https://doi.org/10.5194/egusphere-2026-3188
Preprint. Discussion started: 2 July 2026

The JRC-FASST model: an updated version of the global atmospheric source-receptor model based on EMEP MSC-W chemical transport model

Luca Pozzoli[1,*], Andreas Gavros[1], Alexander De Meij[2], Rita Van Dingenen[3], Claudio A. Belis[3]

[1] Fincons SpA, 20871 Vimercate, Italy
[2] MetClim, 21025, Varese, Italy
[3] European Commission, Joint Research Centre, Ispra, Italy
* now at: NILU, Instituttveien 18, 2007 Kjeller, Norway

Correspondence to: Claudio A. Belis (claudio.belis@ec.europa.eu)

Abstract. Air pollution remains a major global challenge, affecting human health, agricultural productivity, and climate. Reduced-form models have been widely used to support rapid assessment of emission control strategies. This study presents an updated version of a global air quality screening tool, JRC-FASST, developed using the EMEP chemical transport model. JRC-FASST is a reduced-form Source-Receptor model, which translates changes in emissions of air pollutants from different source regions into changes in atmospheric concentrations. The new model version improves the representation of air pollution, by increasing spatial detail and refining the definition of emission source regions, leading to a more accurate estimation of pollutant concentrations and population and ecosystem exposure. A key enhancement of JRC-FASST is the expanded and refined set of source regions. JRC-FASST employs 76 source regions globally simulated at 0.5° × 0.5° resolution, including 41 individual countries in Europe simulated at 0.1° × 0.1° resolution. This allows a more detailed representation of national emissions and their transboundary impacts. It incorporates an expanded set of air quality indicators, including particulate matter, nitrogen dioxide, and multiple ozone metrics relevant for both health and crop impacts. JRC-FASST reproduces the results of the full atmospheric model with high accuracy, particularly for particulate matter and ozone, while maintaining computational efficiency suitable for policy screening. Overall, the updated model provides a more robust and flexible tool for exploring air quality policies at national, regional and global scales. Moreover, the current version establishes the methodological foundation for a continuously evolving platform.

https://doi.org/10.5194/egusphere-2026-3188
Preprint. Discussion started: 2 July 2026

1 Introduction

Air pollution affects human health, agricultural productivity, natural ecosystems and climate at the global level. Exposure to air pollution comes from a complex mixture of gases and particles (e.g. particulate matter, ozone, nitrogen dioxide, sulphur dioxide, carbon monoxide) and has significant adverse health effects, leading to nearly 13% of premature deaths globally (HEI, 2025). Air pollution affects all age groups, from unborn children to older people, in both high- and low-income nations. Although strongest evidence exists for respiratory and cardiovascular diseases, exposure to air pollution affects nearly every organ system (WHO, 2025). Tropospheric ozone harms natural vegetation (forests, grasslands) leading to reduced biodiversity and agricultural crops causing lower yields. From 2000 to 2020, there was a general decline in the proportion of agricultural land in EEA member countries exposed to ozone levels above the protective target for vegetation, reaching a minimum of 6 % in 2020 (Sonwani et al. 2022). However, in 2020, critical thresholds for forest protection were surpassed in 59% of the total forest area of the 32 European Environment Agency (EEA) member states (Maes et al. 2023). Reduction of wheat yields due to ozone exposure have been reported in India and China (Anagha and Kuttippurath 2025; Xu et al. 2024). Moreover, the climate penalty has been widely established in the literature for ozone, due to the role of photochemistry (sunlight) in ozone production, whereby increases in air temperatures enhance ozone formation potentially affecting global food security (von Schneidemesser et al. 2020; Fu and Tian, 2019).

Despite the necessary trade-off between the computational efficiency of reduced-form models (RFMs) and their accuracy, regional detail, and flexibility in spatial arrangement of emissions, these models have been successfully applied in many studies at the national, regional and global levels (Gallagher et al., 2023; Zhong et al., 2023; Cao et al., 2023). According to Cao et al. (2023) RFMs can be classified in three groups. The sensitivity based models analyse the response of concentrations to small emission perturbations using full CTMs runs (e.g. brute force, DDM) while the second group is based on simplified equations in which several assumptions are made on chemical, physical and transport processes (e.g. InMAP, APEEP). The third group, statistical models, rely on analysis (e.g. regression) of large datasets and often combine different data sources to approximate nonlinear chemical and physical processes of CTMs through multi- dimension simulation experiments (e.g. RSM). The TM5-FAst Scenario Screening Tool (TM5-FASST) model (Van Dingenen et al., 2018), developed at the European Commission - Joint Research Centre (EC-JRC), is a scenario screening model which falls in the category of sensitivity based models. It estimates the impacts of changes in national or regional emissions on atmospheric pollutant concentrations and on related metrics affecting human health, agriculture, and the radiative forcing of short-lived climate pollutants. It relies on source–receptor (SR) relationships derived from a suite of global TM5 chemistry transport model (CTM) simulations. Due to the computational limitations at the time of development, country level emissions were aggregated into 56 larger source regions which required hundreds of perturbation simulations to construct the SR relationships. Reduced-form SR models have been extensively used in global air quality modelling (Wild et al., 2012; Turnock et al., 2018; Ye et al., 2021), cost optimisation and cost-benefit analysis in support of policy development (e.g. Amann et al., 2011) and in source apportionment studies (e.g. Thunis et al., 2018). TM5-FASST has long served as a global reduced form air quality assessment tool to support the

https://doi.org/10.5194/egusphere-2026-3188
Preprint. Discussion started: 2 July 2026

exploration of air quality impacts (on health, agriculture, etc.) and air quality - climate interactions (e.g. Belis et al., 2022), including sector and spatial resolved output (e.g. Belis and Van Dingenen, 2023), with a view to designing emission control strategies. Due to its reliability and versatility, TM5-FASST has been used to describe the role of air pollutants in many global assessments (e.g. OCSE, 2025; UNEP, 2025; IPCC AR6, 2021) and key international scientific studies (e.g. Gu et al., 2021; Harmsen et al., 2020; Vandyck et al., 2018; Rao et al., 2017).

Substantial advances in atmospheric modelling and high-performance computing over the last decade now allow full CTM simulations at significantly higher horizontal resolutions within feasible computing times. Alongside these developments, major improvements in chemical mechanisms, physical process representations, and emission inventories further motivate an update to the FASST framework to improve the accuracy and spatial relevance of its SR relationships.

In this context, a new version of the FASST model has been developed using the European Monitoring and Evaluation Programme (EMEP hereafter) Meteorological Synthesizing Centre-West (MSC-W hereafter) chemical transport model (Simpson et al., 2012). The newly developed JRC-FASST version benefits from EMEP simulations higher resolution over Europe and globally, providing a largely improved representation of spatial variability between urban, suburban, rural, and remote environments compared with the previous TM5 based version. This higher resolution enables more accurate estimation of population exposure, crop damage, and transboundary pollution contributions. In addition, the new model relies on updated anthropogenic emissions.

The objective of this work is to achieve a more detailed representation of the influence of emissions and their transboundary impacts through the use of a more recent and higher resolution EMEP output, extending the number of pollutant metrics, including speciated particulate matter, nitrogen and sulphur deposition, and a comprehensive set of ozone health and crop-related metrics, and an expanded set of source regions.

This paper is structured as follows. Sect. 2 describes the methodology underlying the new model, including the configuration of the EMEP MSC-W simulations (section 2.1), the baseline emissions from EDGAR v5.0 for 2015 (section 2.2), the derivation of source–receptor relationships and the treatment of non-linearities (section 2.3), the implementation of health (section 2.4) and crop impact calculations (section 2.5). Sect. 3 presents the main results, including baseline model evaluation (section 3.1), tests of linearity and additivity (section 3.2.1 and 3.2.2), comparisons between JRC-FASST and EMEP (section 3.2.3), and an analysis of population and area-weighted exposure for O_3, NO_2, and $PM_{2.5}$ under different emission reduction scenarios (sections 3.3 to 3.5). Sect. 4 summarises the main findings, identifying the strengths and limitations of the updated model, and outlining key directions for future development.

2 Methods

2.1 The native EMEP MSC-W chemical transport model

The MSC-W of the EMEP, is a three-dimensional chemical transport model that simulates transport, chemical processes, and deposition of atmospheric trace gases and particulate matter. The EMEP model has been used for more than 30 years to support

https://doi.org/10.5194/egusphere-2026-3188
Preprint. Discussion started: 2 July 2026

the Convention on Long Range Transboundary Air Pollution (CLRTAP), and it is one of the key tools within European air pollution policy assessments. We limit here the description of the EMEP model to the main settings used to perform the model simulations, which are at the basis of the JRC-FASST source receptor model.

The EMEP model (Simpson et al., 2012) version rv_34 (https://github.com/metno/emep-ctm) is used over Europe and global scale to study to perform the emissions reductions that serves as an input to FASST. On the European domain, the model stretches from -15.05° to 36.95° longitude and 30.05° to 71.45° latitude with a horizontal resolution of 0.1° x 0.1°. The model has 20 vertical levels, with the first level around 45 m. The global domain has a horizontal resolution of 0.5° x 0.5°. Compared to the version documented in Simpson et al. 2012, the main changes are documented in the EMEP Status Report 1/2020. The initial and background concentrations for ozone are based on Logan (1998) climatology, as described in Simpson et al. (2003). The sources of natural mineral dust in the model include windblown dust from deserts, semi-arid areas, agricultural and bare lands and dust produced on African deserts (Simpson et al., 2012). For the other species, background/initial conditions are set within the model using functions based on observations (Simpson et al., 2003 and EMEP Status Report 1/04). Detailed information on the land cover, model physics are described in Simpson et al. (2012) and in the EMEP Status Report 1/2017.

The model uses meteorological initial conditions and lateral boundary conditions from the Weather Research Forecast model (WRF, http://wrf-model.org/index.php, Skamarock et al. 2005) version 3.9.1. The WRF-ARW system is a non-hydrostatic model (with a hydrostatic option) using terrain- following vertical coordinate based on hydrostatic pressure. The terrestrial data sets for WRF are built using the NCEP geographical data. These consist in global data sets for soil categories, land-use, terrain height, annual mean deep soil temperature, monthly vegetation fraction, monthly albedo, maximum snow albedo and slopes.

WRF uses land-use categories from United States Geological Survey (USGS) 24-category data, which are available for different horizontal resolutions (10', 5', 2', 30"; " denotes arc seconds and ' denotes arc minutes). The horizontal resolution is set by the user in the pre-processing step in WPS. The vertical discretization of WRF involves 29 levels up to about 18 km. The model is set up using WRF Single-moment 5-class (WSM5, Hong et al., 2004). The model uses the 5-layer thermal diffusion with soil temperature in 5 layers. The planetary boundary layer (PBL) Yonsei University (YSU) scheme is used (Hong et.,al., 2006). In the YSU scheme, the top of the PBL is described by the critical Richardson number which is the value of the gradient Richardson number below which air becomes dynamically unstable and turbulent. The Richardson number is used to indicate the dynamic stability and the formation of turbulence. The MM5 similarity theory is used for the surface layer (Janić, 2001). Both longwave and shortwave radiation are simulated by the RRTMG scheme (Mlawer et al., 1997; Matsui et al., 2018). The default diffusion scheme is selected. The cumulus scheme is only activated for the mother domain according to the Grell-Devenyi (Grell 3D) scheme (Grell and Dévényi, 2002). It is recommended to activate the cumulus scheme on coarser grids e.g. > 10 km x 10 km, when it is not resolved by the model. The meteorological year is 2015.

The EMEP MSC-W model calculates roughness length and depositions from its own land cover. The EMEP-WRF modelling system has previously been evaluated well against field measurements at high resolution regional version (Vieno et al., 2010, 2014, 2016) at lower resolution global version (Ge et al. 2021a; Ge et al. 2021b).

https://doi.org/10.5194/egusphere-2026-3188
Preprint. Discussion started: 2 July 2026

Two sets of simulations were performed for the development of the JRC-FASST model (Sect. 2.3). Global simulations were performed at the horizontal resolution of 0.5° x 0.5° degrees, combined with regional simulations at 0.1° x 0.1° resolution to cover Europe.

2.2 Emission inventory

The EDGAR v5.0 for year 2015 (Crippa et al., 2019, at the time the model development started this was the most updated version and year available) was used as the emission inventory of air pollutants for the baseline simulations, replacing the earlier inventory for the year 2000 used in TM5-FASST. EDGAR provides emissions per country and sector for ozone precursor gases (carbon monoxide, CO, nitrogen oxides, NOx, non-methane volatile organic compounds, NMVOC, and methane, CH4), acidifying gases (ammonia, NH_3, and sulphur dioxide, SO_2), and primary particulate matter (PM10, $PM_{2.5}$ and carbonaceous speciation, black carbon, BC, and organic carbon, OC). The activity data for the energy related sectors are based on the energy balance statistics of IEA (2017), whereas the activity data for the agricultural sectors originate mainly from FAO (https://www.fao.org/faostat/en/#home). The EDGAR emissions are provided at the horizontal resolution of 0.1° x 0.1° degrees. The original resolution was used for the model simulations over the European domain, while the emissions for the global model simulations were aggregated at the 0.5° x 0.5° degrees resolution.

Table 1: Summary table with total emissions (ktonnes) of air pollutants from EDGAR v5.0 for year 2015.

Country or Region	NOx	CO	NMVOC	SO_2	NH_3	$PM_{2.5}$	PM_{coarse}	POM	BC	$RemPM_{2.5}$
China	26365	129684	30868	30901	8733	11055	4967	2137	1476	7442
United States	13860	50885	10972	8553	3940	1457	777	447	214	797
India	10420	73195	13455	11480	5795	6154	3491	1594	857	3703
EU27	6351	19612	7250	4068	5107	1275	772	432	213	629
Rest of Europe	1295	3094	1438	1012	777	232	130	69	34	128
Russian federation	3860	8888	4462	2351	1130	335	181	100	35	200
Rest of former Soviet Union	2106	5787	2419	2793	1373	311	143	117	41	153
Middle East	8874	21776	10750	9921	1835	687	335	219	104	364
South America	7451	54764	10603	4054	5000	2541	1365	694	400	1448
South-East Asia	6113	68438	17534	5320	4183	3650	2243	1304	639	1707
Africa	5970	96180	24884	5023	5639	5976	7086	2518	1083	2376
Rest of North and Central America	5052	24962	6062	3428	2009	851	577	286	137	428
Rest of East Asia	4822	14344	3687	3423	706	553	306	101	70	382
Rest of South Asia	1862	18873	3723	1479	1971	1115	822	469	207	438
Oceania	1584	3450	1165	1091	798	236	90	71	39	126
Global	105986	593932	149273	94897	48996	36428	23286	10558	5550	20319

https://doi.org/10.5194/egusphere-2026-3188
Preprint. Discussion started: 2 July 2026

Table 1 presents a summary of the total emissions of all air pollutants for the countries or group of countries with largest emission levels (China, United States, India, the Russian federation and EU27) as well as other regions of the world and global emissions. PM_{coarse} represents the coarse fraction of particulate matter (PM_{coarse} = PM10 – $PM_{2.5}$), while the fine fraction of primary particulate matter, $PM_{2.5}$, is further speciated in black carbon (BC), primary organic matter (POM), and remaining primary $PM_{2.5}$ ($RemPM_{2.5}$).

2.3 Air pollutant SR relations

The background foundation of the newly developed JRC-FASST model remains the same as the previous TM5-FASST version (Van Dingenen et al., 2018). Air Quality Source-Receptor Models (AQ-SRMs) connect pollutant emissions from a specific source region to their concentrations and impacts in the same region and in downwind receptor regions. The effects of meteorology (in this case the meteorology of year 2015) and of atmospheric chemical and physical processes are implicitly included in the simplified AQ-SRM as the SR relationship are based on a set model simulations performed with a Chemical Transport Model (CTM), which include a comprehensive description of the chemical and physical processes in the atmosphere. The newly developed JRC-FASST model, like the previous TM5-FASST, is a reduced-form SR model, i.e. a simple linear function that approximates the meteorological and chemical processes to estimate the concentration of a pollutant or another metric m included in the CTM model simulations at receptor R resulting from the emissions of a pollutant precursor p from source S:

$$dC_{R,m} = \mathrm{SRC} \times \mathrm{d}E_{S,p} \,, \qquad (1)$$

where $dC_{R,m}$ is the change in the concentration of pollutant or metric m compared to a reference concentration in the receptor region R due to a change in the emissions $dE_{S,p}$ of a pollutant precursor p compared to a reference emission in the source region S. SRC is the SR coefficient for the specific pairs of precursor-pollutant and source-receptor regions.

The SRCs are derived for each precursor and for any grid-cell in the full model domain and for all the outputs available in the EMEP model simulations. This represents the great advantage of having the full set of pollutants and metrics simulated by the EMEP model and that can be aggregated at a later stage for any specific receptor country or region. An overview of all precursor–pollutant (or metric) links that have been included in this new version is shown in Table 2. Compared to the previous TM5-FASST version we have a much larger pool of components and metrics that we can estimate.

The list of relevant components and metrics is provided in Table A1 in Appendix A. However, this version does not include CH4 as a precursor and radiative forcing as an output metric. These two aspects remain as main developments of the next version of the JRC-FASST (see Sect. 4).

https://doi.org/10.5194/egusphere-2026-3188
Preprint. Discussion started: 2 July 2026

Table 2: Relevant precursor–pollutant relationships included in JRC-FASST. ●: direct emission or immediate product; ○: effect via thermodynamic equilibration; □: effect via first-order oxidation products (OH) affecting the lifetime of other precursor (adapted from Table 1 in Van Dingenen et al., 2018). S_{ox} Deposition: Total (dry and wet) deposition of oxidized sulphur (S) compounds; N_{ox} Deposition: Total (dry and wet) deposition of oxidized nitrogen (N) compounds; N_{red} Deposition: Total deposition of reduced nitrogen (N) compounds; PODy: Phyto-toxic ozone doses are available from the EMEP model for the European domain only. Different POD calculations are available for different threshold levels y and for different land cover categories (Simpson et al., 2012); SOMO35: The Sum of Ozone Means Over 35 ppb is the indicator for health impact assessment recommended by WHO; AOT40: accumulated amount of ozone over the threshold value of 40 ppb. Different AOT40 calculations are available with different methodologies and for different land cover categories (Simpson et al., 2012).

Pollutant (metric) / Precursor	SO_2	NO_2	NH_3	O_3	SO_4^{2-} (in $PM_{2.5}$)	NO_3^- (in $PM_{2.5}$)	NH_4^+ (in $PM_{2.5}$)	$PM_{2.5}$	EC (in $PM_{2.5}$)	OM (in $PM_{2.5}$)	S_{ox} Deposition	N_{ox} Deposition	N_{red} Deposition	PODy	SOM35	AOT40
NOx	□	●	○	●	○	●	○	●			□	●	●	●	●	●
NMVOC	□	□		●	□	□	□			□	□			●	●	●
CO				●										●	●	●
NH_3	□	□	●	□	○	○	●	●			□	●	●	□	□	□
SO_2	●	□	○	□	●	○	○	●			●			□	□	□
Primary $PM_{2.5}$								●	●	●						

The JRC-FASST model includes 76 source regions (Figure 1), 34 of them correspond to the same regions of the older TM5-FASST version, such as the main source regions in the northern hemisphere like USA (United States of America), CHN (China, Hong Kong, Macao) and IND (India, Maldives and Sri Lanka). Also, the source regions in Africa, South America, Central America, South Asia and East Asia maintain the same aggregation of countries as in the TM5-FASST version. In the new JRC-FASST version the Russian Federation is considered as a single source region (RUS), while in the TM5-FASST version RUS was the aggregation of the western part of the Russian Federation, Georgia, Armenia and Azerbaijan, while the Eastern part of the Russian Federation (RUE) was a separate source region. All these 34 source regions and RUS are simulated at the global model resolution of 0.5° × 0.5° degrees. The most significant improvement in the new JRC-FASST model version is the larger number of European continent and the Caucasus source regions included in the model, simulated as single countries and at the higher model resolution of 0.1° × 0.1° degrees. The countries in these regions were previously aggregated in 18 source regions at the resolution of 1° x 1° degrees. The new JRC-FASST version reorganise the countries of the same area in 41 source regions (Figure 2). All the EU27 countries are considered separately (with the exception of Malta included in the source region of Italy, ITA) and then Switzerland (CHE), Great Britain (GBR), Norway and Iceland (NOR), Albania (ALB), Bosnia and Herzegovina (BIH), North Makedonia (MKD), Montenegro (MNE), Serbia and Kosovo under UNSCR 1244/99 (SRB), Ukraine (UKR), Moldova (MDA), Belarus (BLR), Türkiye (TUR), Armenia (ARM), Georgia (GEO), and Azerbaijan (AZE).

https://doi.org/10.5194/egusphere-2026-3188
Preprint. Discussion started: 2 July 2026

As the new JRC-FASST is based on two sets of EMEP model simulations with different resolutions, 0.5° × 0.5° degrees for simulations covering the whole globe (GLB) and 0.1° × 0.1° degrees for simulations covering the European continent (EU), the impact of non-European source regions (GLB) on receptor regions in Europe is accounted by nearest neighbour interpolation of the GLB simulations at 0.1° × 0.1° degrees over the EU domain. However, the impact of emissions from the European source regions in the EU domain does not extend to the receptor regions outside the EU domain as single source regions. Due to the large number of EMEP simulations that would be needed to perform for all the 41 European source regions at the global scale, the countries of the European region are grouped into four additional source regions in the GLB domain were included in the model (Figure 2):

- EUR (Europe): the EU27 countries plus Switzerland (CHE), Norway and Iceland (NOR) and Great Britain (GBR);
- WEB (Western Balkans countries): Albania (ALB), Bosnia and Herzegovina (BIH), North Makedonia (MKD), Montenegro (MNE), Serbia and Kosovo under UNSCR 1244/99 (SRB);
- UKRP: Ukraine (UKR), Moldova (MDA) and Belarus (BLR);
- TURP: Türkiye (TUR), Armenia (ARM), Azerbaijan (AZE), and Georgia (GEO).

This simplified aggregation of the European source regions in the GLB domain considers groups of countries implementing air quality policies with the same or very similar levels of air quality targets (EUR and WEB), compared to the other countries grouped by their geographical proximity (UKRP and TURP).

In summary, the global (GLB) domain contains a total of 39 source regions, $n_{S,GLBall}$, which are used when the receptor region lies outside Europe. When the receptor region is inside Europe, emissions from only 35 GLB source regions, $n_{S,GLBnotEU}$ — that is, all GLB regions except EUR, WEB, UKRP, and TURP — are included, together with 41 source regions from the higher-resolution European (EU) domain, $n_{S,EU}$. This results in a total of 76 source regions used for simulations within Europe. The concentration response upon a change in emissions in each source region, have been derived from a set of simulations with the full chemical transport model EMEP by applying −20 % emission perturbations for each of the 76 defined source regions, for all relevant anthropogenic precursor components, in comparison to a set of unperturbed simulations, hereafter denoted as “base simulations”. This is the same assumption used in the previous TM5-FASST version and widely used to establish SR emission concentration sensitivities (Alcamo et al., 1990; Amann et al., 2011; Dentener et al., 2010). The applicability of the established SRs for larger emission perturbations depends on the linearity of the emission concentration responses and was extensively evaluated in the previous TM5-FASST version (Van Dingenen et al., 2018). In Sect. 3.2 is reported the analysis accomplished to ensure that the same assumptions hold in the new JRC-FASST simulations, done with a different CTM and at a higher spatial resolution. Natural emissions, such as biogenic organic components (isoprene and monoterpenes) from vegetation (BSOA), NO from soil, natural dust, marine DMS and sea salt sprays are simulated in the EMEP model as a space-time varying component (Simpson et al., 2012) but did not vary in the model sensitivity simulations. Consequently, absolute concentrations of BSOA or natural dust in $PM_{2.5}$ were identical across base and perturbation simulations.

https://doi.org/10.5194/egusphere-2026-3188
Preprint. Discussion started: 2 July 2026

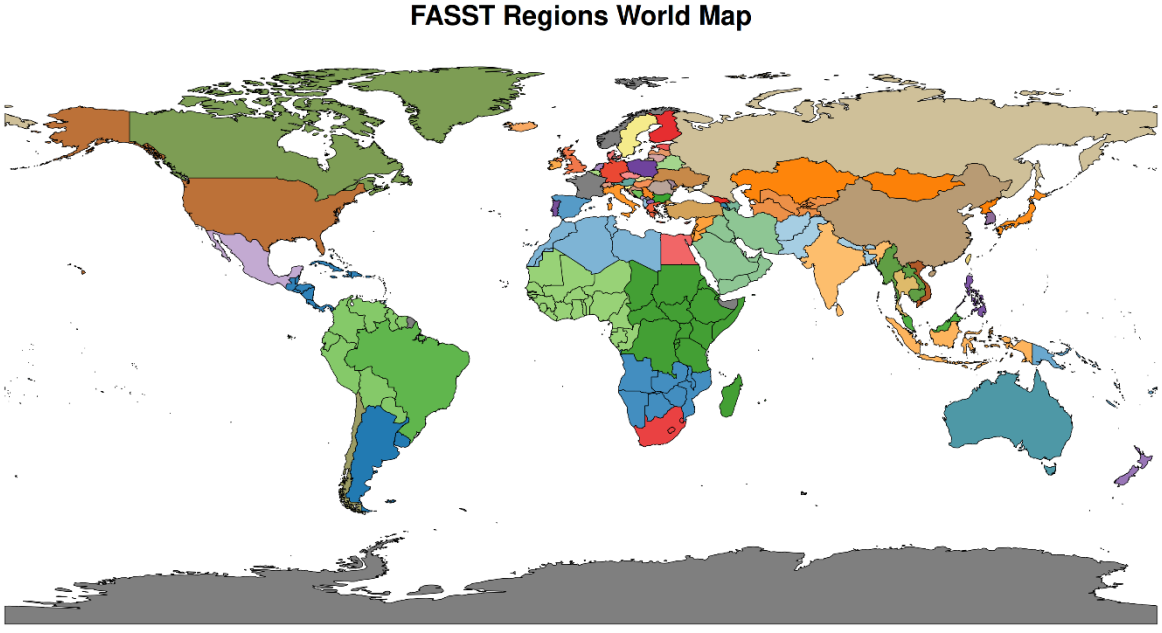

Figure 1: The 76 continental emission source regions in JRC-FASST. See Table A2 in Appendix A for the mapping between regions and countries.

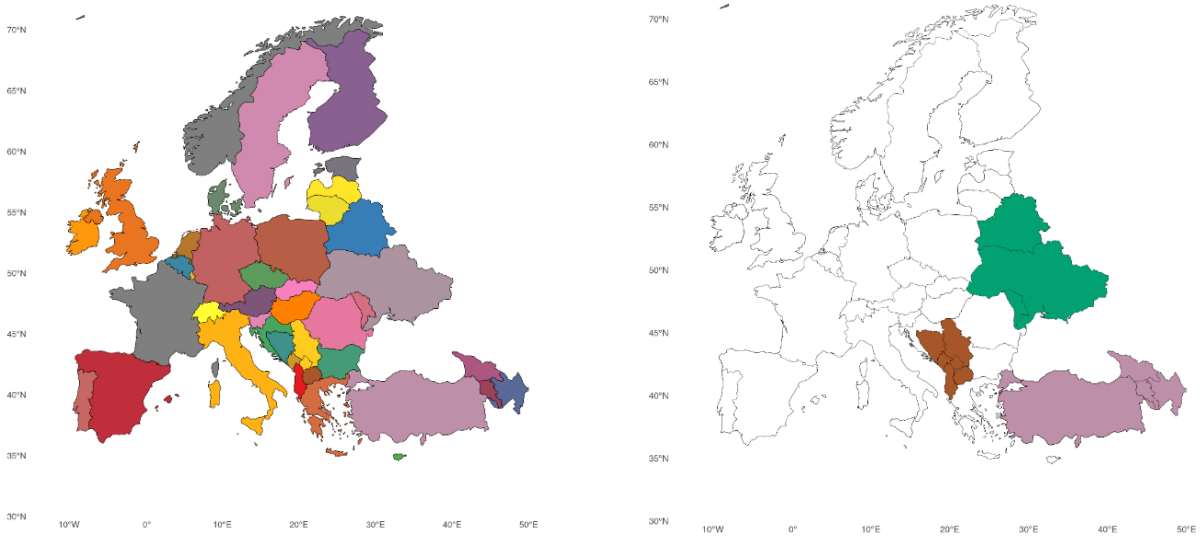

Figure 2: The 41 emission source regions in JRC-FASST over the European continent (left). The 4 source regions in Europe (EUR, WEB, TURP, UKRP) considered in the global domain (right). See Table A3 in Appendix A for the detailed list of source regions in Europe and comparison with previous TM5-FASST version.

In the GLB domain, the total concentration of a component (or metric) at any receptor point (i.e. grid cell in the GLB domain EMEP simulation), C_{GLB}, resulting from arbitrary emissions of all precursors p at all source regions s, is calculated as a

https://doi.org/10.5194/egusphere-2026-3188
Preprint. Discussion started: 2 July 2026

perturbation of the base simulation, $C_{GLB,base}$, by adding all the SR coefficients scaled by the emission perturbations, as in Eq. 2:

$$C_{GLB} = C_{GLB,base} + \sum_{s=1}^{n_{S,GLBall=39}} \sum_{p=1}^{n_P} \frac{\Delta C_{GLB}(s,p)}{\Delta E(s,p)} \cdot [E_x(s,p) - E_{base}(s,p)] \quad (2)$$

Where $\frac{\Delta C_{GLB}(s,p)}{\Delta E(s,p)}$, is the SR coefficient as the ratio between $\Delta C_{GLB}(s,p)$, the change in the component simulated with the EMEP model due to the 20% emission reduction, $\Delta E(s,p) = 0.20 \cdot E_{base}(s,p)$, and $[E_x(s,p) - E_{base}(s,p)]$ is the emission perturbation E_x for each precursor p and each source region s, compared to the emissions used in the base case EMEP simulation, E_{base}. For receptors in the GLB domain, all the 39 source regions in the GLB domain are included.

In the EU domain, similarly to Eq. 2, the total concentration of a component (or metric) at any receptor point (i.e. grid cell in the EU domain EMEP simulation), C_{EU}, resulting from arbitrary emissions of all precursors p at all the 41, $n_{S,EU}$, source regions s within the EU domain, $C_{EU,base}$, by adding all the SR coefficients scaled by the emission perturbations, as in Eq. 2, but with an additional term for the perturbations occurring in all the 35 source regions outside Europe in the GLB domain, $n_{S,GLBnotEU}$, as in in Eq. 3:

$$C_{EU} = C_{EU,base} + \sum_{s=1}^{n_{S,EU}=41} \sum_{p=1}^{n_P} \frac{\Delta C_{EU}(s,p)}{\Delta E(s,p)} \cdot [E_x(s,p) - E_{base}(s,p)] + \sum_{s=1}^{n_{S,GLBnotEU}=35} \sum_{p=1}^{n_P} \frac{\Delta C'_{GLB}(s,p)}{\Delta E(s,p)} \cdot [E_x(s,p) - E_{base}(s,p)] \quad (3)$$

where $\Delta C'_{GLB}(s,p)$ is the change in the component due to the 20% emission reduction in source region s and precursor p, interpolated at the same resolution of the EU domain.

The $\Delta C_{GLB}(s,p)$ and $\Delta C_{EU}(s,p)$ generated as annual mean responses to annual emission changes of 20% allow the output of the JRC-FASST to be customised according to different needs. The main output variables include:

- gas pollutants, such as O_3, NO, NO_2, NH_3, HNO_3, SO_2 and CO;
- total $PM_{2.5}$, both dry and at 50% relative humidity;
- speciation of the PM components in the fine ($PM_{2.5}$) and coarse (PM_{10}) fractions: the secondary inorganic components, nitrate (NO_3^-), ammonium (NH_4^+) and sulphate (SO_4^{2-}); the secondary organic biogenic and anthropogenic aerosols (BSOA and ASOA); the total primary component of $PM_{2.5}$ which is further speciated in primary organic matter (POM), elemental carbon (EC) and remaining primary $PM_{2.5}$;
- wet and dry deposition of SOx, oxidised and reduced N separately;
- O_3 metrics used in the health and crop impact assessments such as the SOMO35, AOT40, and phytotoxic ozone doses (POD).

In addition to the O_3 metrics included in the EMEP model output, surface ozone fields from both the base and perturbation experiments were saved at hourly intervals. This enabled the calculation of additional ozone metrics relevant to vegetation and human health, which are typically based on hourly or daytime ozone concentration thresholds. These hourly surface ozone

https://doi.org/10.5194/egusphere-2026-3188
Preprint. Discussion started: 2 July 2026

data were then used to derive annual emission responses for O_3 key metrics for specific seasons and daytime averages, including:

- AOT40: Accumulated hourly ozone concentrations above 40 ppb during a 3-month crop growing season;
- M7 and M12: 3-month averages of 7-hour or 12-hour daytime ozone concentrations during the crop growing season;
- 6mDMA1: The maximum 6-month running average of daily maximum hourly ozone.

The list of the EMEP output variables relevant for the JRC-FASST model is provided in Table A1 in Appendix A.

Table 3: Overview of the EMEP simulations performed for the calculation of the source-receptor matrices and the development of the new JRC-FASST model.

Simulation	Domain and resolution	Emission perturbations	Applied to source regions	Scope
$P0_{Global}$	Global (0.5° × 0.5°)	No perturbation		Base simulation for the global domain
$P1_{Global}$	Global (0.5° × 0.5°)	20% NO_x emission reductions	All 39 source regions in the global domain	Independent SR for NO_x
$P2_{Global}$	Global (0.5° × 0.5°)	20% SO_2 emission reductions	All 39 source regions in the global domain	Independent SR for SO_2
$P3_{Global}$	Global (0.5° × 0.5°)	20% NH_3, NMVOCs emission reductions	All 39 source regions in the global domain	SR matrices for NH_3 and NMVOCs, assuming little chemical interaction among the selected precursors in the formation of O_3 and NH_4^+
$P4_{Global}$	Global (0.5° × 0.5°)	20% $PM_{2.5}$, CO emission reductions	All 39 source regions in the global domain	SR matrices for $PM_{2.5}$ and CO, assuming little chemical interaction among the selected precursors
$P0_{Europe}$	Europe (0.1° × 0.1°)	EDGARv5.0, No perturbation		Base simulation for the European domain
$P1_{Europe}$	Europe (0.1° × 0.1°)	20% NO_x emission reductions	All 41 source regions in Europe	Independent SR for NO_x
$P2_{Europe}$	Europe (0.5° × 0.5°)	20% SO_2 emission reductions	All 41 source regions in Europe	Independent SR for SO_2
$P3_{Europe}$	Europe (0.5° × 0.5°)	20% NH_3, NMVOCs emission reductions	All 41 source regions in Europe	SR matrices for NH_3 and NMVOCs, assuming little chemical interaction among the selected precursors in the formation of O_3 and NH_4^+
$P4_{Europe}$	Europe (0.5° × 0.5°)	20% $PM_{2.5}$, CO emission reductions	All 41 source regions in Europe	SR matrices for $PM_{2.5}$ and CO, assuming little chemical interaction among the selected precursors

https://doi.org/10.5194/egusphere-2026-3188
Preprint. Discussion started: 2 July 2026

Table 3 lists the set of EMEP simulations, including the baseline simulations for the Global and European domain (P0), and the -20% perturbation simulations for combined or single precursors (P1 to P4). In total, perturbations are calculated for 6 precursors (NO_x, SO_2, NH_3, NMVOC, CO and $PM_{2.5}$) for all individual source regions, 39 in the global and 41 in the European domains. NO_x (P1) and SO_2 (P2) perturbations were computed singularly for all individual source regions. Precursors that are not expected to interact chemically were perturbed simultaneously to reduce the number of CTM simulations and computing time. P3 combines NH_3 and NMVOC perturbations, P4 combines $PM_{2.5}$ and CO perturbations.

2.4 Health impact assessment

In the new JRC-FASST version, Health Impact Assessment (HIA) and costing methods follow Belis et al. (2023) methodology. HIA can be implemented through two different methodological frameworks, with population-weighted pollutant concentrations derived from the JRC-FASST tool serving as the input for all subsequent calculations.

Two complementary approaches are used to estimate the long-term health impacts of ambient air pollution:

- **Concentration–Response Functions (CRF):** log-linear CRFs are applied to estimate all-cause mortality (deaths and Years of Life Lost-YLL) and morbidity attributable to $PM_{2.5}$, O_3, and NO_2. For mortality, CRFs are taken from Chen & Hoek (2020), Huangfu & Atkinson (2020) and Kasdagli et al. (2024). Morbidity endpoints associated with particulate matter include bronchitis in children, chronic bronchitis in adults, hospital admissions for cardiovascular and respiratory diseases, restricted activity days, and work-loss days, parameterized mainly following Héroux et al. (2015); additional $PM_{2.5}$ attributable outcomes include childhood asthma (Khreis et al., 2017), lung cancer (Hamra et al., 2014), myocardial infarction and cerebrovascular disease (Alexeeff et al., 2021), diabetes mellitus type 2 (Yang et al., 2020), and Chronic Obstructive Pulmonary Disease (COPD) (Park et al., 2021). Post neonatal infant mortality followed Héroux et al. (2015). A detailed description of the methodology including CRF parameter values, cutoffs, and exposure metrics (including use of SOMO35 for O_3 where applicable) are reported in Tables 2 and 3 of Belis et al. (2023). Moreover, JRC- FASST implements the CRF recommended by the EMAPEC study for the assessment of morbidity attributable to the considered air pollutants (Forastiere et al., 2024).
- **Global Burden of Disease framework (GBD):** in parallel, cause-specific mortality for six outcomes—lower respiratory infections, lung cancer, stroke, type-2 diabetes, ischemic heart disease, and COPD— are estimated using GBD2021 relative risk curves defined over a broad $PM_{2.5}$ range and fitted with splines (Brauer, et al., 2024).

Health impacts are monetised using Value of a Statistical Life (VSL) and Value of a Life Year (VOLY) derived by benefit transfer (BT) from a nonmarket global econometric model which incorporates economic (GDP), socio-economic (GINI), demographic (population), and health (number of doctors) proxies to tailor VSL estimates specific for each country (Ciarlantini et al., 2025). VOLY is estimated from the VSL considering the discount period (remaining expected life years), and the discount rate (Ananthapavan et al., 2021).

https://doi.org/10.5194/egusphere-2026-3188
Preprint. Discussion started: 2 July 2026

2.5 Crop impacts

The JRC-FASST tool can be used to quantify how changes in anthropogenic emissions translate into variations in surface ozone concentrations and, in turn, influence agricultural productivity. From the linearised source–receptor relationships derived from the full EMEP chemistry–transport model, the tool estimates crop yield losses based on established concentration-based ozone exposure metrics and applies these to global and regional ecosystems and agricultural systems. This framework allows rapid evaluation of how different emission scenarios affect crop damage, providing consistent results with detailed CTM simulations while remaining computationally efficient. For comparability with TM5- FASST (Van Dingenen et al., 2018) the traditional crop ozone exposure metrics are included, such as the 3-monthly accumulated ozone above 40 ppbV (AOT40) and seasonal mean 7 or 12 hours daytime ozone concentration (M7, M12) for which exposure-response functions are available from the literature (Mills et al., 2007; Wang and Mauzerall, 2004).

On the other hand, the stomatal flux (i.e. the uptake of O_3 through the stomatal leaf pores) is more strongly related than atmospheric concentration to the impacts of O_3 on vegetation. The stomatal flux responds to environmental conditions, such as temperature, light, air humidity, soil moisture, and plant growth stage. For these reasons, the flux-based metric, such as the Phytotoxic O_3 Dose above a threshold flux of y (PODy), is preferred in risk assessment over the concentration-based metrics, such as AOT40. This is particularly relevant for large scale studies (e.g. pan-European), with large climate differences (UNECE, 2017).

The full EMEP chemistry-transport model includes different types of metrics for stomatal flux-based critical levels, and which can be used in the JRC-FASST tool over the European domain only:

- PODySPEC is a species or group of species-specific PODy that requires comprehensive input data and is suitable for detailed risk assessment: the Phytotoxic O_3 Dose above 1 nmol/m^2/s is calculated for conifer (POD1_CF) and deciduous (POD1_DF) forests, while for all crop types the POD is calculated at 3 nmol/m^2/s (POD3_TC).
- PODyIAM is a vegetation-type specific PODy that requires less input data and is suitable for large-scale modelling, including integrated assessment modelling. A number of metrics is provided by EMEP output for IAM, without flux threshold (POD0_IAM_CR, POD0_IAM_CF, and POD0_IAM_CR), at 1 nmol/m^2/s (POD1_IAM_CR, POD1_IAM_CF, and POD1_IAM_CR), and at 3 nmol/m^2/s only for corps (POD3_IAM_CR).

A guideline to choose the O_3 metrics for crops and vegetation is provided in UNECE (2017, Figure III.2). The biologically most relevant metrics are the PODySPEC which can be used for plant species/group of species-specific risk assessment, while the PODyIAM metrics can be used for indicative risk assessment for vegetation types and quantify the risk for the most sensitive vegetation. The AOT40 (biologically least relevant) is suitable for vegetation types at risk in areas with higher ozone concentrations and for areas where no climatic or water restrictions to stomatal O_3 flux are expected. Due to difficulties in estimating the O_3 flux using Y = 6 nmol m^{-2} s^{-1} in large scale modelling and IAM arising from the strong increase in the uncertainty in modelled POD with increasing Y, Y= 3 nmol m^{-2} s^{-1} is to be used for crops (POD3_TC and POD3_IAM_CR, UNECE, 2017). For forest trees and semi-natural vegetation Y = 1 nmol m^{-2} s^{-1} is used (POD1_CF, POD1_DF,

https://doi.org/10.5194/egusphere-2026-3188
Preprint. Discussion started: 2 July 2026

POD1_IAM_DF, and POD1_MF). The distribution over Europe of AOT40 and POD3 values as calculated by the full EMEP chemistry transport model is shown in Figure 3.

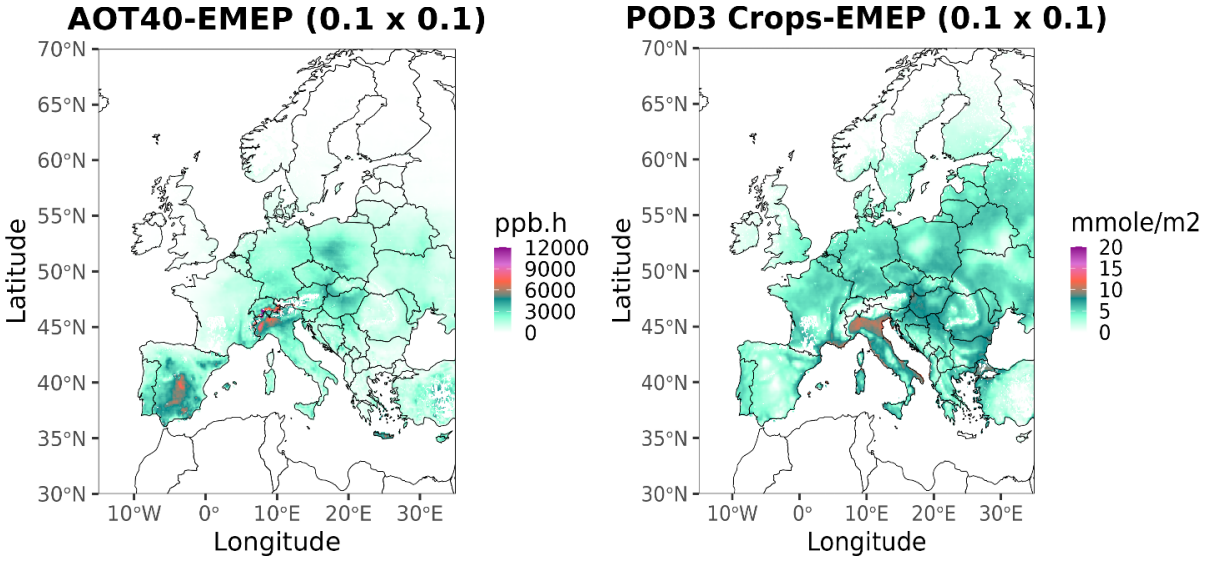

Figure 3: Map of annual AOT40 (MMAOT_TC, Table A1 in Appendix A) and annual mean POD3 for crops (POD3_TC, Table A1 in Appendix A) as calculated by the EMEP full chemistry-transport mode over Europe at the horizontal resolution of 0.1° x 0.1°.

3 Results

3.1 EMEP Baseline concentrations and validation

Figure 4 shows the annual mean concentrations for O_3, NO_x and $PM_{2.5}$ as simulated in the baseline EMEP simulation ($P0_{Global}$). The simulations with the EMEP model at the finer resolution of 0.5° x 0.5° provides a significant improvement compared to the JRC-FASST estimates of population exposure to atmospheric pollutants and thus on their impacts on health and crops production.

The JRC-FASST model is designed to estimate a change in pollutant concentrations, mortality, and crop production due to a changing emission level, relative to a base scenario. For this reason, the model biases in atmospheric concentrations compared to observations have a minor impact on the final output expressed as relative change to a base scenario. On the other hand a bias in the JRC-FASST approach could be due to the model resolution which affects the source-receptor matrices (e.g. offsetting the share of local vs imported pollution in a given region, Van Dingenen et al., 2018).

Considering that the EMEP model has been extensively and regularly evaluated in Europe (Ménégoz et al., 2009; Simpson et al., 2012) and in the international context (Pommier et al., 2018; Ge et al., 2021; van Caspel et al., 2023; Pachón et al., 2024) the reader is referred to the literature for a detailed description of the EMEP model validation.

https://doi.org/10.5194/egusphere-2026-3188
Preprint. Discussion started: 2 July 2026

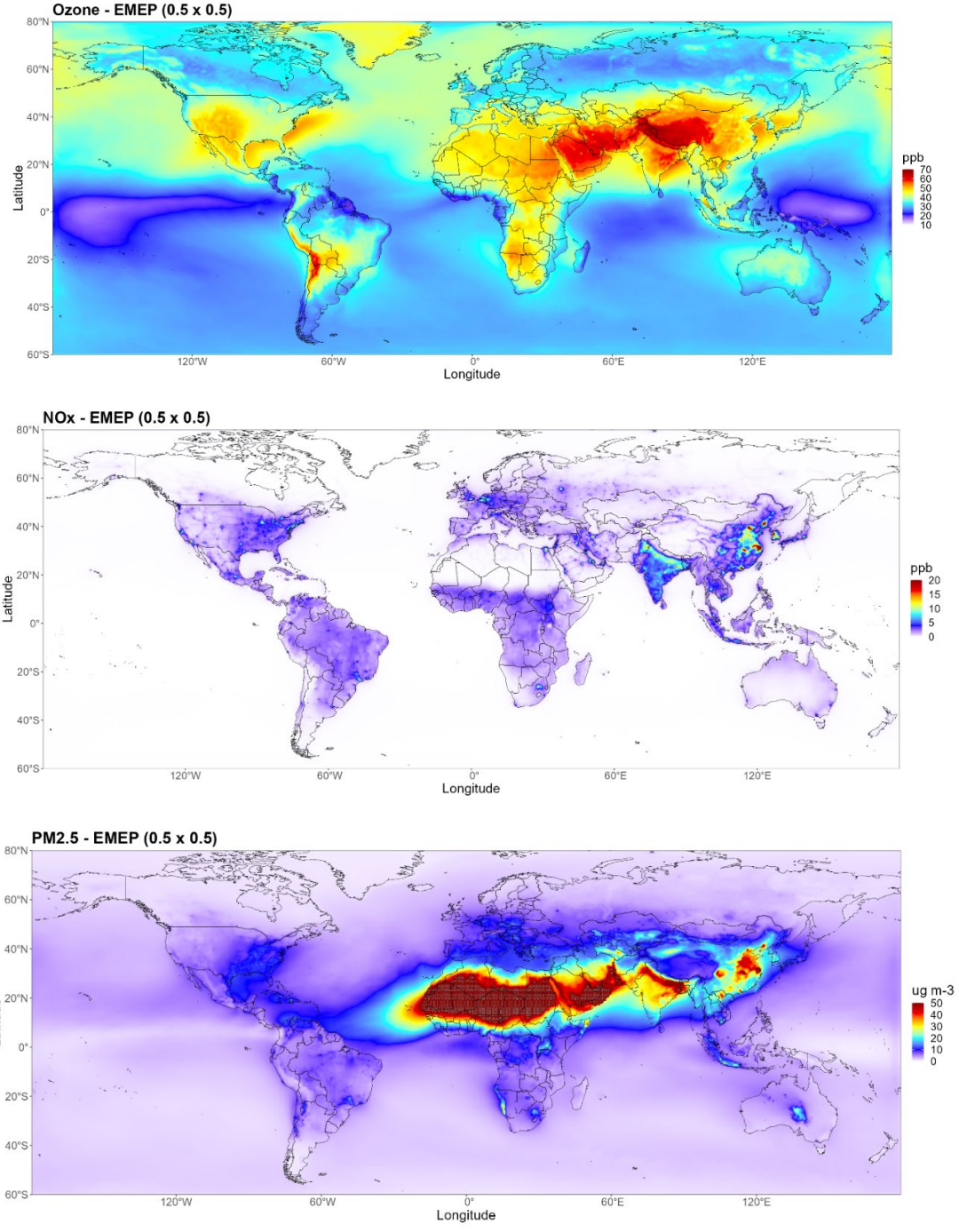

Figure 4: Annual mean O_3 (top), NO_x (centre) and $PM_{2.5}$ (bottom) concentrations simulated in the baseline simulation $P0_{Global}$ by the EMEP model.

https://doi.org/10.5194/egusphere-2026-3188
Preprint. Discussion started: 2 July 2026

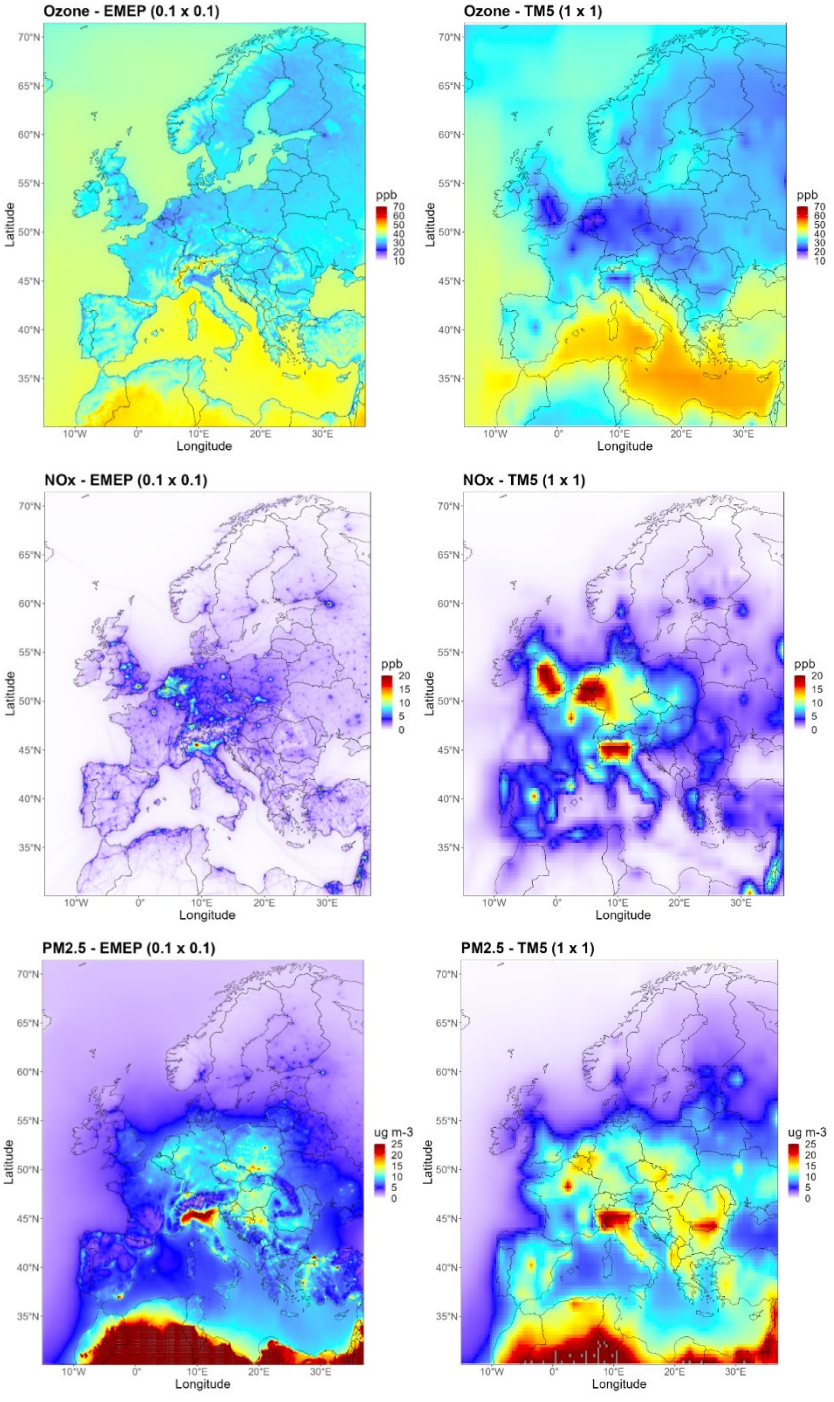

Figure 5: Annual mean O_3 (top), NO_x (centre) and $PM_{2.5}$ (bottom) concentrations simulated over Europe in the baseline simulation $P0_{Europe}$ by the EMEP model (left) and the previous TM5-FASST model (right).

https://doi.org/10.5194/egusphere-2026-3188
Preprint. Discussion started: 2 July 2026

The largest improvements in the new JRC-FASST version, compared to the previous TM5-FASST, is expected in the European domain, mainly due to the higher horizontal resolution. Figure 5 shows the comparison between the EMEP baseline simulation $P0_{Europe}$ used for the new JRC-FASST, compared to the previous TM5 baseline. Even if a quantitative comparison between the baselines of the two models is meaningless, due to the different emission inventories used in each of them, the more detailed spatial distribution of the pollutants, in particular NO_x and $PM_{2.5}$, is evident. The concentrations calculated at the horizontal resolution at 0.1° × 0.1° degrees (corresponding to about 9 km x 11 km at 35N and 5 km x 11 km at 65N) are suitable to depict the urban background concentrations with the consequent improvement in estimating population and ecosystem exposures.

To highlight the capability of the EMEP base case scenario to better represent the geographical gradients due to the higher resolution, compared to TM5, we compare observed and simulated annual mean O_3, $PM_{2.5}$ and NO_2 concentrations which are the target pollutants used in TM5-FASST to estimate the impacts on health and crop production (Figure 6). Observation data were retrieved from the EEA Air Quality e-Reporting portal (https://aqportal.discomap.eea.europa.eu/). Air quality sampling points are defined by type (background, industrial and traffic) and by area (rural, suburban ad urban). The TM5 simulated concentrations are compared with observations of year 2001 (as the meteorology used for its base case scenario and emissions are from year 2000), while EMEP is compared to observations of year 2015 (meteorology and emissions of the same year). The $PM_{2.5}$ concentrations in the TM5 model are calculated as the sum of the inorganic aerosols (SO_4^{2-}, NH_4^+, and NO_3^-), primary anthropogenic aerosols (BC and POM) and $PM_{2.5}$ fractions of natural mineral dust and sea salt aerosols. The EMEP model provides a $PM_{2.5}$ concentration at the relative humidity of 50%, which is the standard for comparisons with observed $PM_{2.5}$. The new JRC-FASST version based on EMEP shows improvements compared to observed values in Europe for all three pollutants, with increased correlation coefficient (R) and reduced root mean square error (RMSE) as depicted in the Taylor diagrams (Figure 6).

The largest improvements are observed in the $PM_{2.5}$ concentrations, for all stations areas and types. The $PM_{2.5}$ concentrations simulated by the EMEP model shows substantial improvement over the TM5 model. Across different sampling point areas (rural, urban, and suburban) and types (traffic, industrial, and background), the RMSE is reduced by between 0.02 and 2.99, and R is ranging between 0.55 and 0.88. Improvements compared to the TM5 are also observed in O_3 concentrations, the RMSE is reduced by between 1.73 and 7.23, and R is ranging between 0.49 and 0.68. As for NO_2 we see a large improvement in the background and industrial stations, while, as expected, NO_2 concentrations at traffic stations would require a higher horizontal resolution. The RMSE is reduced by between 0.24 and 1.25, R s ranging between 0.12 (traffic rural sampling points) and 0.83. Only four traffic rural sampling points are available for $PM_{2.5}$ and O_3, while 12 are available for NO_2. Due to the limited number, traffic rural sampling points were excluded from the analysis of $PM_{2.5}$ and O_3. The scatterplots of simulated value in $P0_{Europe}$ compared to observations are shown in the Figures A1, A2, and A3 in Appendix A.

https://doi.org/10.5194/egusphere-2026-3188
Preprint. Discussion started: 2 July 2026

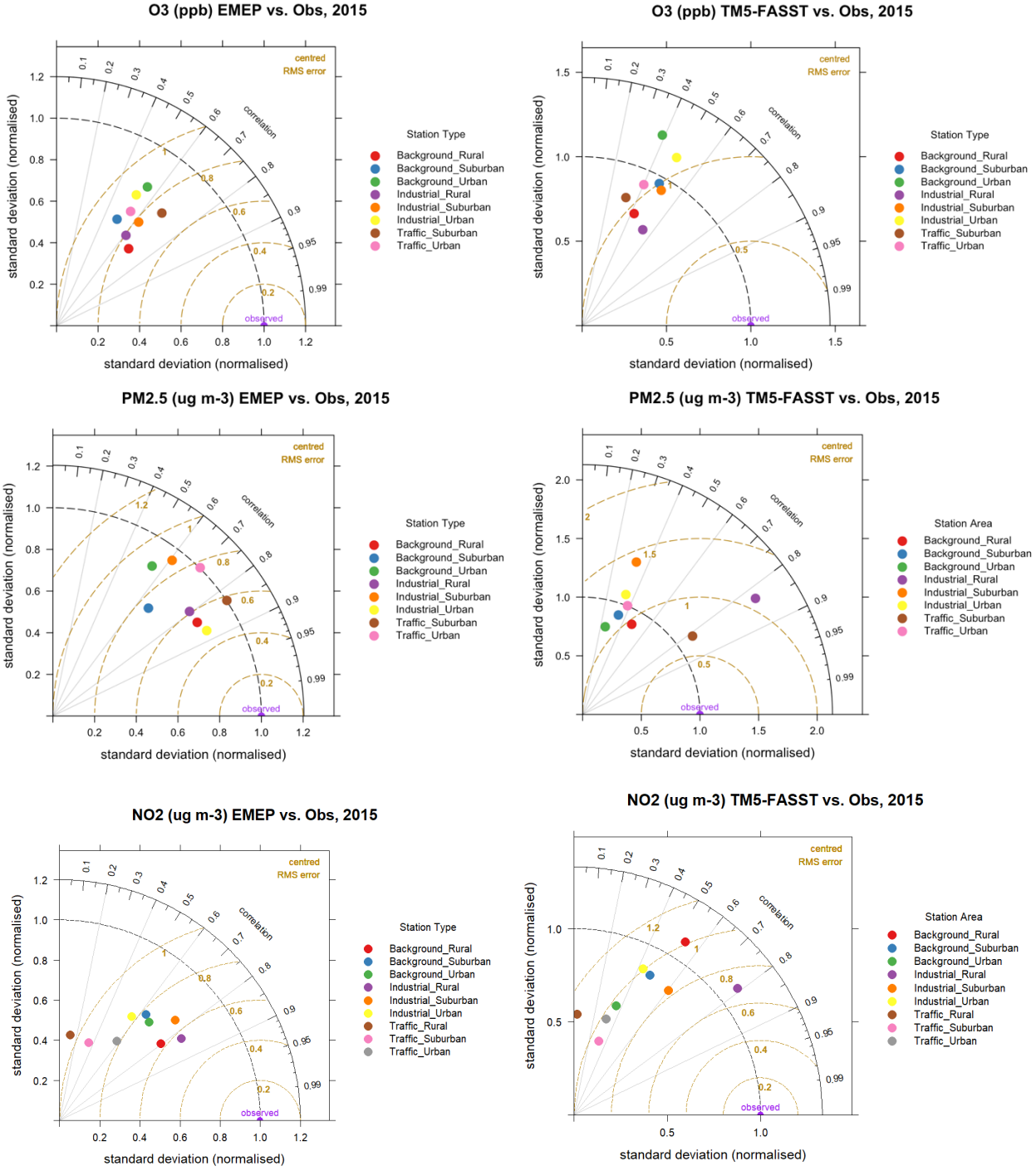

Figure 6: Taylor diagrams (Taylor et al., 2001) for the $P0_{Europe}$ (EMEP) and baseline simulation from the previous TM5-FASST model, for O_3, $PM_{2.5}$ and NO_2 concentrations simulated at different observation sampling points in Europe.

https://doi.org/10.5194/egusphere-2026-3188
Preprint. Discussion started: 2 July 2026

3.2 Validation of the reduced-form JRC-FASST

The FASST approach is based on perturbations with the assumption of linearity for the difference between scenario and reference emissions at different perturbation levels. A standard set of -20% emission perturbation simulations was performed for each source region and precursor (Table 3). This approach was extensively tested to verify the additivity of individual pollutants responses as an approximation for the response to combined precursor perturbations and the linearity of the emission responses for perturbations extending beyond the 20%. For further details, refer to Van Dingenen et al. (2018). In this study, a limited number of additional perturbations were performed in order to verify the assumption of the FASST approach with the new EMEP simulations. We repeated the linearity test of the emission responses for perturbations extending beyond 20% for a limited number of source regions, corresponding to the main emitters in different parts of the world: USA, Russia, China, India and Germany.

Following the same validation approach used for TM5-FASST model (Van Dingenen et al., 2018), in this section we discuss the linearity of the emission responses for perturbations extending beyond the 20% for O_3 and its health and crop exposure metrics (Sect. 3.2.1) and for $PM_{2.5}$ (Sect. 3.2.2).

An additional set of simulations was added for a reduced number of countries (USA, Russia, China, India and Germany) including perturbations of -80%, -50%, and +50%. These additional perturbations are used to validate the linearised reduced-form approach against the EMEP model, exploring chemical feedback mechanisms, and the extrapolation of the -20% response sensitivity towards larger emission perturbations. These two validations are particularly relevant for the NO_x-NMVOC-O_3 chemistry and the secondary $PM_{2.5}$ components (NO_3^- - NH_4^+ - SO_4^{2-}).

3.2.1 Linearity of ozone responses to precursor emissions

The additivity hypothesis in the FASST approach assumes that the O_3 response to combined NO_x and VOC perturbations can be approximated by the sum of the responses to the single component perturbations. This hypothesis was already verified for the FASST model based on TM5 CTM simulations at a coarse resolution. Most countries show a reverse response in O_3 concentrations to NO_x emission reduction due to O_3 titration by NO. On the other hand, just like in the TM5-FASST model, the linearised responses as a sum of the -20% individual precursor responses do not change the prevailing O_3 regime, thus the additivity hypothesis is not further tested here.

However, as shown by the TM5-FASST model, extending the O_3 linearised responses towards more extreme perturbation ranges is a challenge, as the individual perturbation of one of the precursors may change the O_3 formation regime. Figure 7 shows the O_3 response and exposure metrics to individual NO_x and NMVOC perturbations of -80%, -50%, -20%, and +50%. As expected, the response to NMVOC perturbations is near-linear and monotonically increases over the -80% to 50% range. The response to NO_x emissions is non-linear for the largest perturbations, which is in agreement with previous studies such as Xiao et al., (2010), Harrison et al., (2022), and Tian et al., (2025).

https://doi.org/10.5194/egusphere-2026-3188
Preprint. Discussion started: 2 July 2026

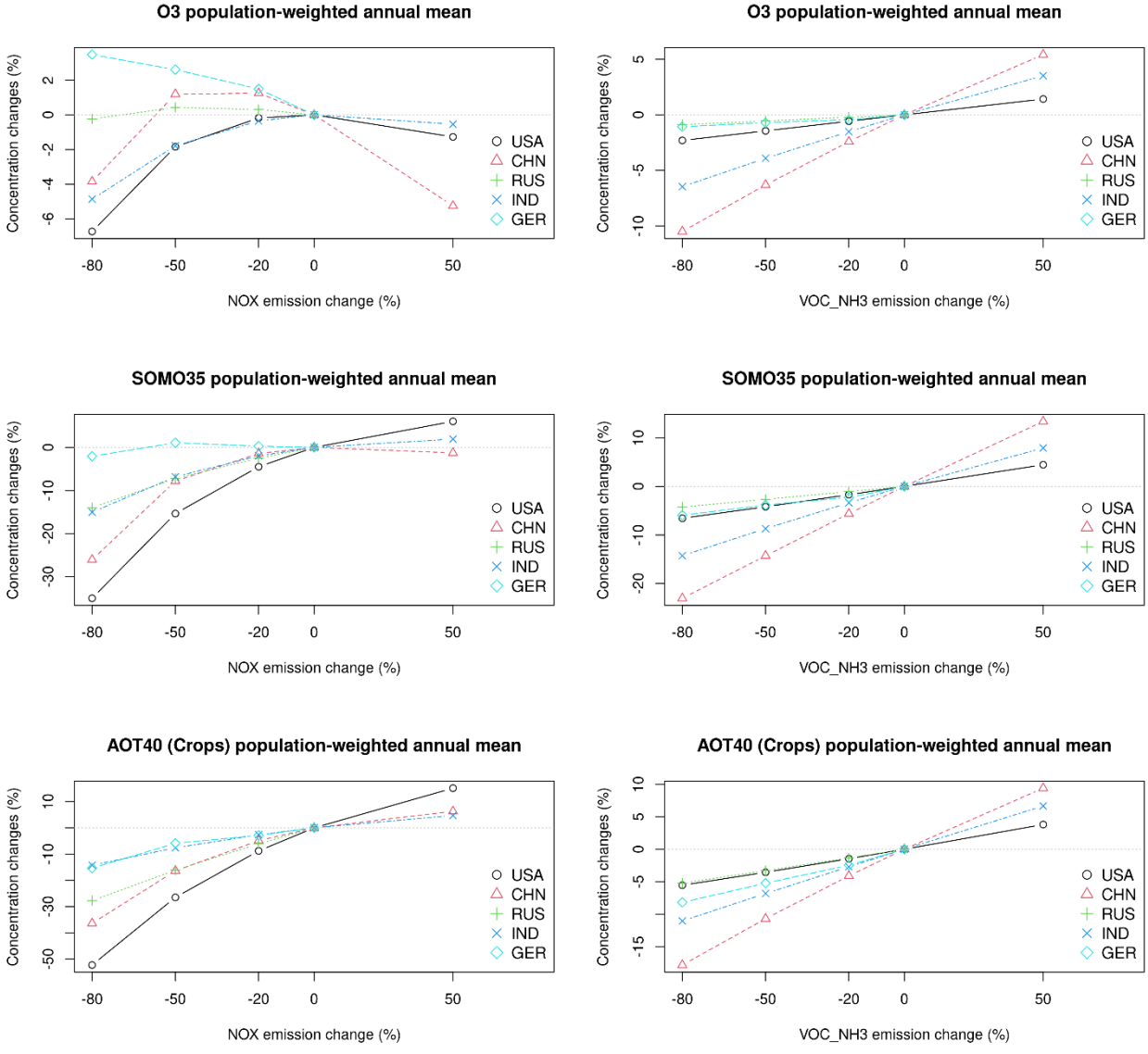

Figure 7: EMEP responses in population-weighted annual mean O_3, health exposure metric SOMO35, and AOT40 crop exposure metric as a function of precursors NO_x and NMVOC emission perturbation strength (USA: United States; CHN: China; RUS: Russian Federation; IND: India; GER: Germany).

However, O_3 annual mean is not used for the assessment of O_3 impacts on health, vegetation and crops. The responses of the health and crop O_3 impact metrics (SOMO35 and AOT40) to individual NO_x perturbations have opposite slopes compared to the O_3 concentration responses to perturbations of NO_x emissions. These metrics are mainly determined by summer O_3 concentrations, thus less sensitive to wintertime O_3 titration by high NO_x conditions, and for this reason behave more linearly and with opposite impact compared to the O_3 concentration response. The O_3 health impact metric, SOMO35, is the sum of O_3 means over 35 ppb, it behaves less linearly at larger perturbation ranges (above 50%), compared to the crop impact metrics,

https://doi.org/10.5194/egusphere-2026-3188
Preprint. Discussion started: 2 July 2026

AOT40. The FASST approach applied to EMEP model simulations shows more linear behaviour of the O_3 crop exposure metric AOT40 compared to the previous TM5-FASST version. However, this preliminary analysis over selected source regions indicates that the linearised approximation in JRC-FASST underestimates the O_3 metric response (SOMO35 and AOT40) to a high decrease of NOx emissions in particular in the USA and China, while for the other regions the linear approach is acceptable over the entire range of emission reduction. For the next phase version of JRC-FASST we envisage the development of a second-order correction on the ozone response to strong NOx emissions, based on additional perturbation runs (see Sect. 4).

3.2.2 Linearity of secondary inorganic $PM_{2.5}$ responses

Figure 8, Figure 9 and Figure 10 summarise the changes in country population-weighted means of fine particulate sulphate, nitrate, ammonium and total secondary inorganic aerosols (SIA) due to reductions in SO_2, NH_3 and NO_x emissions.

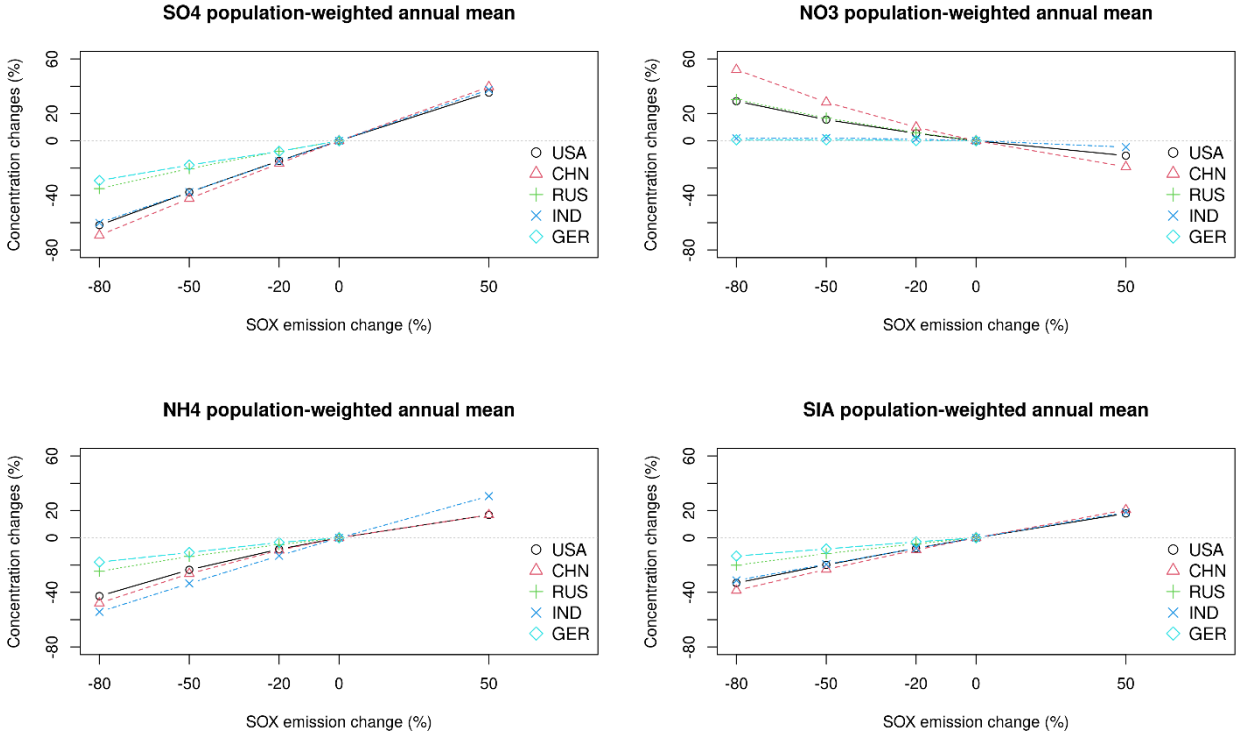

Figure 8: EMEP responses in population-weighted annual mean secondary inorganic aerosols in $PM_{2.5}$ (sulphate, SO_4^{2-}; nitrate, NO_3^-; ammonium, NH_4^+; total secondary inorganic aerosols, SIA) as a function of precursor SO_x emission perturbation strength (USA: United States; CHN: China; RUS: Russian Federation; IND: India; GER: Germany).

The changes in sulphate (SO_4^{2-}) concentrations are mainly driven by SO_2 emissions with large decreases in all countries. Sulphate concentrations slightly decrease with decreasing NH_3 emissions, due to lower sulphate neutralisation with ammonium, and is on average 25% of the sensitivity to SO_2 emission. The sensitivity of sulphate concentrations to NO_x

https://doi.org/10.5194/egusphere-2026-3188
Preprint. Discussion started: 2 July 2026

emissions is on average 7% and opposite sign of the sensitivity to SO_2 emissions. The sensitivity of nitrate (NO_3^-) concentrations to NH_3 and NO_x emission reductions is of the same order of magnitude, on average NH_3 emissions cause larger changes in NO_3^- concentrations than NO_x emissions by about 20%. The effect of SO_2 emissions on NO_3^- concentration is minor compared to the other precursors. The impacts of emission reductions on ammonium (NH_4^+) concentrations are in the same order of magnitude for the three precursors (SO_2, NO_x, and NH_3), with generally lower changes due to NO_x emissions.

The response of total sulphate, ammonium and nitrate to combined NO_x and SO_2 perturbation can be approximated by the sum of the responses to the individual perturbations, as shown by the previous TM5-FASST version (Figure 2 and S7.1 in Van Dingenen et al., 2018).

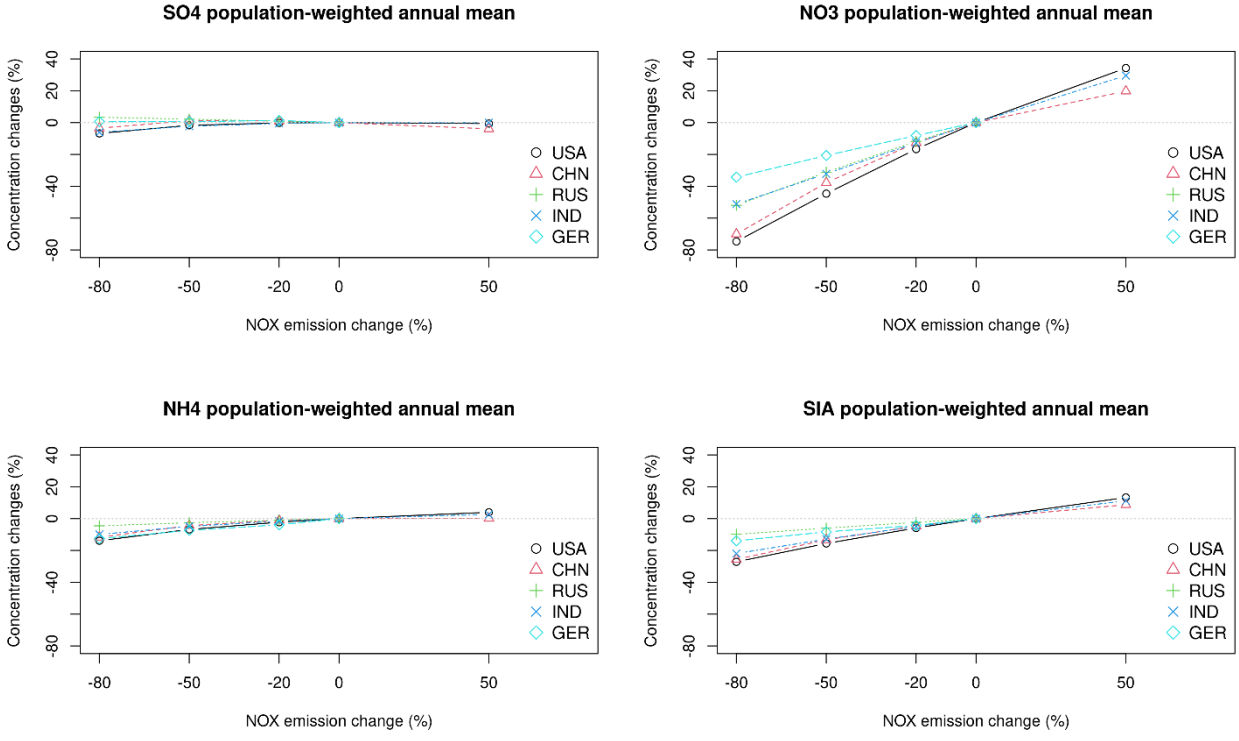

Figure 9: EMEP responses in population-weighted annual mean secondary inorganic aerosols in $PM_{2.5}$ (sulphate, SO_4^{2-}; nitrate, NO_3^-; ammonium, NH_4^+; total secondary inorganic aerosols, SIA) as a function of precursor NO_x emission perturbation strength (USA: United States; CHN: China; RUS: Russian Federation; IND: India; GER: Germany).

Total secondary inorganic aerosols (SIA) and their single components (SO_4^{2-}, NH_4^+, and NO_3^-) show a near-linear behaviour towards emission perturbations of SO_2 emissions between -20% and -80%. The responses of SIA to NO_x emissions show small deviations from linearity for perturbations above 50%, while more evident non-linear responses of ammonium and nitrate result from NH_3 perturbations above 50%, which agrees earlier studies by Clappier et al., (2021), Thunis et al., (2021) and Belis et al., (2021). The deviation from linearity in SIA responses towards NH_3 perturbations was also shown in the previous

https://doi.org/10.5194/egusphere-2026-3188
Preprint. Discussion started: 2 July 2026

FASST version based on TM5 simulations, more pronounced for NH_3 reduction at -80% than 100% increase (Figure 4c, Van Dingenen et al., 2018).

Figure 10 compares the -20% perturbation rate of VOC- NH3 emissions extrapolated to larger perturbation ranges with the EMEP model simulations. The concave-shaped scatter plots indicate a tendency of JRC-FASST to over predict secondary inorganic aerosols. This behaviour is more pronounced for extrapolations at -80% of emission perturbations of NO_x and NH_3, while the extrapolation at a rate of 50% behaves quite linearly. While the linearity and additivity of the combined SO_2 – NO_x perturbation was already tested in the TM5-FASST model, the combined NO_x – NH_3 perturbation was not investigated. The FASST approach applied to the EMEP simulations shows a slight over prediction for the combined NH_3 – NO_x perturbation, in the same range of the single NH_3 and NO_x perturbations. These values are comparable to the normalised bias found in TM5-FASST for Europe (Table 4 in Van Dingenen et al., 2018).

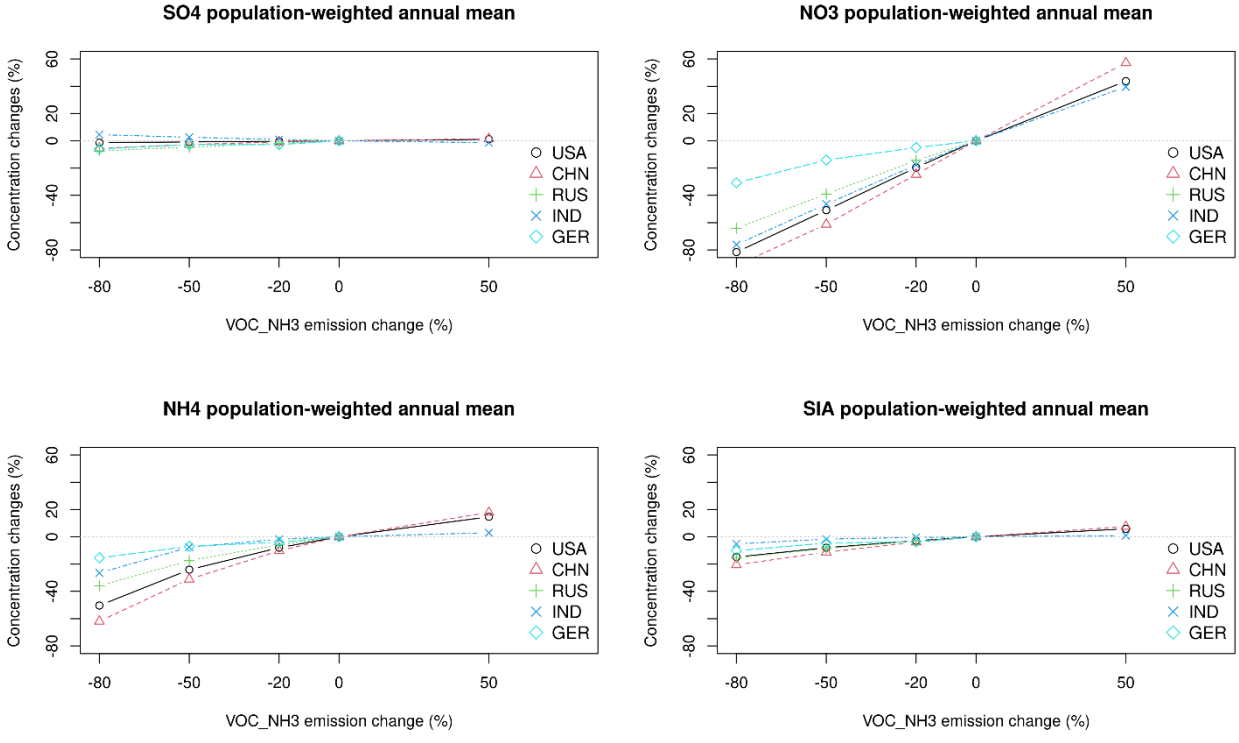

Figure 10: EMEP responses in population-weighted annual mean secondary inorganic aerosols in $PM_{2.5}$ (sulphate, SO_4^{2-}; nitrate, NO_3^-; ammonium, NH_4^+; total secondary inorganic aerosols, SIA) as a function of precursor NMVOC-NH_3 emission perturbation strength (USA: United States; CHN: China; RUS: Russian Federation; IND: India; GER: Germany).

3.2.3 Comparison between JRC-FASST and EMEP model and other approaches/models

The three graphics in Figure 11 present a country comparison of population-weighted annual mean concentrations of $PM_{2.5}$, O_3, and NO_2, as simulated by the JRC-FASST reduced-form model and by the full EMEP chemistry-transport model using EDGAR emissions for the year 2018. In each scatterplot, the population-weighted concentrations from the EMEP model are

https://doi.org/10.5194/egusphere-2026-3188
Preprint. Discussion started: 2 July 2026

placed on the horizontal axis, while those from JRC-FASST are shown on the vertical axis. A one-to-one reference line is included to indicate agreement between the two estimates, accompanied by a fitted regression line that reveals the degree to which the simplified model reproduces the full model behaviour.

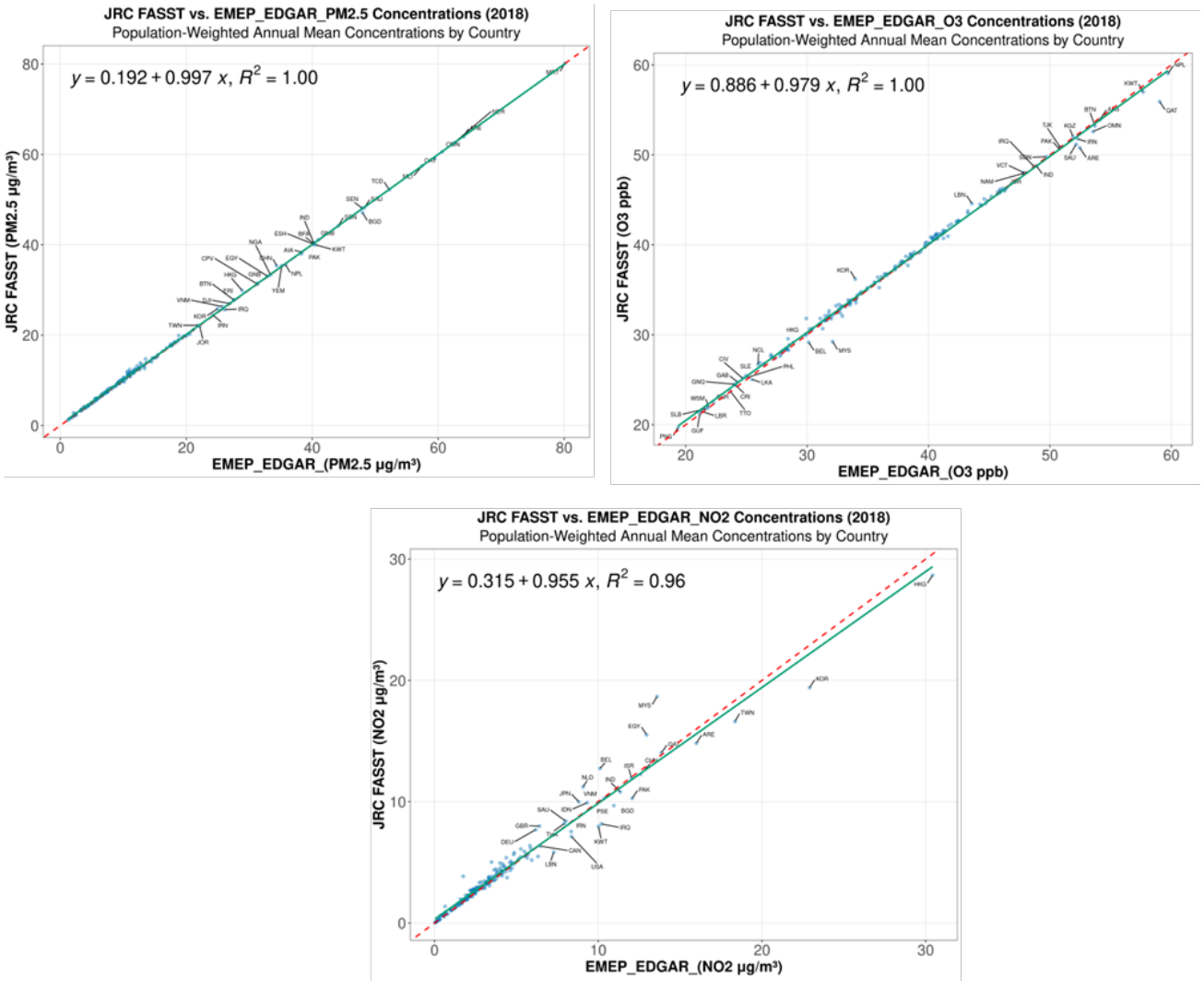

Figure 11: Comparison between simulated population-weighted concentrations of $PM_{2.5}$ (top left), O_3 (top right) and NO_2 (bottom), by the JRC-FASST model and the full EMEP simulation for EDGAR 8.1 emissions in 2018.

For O_3, the comparison demonstrates a close match between the two models. The data points form a narrow band along the 1:1 line, and the regression equation and coefficient of determination show nearly perfect correlation. While a few countries show small positive or negative deviations, these differences remain minor relative to the overall alignment. This result indicates that the reduced-form JRC-FASST approach captures the population-weighted distribution of ozone exposure with remarkable fidelity, despite the simplified formulation.

https://doi.org/10.5194/egusphere-2026-3188
Preprint. Discussion started: 2 July 2026

The depiction of nitrogen dioxide shows a slightly broader spread of country points but still reveals a strong and robust relationship between the two modelling systems. The regression line remains close to the 1:1 relationship, although a tendency appears for JRC-FASST to modestly underpredict NO_2 concentrations in countries with highest EMEP values. This behaviour is consistent with the more localised nature of NO_2 emissions, their steep concentration gradients caused by road traffic emissions and the short lifetime of NO_2, which are more challenging for reduced-form models to reproduce in detail. Nonetheless, the overall agreement confirms that JRC-FASST retains the key spatial and population-exposure characteristics of NO_2 at the country level.

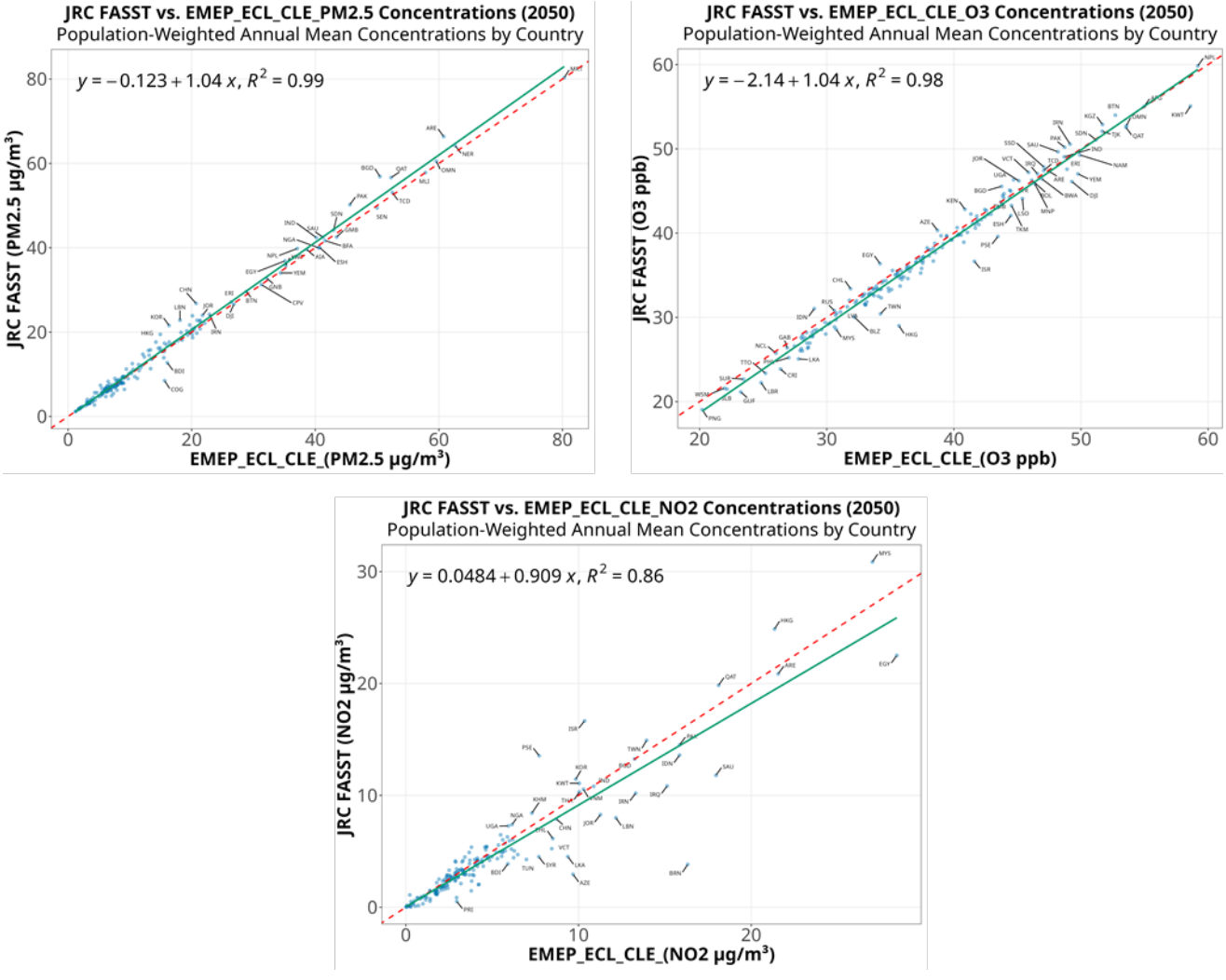

Figure 12: Comparison between simulated population-weighted concentrations of $PM_{2.5}$ (top left), O_3 (top right) and NO_2 (bottom), by the JRC-FASST model and the full EMEP simulation for ECLIPSE V6b CLE emissions in 2050.

A similar analysis to test the ability of the JRC-FASST reduced-form to reproduce population-weighted concentrations when changes in the emissions are significant compared to the base case was accomplished by comparing its output with the one of

https://doi.org/10.5194/egusphere-2026-3188
Preprint. Discussion started: 2 July 2026

the full EMEP model for two different Eclipse v6b scenarios in 2050: the CLE BASE and the MFR BASE (Figure 12 and Figure 13). In the CLE BASE the global emissions of $PM_{2.5}$, NO_x and SO_2 are –44%, -59% and -84% lower than 2015 values, respectively, while in the MFR BASE the reductions are even stronger reaching, -89%, -81% and -94%, respectively (Figure 14). Figure 12 and Figure 13 show a very good match between the two models for O_3 and $PM_{2.5}$ in both scenarios with very high coefficients of determination ($R^2 > 0.99$) and slopes close to the unity. The values corresponding to small countries or islands are those showing the highest differences. The dispersion around the regression line of NO_2 concentrations is higher than the previous pollutants leading to a lower but still satisfactory correlation between the models ($R^2 > 0.75$) and slopes within a 30% range around unity.

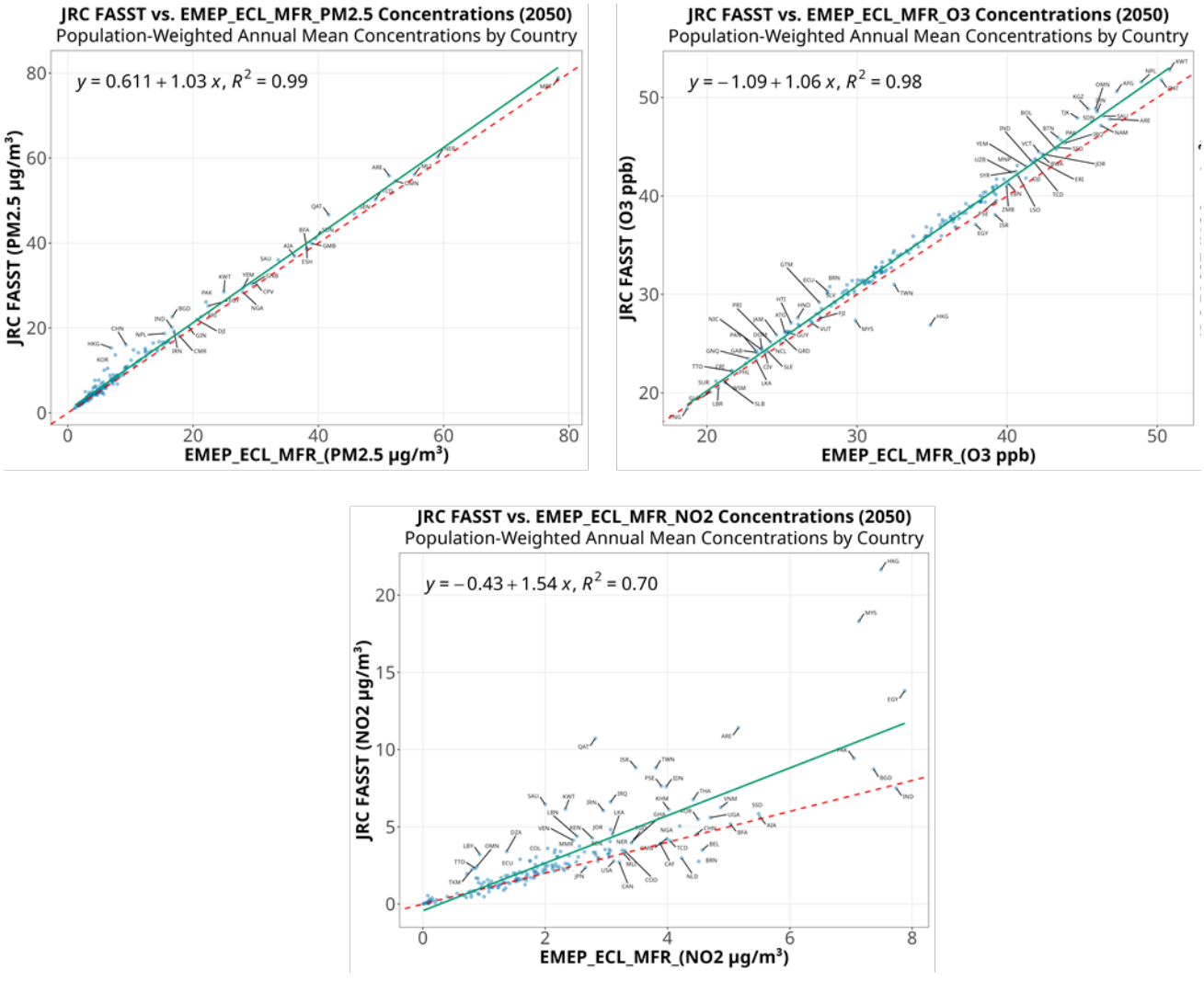

Figure 13: Comparison between simulated population-weighted concentrations of $PM_{2.5}$ (top left), O_3 (top right) and NO_2 (bottom), by the JRC-FASST model and the full EMEP simulation for ECLIPSE V6b MFR emissions in 2050.

https://doi.org/10.5194/egusphere-2026-3188
Preprint. Discussion started: 2 July 2026

The comparison of the JRC-FASST reduced-version model with the full EMEP runs demonstrate the ability of the adopted linearised approach to reproduce $PM_{2.5}$ and O_3 concentrations of the parent model within a range of 5% uncertainty even for considerable reductions of key precursors' emissions way above 80%. The tests show that the NO_2 responses estimated by JRC-FASST are comparable to the parent EMEP model for reductions not higher than 50%.

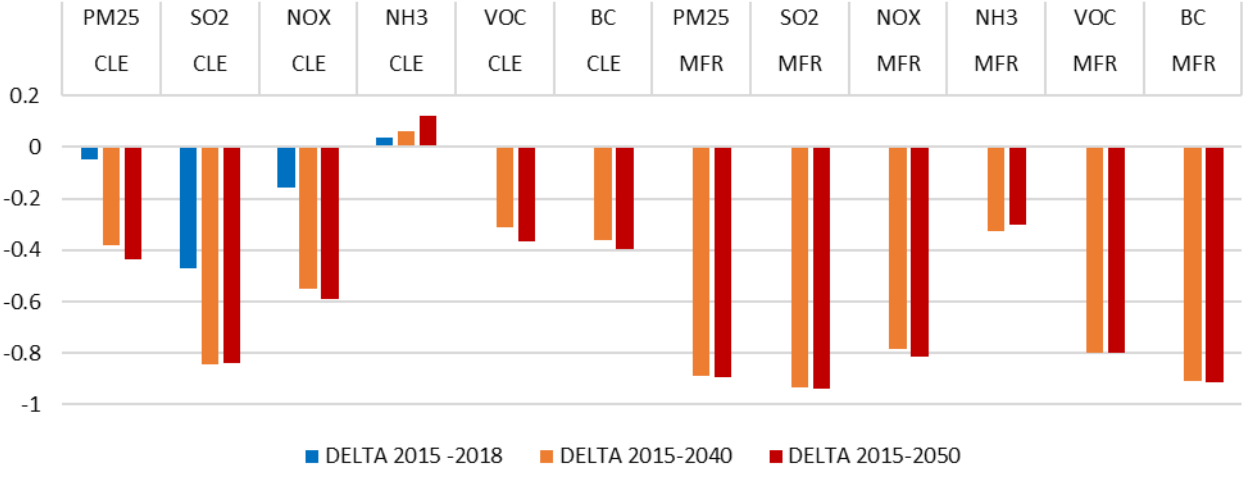

Figure 14: Global emission delta (%) between the EDGAR base case used to training JRC-FASST and the scenarios used for test with the full EMEP simulation: EDGAR 8.1 emissions in 2018, ECLIPSE V6b CLE emissions in 2050, and ECLIPSE V6b MFR emissions in 2050.

The comparison for $PM_{2.5}$ and O_3 shows a very good agreement in all the tests. The scatter points from almost all countries lie tightly along the diagonal, and the regression statistics indicate a close correspondence between the two models. This very close match holds across the entire concentration range, from low exposure to high exposure countries. The performance demonstrates that the simplified JRC-FASST representation is highly effective in capturing national level $PM_{2.5}$ population exposure, reflecting the relatively broad spatial patterns of fine particulate pollution and the strong linearity in its response functions compared to the full EMEP model. The NO_2 concentrations which are comparable in all countries for small emission variations are sensitive to the intensity of emission reductions particularly in regions where NO_x emissions increase by a factor of 2 or 3 (e.g. AZE, MYS) which is beyond the scope of the tool.

Taken together, the three graphics illustrate that the JRC-FASST reduced-form model reproduces population-weighted concentrations from the full EMEP model with bias below 5% for $PM_{2.5}$ and O_3, and below 50% for NO_2. The agreement is strongest for ozone and $PM_{2.5}$, for which correlations approach unity, and remains very good for NO_2 despite the inherently more localised nature of this pollutant.

3.3 Impacts on population-weighted and area-weighted exposure: O_3 exposure and metrics

In this section we analyse how the NO_x and VOC emission perturbations impact the O_3 and SOMO35 (health exposure metric) in some of the main source regions.

https://doi.org/10.5194/egusphere-2026-3188
Preprint. Discussion started: 2 July 2026

Figure A4 in Appendix A illustrates the spatial changes in annual mean ozone (O_3) concentrations resulting from a 20% reduction in anthropogenic NO_x emissions within four major source regions: China, India, the United States, and Europe (EU27, Norway, Switzerland, and the United Kingdom). Each panel presents the modelled O_3 response to the country emission perturbation, highlighting both the magnitude and geographical distribution of the resulting concentration changes.

Across all regions, the patterns reflect the non-linear and regime-dependent chemistry governing O_3 formation. In China and parts of northern India, reductions in NO_x emissions tend to increase O_3 concentrations, particularly in densely populated and high emission regions, consistent with NO_x saturated photochemical environments where lower NO_x levels reduce titration and promote net O_3 formation. The positive O_3 responses in these areas are spatially extensive and can exceed 2 ppb. In contrast, more remote and rural regions generally exhibit decreases in O_3, indicating local transitions toward NO_x limited conditions.

In the United States, the O_3 response shows a more balanced mixture of increases and decreases, reflecting the regional variability of chemical regimes. Urban areas, especially in the eastern and western United States, exhibit slight O_3 increases, whereas many rural and downwind areas show modest reductions.

For Europe, a predominantly positive O_3 response is observed over central and western regions, such as the Benelux, the Po valley in Italy and the main European cities again indicating the prevalence of NO_x saturated conditions in urbanised emission hotspots. Surrounding areas show small O_3 decreases that demonstrate the spatially coupled nature of O_3 production and loss processes.

Overall, the figure highlights the substantial regional heterogeneity in O_3 sensitivity to NO_x emission reductions, emphasising the importance of chemical regime diagnostics when designing effective O_3 mitigation strategies.

Figure 15 summarizes, at the country level, the population-weighted ozone (O_3) responses shown spatially in the previous figure. While the earlier maps illustrate the detailed geographic patterns of O_3 changes, the current figure condenses those spatial effects into national averages for a selected set of countries. Together, the two figures provide a complementary view of the same phenomenon: the maps reveal where O_3 increases or decreases occur within each source region, and the bar chart quantifies how population exposure changes at the country scale.

The ranking shown in the bar chart reflects the dominant chemical regimes highlighted in the previous spatial maps. Countries such as Germany and China show the largest positive population-weighted O_3 responses, consistent with the strong O_3 increases identified over major urban and industrial regions in the corresponding maps, where NO_x saturated conditions lead to reduced O_x titration and net formation of O_3 after NO_x emission cuts. Intermediate responses in countries like Italy and Poland likewise mirror the mixed spatial patterns seen in their respective European or Asian source region panels.

Conversely, countries with smaller or negative population-weighted responses—such as Brazil, India, Indonesia, and especially Nigeria—correspond well to areas where NO_x reductions produced widespread O_3 decreases, characteristic of NO_x limited photochemical environments. India's slight negative value in the bar chart matches the heterogeneous mixture of increases and decreases observed in the Indian subcontinent map, where only highly polluted northern regions experience O_3 increases, while most rural areas show decreases.

https://doi.org/10.5194/egusphere-2026-3188
Preprint. Discussion started: 2 July 2026

By integrating the detailed spatial results into aggregated national metrics, this plot highlights how the chemical regime structure visible in the previous figure translates into net population exposure impacts. Together, the two figures demonstrate that the same emission reduction can lead to opposite O_3 outcomes across different regions, and they emphasize the importance of interpreting spatial O_3 responses in conjunction with population distribution to assess real-world exposure impacts.

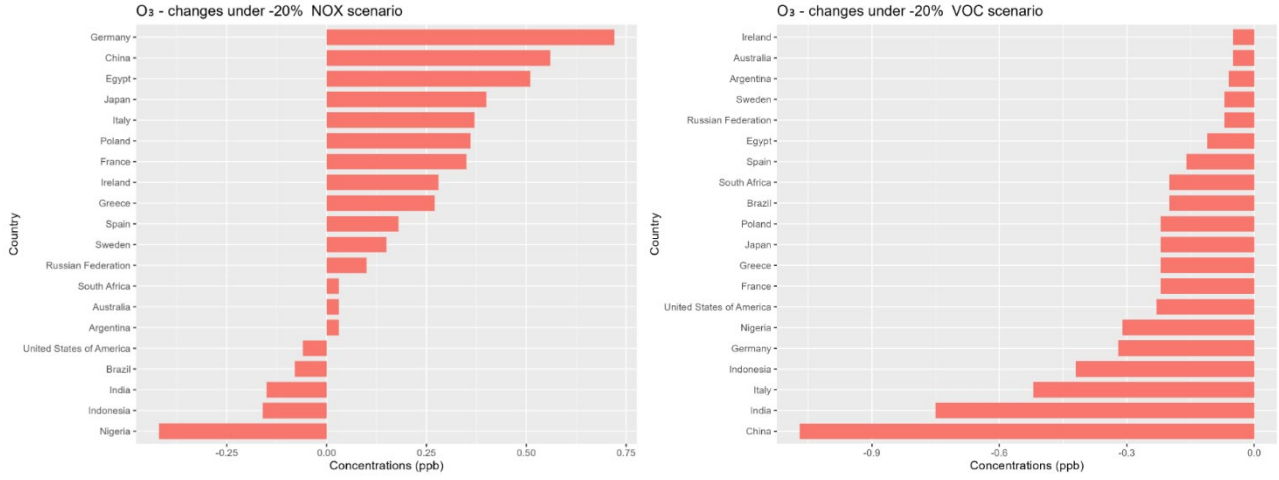

Figure 15: Change in population-weighted ozone (O_3) concentrations for a selected set of countries in response to a 20% reduction in national NO_x emissions (left) and NMVOC emissions (right). For European countries, the perturbation corresponds to a coordinated 20% reduction across the entire European region (EU-27, Norway, Switzerland, and the United Kingdom).

In contrast to the NO_x reduction scenario, the NMVOC emission perturbations show a much more uniform tendency toward O_3 decreases, consistent with the VOC limited conditions prevalent in urban and industrial regions (Figure A5, Appendix A). In China, strong O_3 reductions appear across major population and industrial centres, extending throughout the North China Plain and surrounding provinces. These decreases often reach more than −2 ppb and cover large spatial areas. A similar pattern is seen in India, where the Indo-Gangetic Plain exhibits the most pronounced reductions, again reflecting VOC limitation in densely populated and emission rich regions. In the United States and Europe, the O_3 response is more moderate but still dominated by decreases over the eastern and central parts of the United States and western and central European emission.

The country level bar chart in Figure 15 aggregates these spatial changes into national average population-weighted O_3 responses. The results contrast sharply with the previous NO_x reduction summary, the VOC reduction scenario yields exclusively negative population-weighted O_3 changes across all countries shown. In Europe, countries such as Germany and Italy show the largest reductions in population-weighted O_3. Similarly, the substantial O_3 decreases over northern India and eastern China seen in the maps translate into significant benefits in these countries. The United States shows a smaller but still clearly negative population-weighted response, reflecting the more moderate spatial reductions observed in its domain.

Figure A6 in Appendix A and Figure 16 show the same maps and plots for the six-month maximum cumulative exceedance of 35 ppb (SOMO35), therefore emphasizing the warm season when photochemistry is strongest. SOMO35 is more representative of summer O_3 than the annual mean. Under summertime conditions, many populated regions shift toward VOC

https://doi.org/10.5194/egusphere-2026-3188
Preprint. Discussion started: 2 July 2026

limited or transitional chemistry, so a 20% NO_x reduction typically reduces photochemical O_3 production and, crucially, also diminishes fresh NO titration effects that otherwise depress O_3 mainly in winter or at night. As a result, the SOMO35 response is predominantly negative across broad regions in the NO_x reduction scenario, in contrast to the mixed-sign changes seen in annual means. The few remaining positive hotspots—visible over the urban/industrial areas—are consistent with strongly NO_x saturated environments, where cutting NO_x can initially lessen titration and shift peroxide radical partitioning in ways that locally increase O_3 during peak episodes. Overall, the maps show that once the metric focuses on the photochemically active months and on exceedances most relevant for health, NO_x controls yield widespread SOMO35 decreases, with increases confined to limited, very high emission cores.

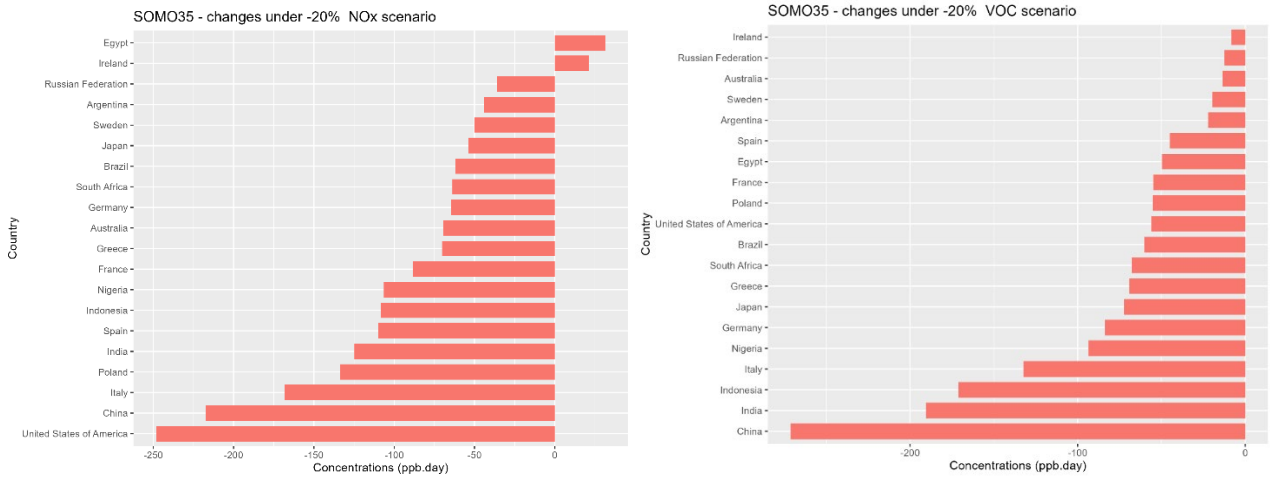

Figure 16: Change in population-weighted SOMO35 for a selected set of countries in response to a 20% reduction in national NO_x emissions (left) and NMVOC emissions (right). For European countries, the perturbation corresponds to a coordinated 20% reduction in NO_x emissions across the entire European region (EU-27, Norway, Switzerland, and the United Kingdom).

The spatial maps for China, India, the United States, and Europe show widespread decreases in SOMO35 due to NMVOC emission reductions (Figure A7, Appendix A). These reductions reflect the strong suppression of peak O_3 production when NMVOC availability is constrained under summertime conditions. The population-weighted SOMO35 responses to a 20% reduction in national NMVOC emissions show a consistently negative pattern across all selected countries (Figure 16). The largest decreases occur in China and India, followed by Indonesia, Italy, Nigeria. Most European countries and the United States also experience moderate reductions, while only a few countries—such as Ireland, the Russian Federation, Australia, and Sweden—show very small or negligible changes. Reducing NOx emissions lead to (a non-linear increase) in ozone concentrations over urban areas, while reducing NMVOC lead to a nearly linear reduction in ozone. The differences in NMVOC/NOx ratios highlight the importance of emitted precursors since these lead to changes in chemical regimes, directly affecting the responses of O_3 concentrations to emission reductions (De Meij et al., 2024).

https://doi.org/10.5194/egusphere-2026-3188
Preprint. Discussion started: 2 July 2026

3.4 Impacts on population-weighted and area-weighted exposure: NO_2 exposure and metrics

Figure A8 in Appendix A shows the spatial patterns in annual mean NO_2 concentrations across four source regions following a 20% reduction in NO_x emissions. Substantial decreases are shown in all regions. The strongest reductions occur in and around major urban and industrial centres—such as the North China Plain, the Indo-Gangetic Plain, the eastern United States and main cities, central Europe and the main inhabited and industrial regions —reflecting the highly localized nature of NO_2 and its strong coupling to NO_x emissions. Outside these hotspots, decreases extend more broadly but with lower magnitude, consistent with rapid chemical transformation and shorter atmospheric lifetime of NO_2. Overall, the maps demonstrate that NO_x emission controls lead to widespread and pronounced improvements in NO_2 air quality, with the largest benefits concentrated in densely populated, high-emission regions.

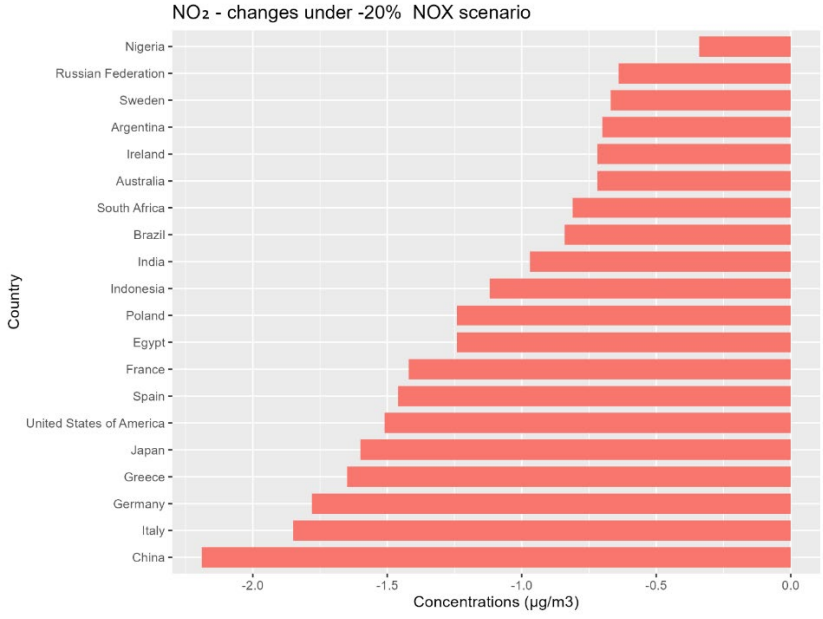

Figure 17: Change in population-weighted NO_2 concentrations for a selected set of countries in response to a 20% reduction in national NO_x emissions. For European countries, the perturbation corresponds to a coordinated 20% reduction in NO_x emissions across the entire European region (EU-27, Norway, Switzerland, and the United Kingdom).

Consequently, Figure 17 shows that population-weighted NO_2 concentrations decrease consistently across all countries following a 20% reduction in national NO_x emissions. The largest reductions occur in China, Italy, Germany, Greece, and Japan, reflecting their high baseline NO_2 levels and dense emission sources. Most other countries—including the United States, Spain, France, Egypt, and Poland—also experience substantial declines, although of smaller magnitude. Overall, the results confirm that NO_x reductions lead to widespread improvements in population-weighted NO_2 exposure, with the greatest benefits occurring in regions with intensive anthropogenic emissions and large urban populations.

https://doi.org/10.5194/egusphere-2026-3188
Preprint. Discussion started: 2 July 2026

3.5 Impacts on population-weighted exposure: $PM_{2.5}$ (primary and secondary inorganic sources)

Figure A9 in Appendix A shows that a 20% reduction in primary $PM_{2.5}$ emissions leads to substantial decreases in annual mean $PM_{2.5}$ concentrations across all four source regions, with the largest reductions occurring directly over major urban and industrial emission hotspots. In China and India, densely populated regions such as the North China Plain and the Indo-Gangetic Plain exhibit decreases often exceeding 3–5 µg/m³, reflecting the strong contribution of primary emissions to local particulate pollution. In the United States and Europe, reductions are more moderate but remain spatially widespread, particularly around large metropolitan areas and industrial regions. Overall, the maps highlight the highly localised and near source nature of primary $PM_{2.5}$, with emission controls producing clear and immediate air quality benefits concentrated in regions with high baseline emissions.

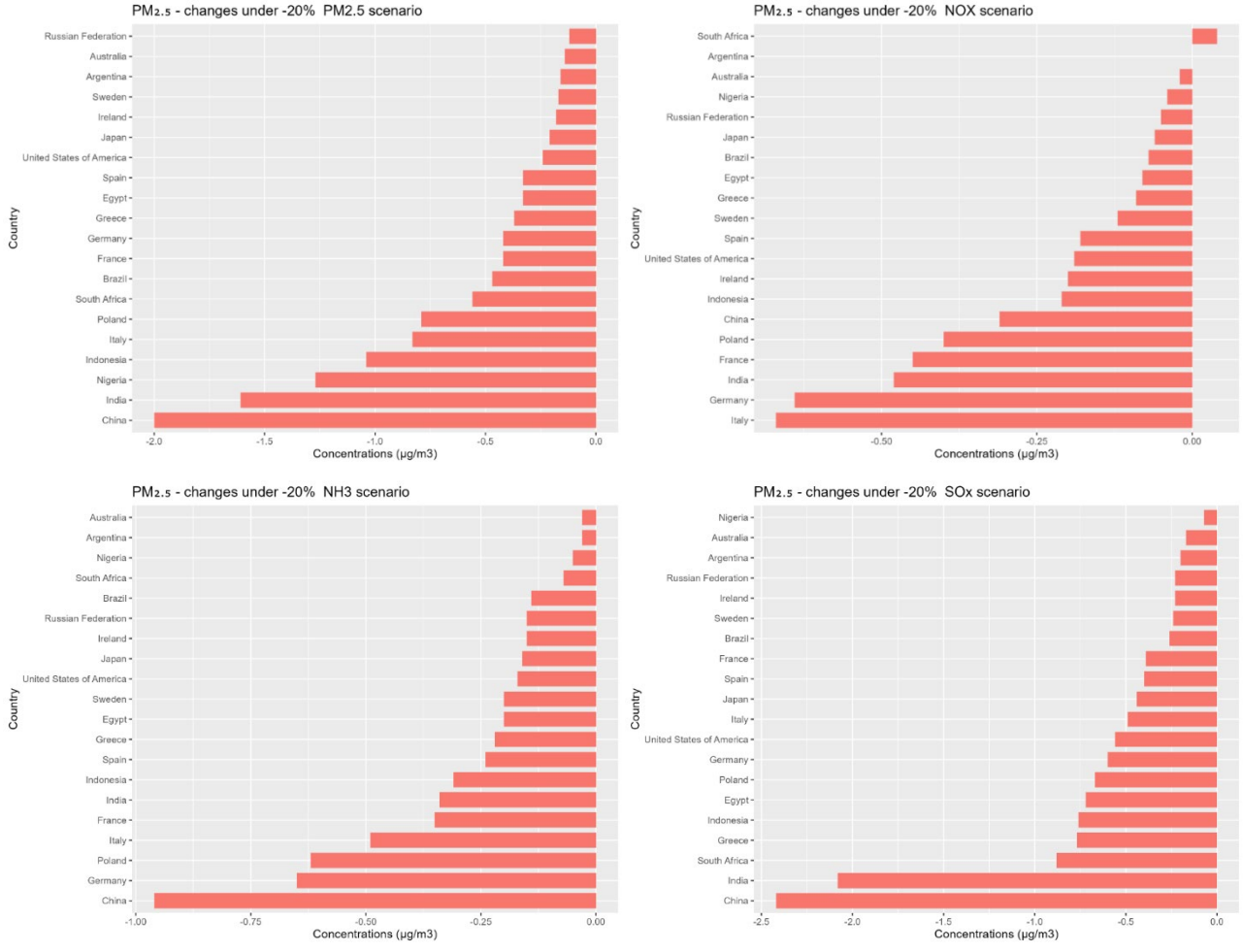

Figure 18: Change in population-weighted $PM_{2.5}$ concentrations for a selected set of countries in response to a 20% reduction in national primary $PM_{2.5}$ emissions (top left), NOx emissions (top right), NH_3 emissions (bottom left) and SOx emissions (bottom right). For European countries, the perturbation corresponds to a coordinated 20% reduction in primary $PM_{2.5}$ emissions across the entire European region (EU-27, Norway, Switzerland, and the United Kingdom).

https://doi.org/10.5194/egusphere-2026-3188
Preprint. Discussion started: 2 July 2026

Figure 18 shows that a 20% reduction in primary $PM_{2.5}$ emissions leads to consistent decreases in population-weighted $PM_{2.5}$ concentrations across all countries included in the analysis. The largest benefits occur in China and India, reflecting their high primary emission sources and large exposed populations. Large reductions are also observed in countries such as Nigeria, Indonesia, Italy, Poland, and South Africa, while countries with lower baseline primary $PM_{2.5}$ emissions—such as Sweden, Ireland, Australia, and the Russian Federation—experience comparatively smaller improvements. Overall, the results demonstrate that primary $PM_{2.5}$ emission controls yield widespread population level air quality benefits, with the magnitude of improvement closely tied to both the initial emission burden and the population distribution within each country.

$PM_{2.5}$ concentrations arise not only from direct primary emissions but also, and very substantially, from the formation of secondary inorganic aerosols (SIA), which depend on emissions of NO_x, NH_3, and SO_x. These precursors interact nonlinearly through atmospheric chemistry to form ammonium nitrate and ammonium sulphate, and the maps (Figure A10, Figure A11 and Figure A12 in Appendix A) and bar charts (Figure 18) clearly highlight the distinct role of each precursor. While reducing primary $PM_{2.5}$ emissions leads to large and highly localised improvements directly over emission hotspots, the effects of precursor reductions are more spatially diffuse and often larger in magnitude when summed across extensive populated areas. NO_x reductions show mixed effects because lowering NO_x decreases the availability of nitric acid for nitrate aerosol formation but simultaneously reduces oxidants, occasionally leading to compensating increases or decreases depending on regional chemical conditions. This yields $PM_{2.5}$ reductions in many areas (e.g., India, Europe, the Eastern U.S.) but also localised increases in some NO_x-saturated urban regions, mainly visible in China and one hotspot in India (Figure S10). The population-weighted results remain consistently negative across most countries (Figure 18), $PM_{2.5}$ reductions below -0.5 $\mu g/m^3$ only in Italy and Germany, though the magnitude tends to be smaller than for SO_x or NH_3, reflecting the more complex and regime-dependent influence of NO_x on SIA formation.

In contrast, NH_3 reductions produce clear and widespread decreases in $PM_{2.5}$ across all source regions. Because ammonium nitrate and ammonium sulphate formation is in the majority of cases NH_3 limited, especially in Europe, China, and parts of India, reducing NH_3 leads to substantial declines in secondary $PM_{2.5}$. The maps show strong reductions in agricultural regions and their downwind urban areas (Figure A11, Appendix A), and the population-weighted bar chart (Figure 18) confirms that NH_3 control is often more effective than NO_x control for reducing total $PM_{2.5}$ exposure. $PM_{2.5}$ reductions between -1 $\mu g/m^3$ and -0.5 $\mu g/m^3$ are estimated in China, Germany, Poland and Italy.

SO_x reductions produce the largest and most robust decreases in $PM_{2.5}$ among all precursor controls, especially in regions where sulphate constitutes a major fraction of total $PM_{2.5}$. Because ammonium sulphate formation is strongly tied to SO_2 oxidation, cutting SO_x emissions sharply suppresses sulphate aerosol, leading to large reductions over the eastern U.S., Europe, India, and China (Figure A12, Appendix A). The population-weighted reductions are consistently substantial, often exceeding those of primary $PM_{2.5}$ emission cuts. This underscores the continued importance of SO_2 controls for regions where coal combustion and industrial activities remain significant. Reductions above -2 $\mu g/m^3$ are found in China and India, moderate reductions, between -1 $\mu g/m^3$ and -0.5 $\mu g/m^3$ are found in South Africa, Greece, Indonesia, Egypt, Poland, Germany and the United States (Figure 18).

https://doi.org/10.5194/egusphere-2026-3188
Preprint. Discussion started: 2 July 2026

When compared to primary $PM_{2.5}$ reductions, which show clear, highly localised benefits, the reductions in secondary aerosol precursors generate broader regional improvements that extend far downwind of the emission sources. In several countries—especially in Europe, China, and India—reductions in NH_3 or SO_x yield equal or greater population-weighted $PM_{2.5}$ decreases than the primary $PM_{2.5}$ scenario, demonstrating that secondary aerosol formation is a significant driver of total $PM_{2.5}$ exposure. Overall, the results highlight that effective $PM_{2.5}$ mitigation requires a combination of strategies: reducing primary emissions to address local hotspots, and controlling precursor emissions (NO_x, NH_3, SO_x) to suppress secondary aerosol formation that affects population exposure at a broader regional scale.

4 Conclusions and way forward

In this study we present the global reduced form air quality assessment model JRC-FASST, an updated version of the TM5-FASST model, built from EMEP full CTM simulations at 0.5° × 0.5° globally and 0.1° × 0.1° over Europe and driven by EDGAR v5.0 (2015) emissions. Overall, the new JRC-FASST represents a significant methodological and technical advancement, integrating modern CTM capabilities, updated emissions, and higher spatial resolution to deliver a global reduced-form model better suited for policy screening, air quality planning, health and crop impact assessment at national and subnational scales.

Relative to the TM5 based predecessor, EMEP based JRC-FASST offers a finer representation of pollutant concentration gradients, a much expanded and more granular set of source regions (76 compared to 56 globally; 41 individual European countries compared to 6), and a broader portfolio of pollutant metrics, including detailed PM speciation, nitrogen oxides, and multiple ozone indicators for health and crops. These advances directly translate into more realistic estimates of population and area weighted exposure and improved support for policy screening at national and sub national scales.

Baseline evaluation indicates that EMEP captures the continental scale patterns of pollutants and significantly improves the performance over Europe compared with the earlier TM5 baseline, particularly for $PM_{2.5}$ (RMSE drop 0.02 - 2.99), NO_2 (RMSE drop 0.24 - 1.25) where higher resolution is most impactful and also for O_3 (RMSE drop 1.73 - 7.23). While remaining biases exist — especially for localised NO_2 in densely populated urban centres — the EMEP population-weighted national exposures that underpin JRC-FASST are reproduced with high level of detail compared to observations (centred RMSE 0.7 to 0.9, 0.5 to 0.9 and 0.5 to 1.1 for O_3, $PM_{2.5}$ and NO_2, respectively.

The comparison of the JRC-FASST reduced-form model with the source EMEP CTM runs demonstrates the ability of the adopted linearised approach to reproduce $PM_{2.5}$ and O_3 concentrations of the parent model at the country level within a range of 5% uncertainty even for considerable reductions of key precursors' emissions way above 80%. The tests show that the NO_2 responses estimated by JRC-FASST are comparable to the parent EMEP model for reductions not higher than 50%.

A comparison of JRC-FASST with another global air quality model based on source-receptor relationships (GNAQPMS-SM, Ye et al., 2021) shows similar global average concentrations for O_3, NO_2 and $PM_{2.5}$ in 2018 (37 ppb vs 32.ppb, 4.1 $\mu g/m^3$ vs 3.6 $\mu g/m^3$ and 14.3 $\mu g/m^3$ vs 18.5 $\mu g/m^3$, respectively). However, the comparison between emulators is of little added value,

https://doi.org/10.5194/egusphere-2026-3188
Preprint. Discussion started: 2 July 2026

firstly because this kind of models are designed to reproduce the results of a full CTM, which is the reference and, secondly, because there are many methodological aspects that may affect the results (e.g. emission inventory, meteorological variability, reference year, spatial resolution, number of source regions).The scenario (-20% emission perturbations) analysis confirms and highlights well known priorities. For O_3, reducing VOCs consistently lowers exposure across regions (delta range in 20 selected countries -0.05 ppb to -1.2 ppb), whereas the effect of NO_x reductions is regime dependent in annual means (delta range in 20 selected countries -0.4 ppb to +0.7 ppb) but becomes predominantly beneficial for SOMO35 during the warm season (delta range in 20 selected countries -250 ppb.day to +30 ppb.day). For $PM_{2.5}$, controls on SO_x and NH_3 deliver the largest and most robust population-weighted reductions across many countries (delta range in 20 selected countries -0.1 µg/m^3 to -2.4 µg/m^3 and -0.5 µg/m^3 to -0.9 µg/m^3, respectively), often exceeding the benefits of primary $PM_{2.5}$ controls when averaged nationally; NO_x controls can contribute but show mixed effects where nitrate formation is oxidant limited or NO_x saturated (delta range in 20 selected countries +0.05 µg/m^3 to -0.65 µg/m^3). Together, these results confirm the need for integrated strategies that combine primary PM controls in hotspots with precursor controls (SO_x, NH_3, and context dependent NO_x/VOC) to suppress secondary aerosol and ozone formation at regional scales.

Reduced form model validation confirms that the linearity assumption underpinning the FASST approach remains appropriate over the intended perturbation range. O_3 concentration responses to VOC emission reductions are near linear while their responses to NO_x emission reduction become non-linear at large perturbations, consistent with chemical regime changes. However, the responses of the health and crop O_3 impact metrics (SOMO35 and AOT40) to individual NO_x perturbations behave more linearly compared to the O_3 concentration responses. Secondary inorganic aerosols concentrations respond nearly linearly to SO_2 reductions while showing stronger non-linearity under large NH_3 changes. Extrapolation of −20% sensitivities beyond ~±50% can introduce a modest over prediction in SIA reductions, underscoring that JRC-FASST is best suited for screening and policy exploration rather than as a substitute for full CTM analysis of very large perturbations.

A preliminary analysis of dedicated EMEP runs over selected source regions applying stronger NO_x emission perturbations beyond 20%, indicates that the linearised approximation in JRC-FASST may underestimate the O_3 concentration response for decreasing NO_x emissions in particular in the USA and China, while for the other regions the linear approach is acceptable. In a next version of the reduced-form model we envisage the development of a second-order correction on the ozone response to strong NO_x emissions, based on additional perturbation runs.

This work represents the first step toward the full development of the JRC-FASST model. The current version establishes the methodological foundation—high-resolution EMEP-based source–receptor relationships, updated emissions, and an expanded set of pollutant metrics—while the model is envisioned as a continuously evolving platform. New modules, improved parameterisations, and additional diagnostics will be progressively integrated to enhance its scientific robustness, policy relevance, and compatibility with emerging datasets. Future developments already identified include the incorporation of nitrogen and sulphur deposition module, enabling the representation of long-lived ozone formation pathways; the addition of radiative forcing calculations for short-lived climate forcers to support climate–air-quality co-assessment; and further refinement of non-linearity corrections, particularly for ozone and secondary aerosol chemistry. Extensions to the

https://doi.org/10.5194/egusphere-2026-3188
Preprint. Discussion started: 2 July 2026

health-impact module, including the use of hourly metrics and updated exposure–response functions, as well as the inclusion of additional vegetation and crop indicators derived from EMEP's hourly ozone output, are also planned. Altogether, these steps will ensure that JRC-FASST remains a living, up-to-date modelling framework capable of supporting a wide range of scientific and policy applications.

https://doi.org/10.5194/egusphere-2026-3188
Preprint. Discussion started: 2 July 2026

Appendix A

Table A1: List of relevant metrics simulated by the EMEP model and available in the JRC-FASST simulations.

Short name	Description	Units
	Surface Concentrations (gases)	
SURF_ppb_O3	O_3	ppb
SURF_ppb_NO	NO	ppb
SURF_ug_NO	NO	µg/m^3
SURF_ppb_NO2	NO_2	ppb
SURF_ug_NO2	NO_2	µg/m^3
SURF_ppb_SO2	SO_2	ppb
SURF_ug_SO2	SO_2	µg/m^3
SURF_ppbC_VOC	VOC	ppb
SURF_ppb_HNO3	HNO_3	ppb
SURF_ug_HNO3	HNO_3	µg/m^3
SURF_ppb_NH_3	NH_3	ppb
SURF_ug_NH_3	NH_3	µg/m^3
SURF_ppb_HCHO	HCHO	ppb
SURF_ppb_CO	CO	ppb
	Surface concentrations (aerosols)	
SURF_ug_PM10	PM_{10} dry	µg/m^3
SURF_ug_PM10_rh50	PM_{10} with particle water at 50% relative humidity	µg/m^3
SURF_ug_PM25	$PM_{2.5}$ dry includes fine PM and 27% of coarse NO_3^-	µg/m^3
SURF_ug_PM25_rh50	PM_{10} with particle water at 50% relative humidity	µg/m^3
SURF_ug_PM25X	$PM_{2.5}$ dry includesfinePMand27%ofcoarse NO_3^--, EC and OM	µg/m^3
SURF_ug_PM25X_rh50	$PM_{2.5}$ as PM25X + particle water at 50% relative humidity	µg/m^3
SURF_ug_PMFINE	Fine PM, sum of all fine aerosols	µg/m^3
SURF_ug_PPM_C	Primary coarse PM from anthropogenic emissions	µg/m^3
SURF_ug_PPM25	Primary $PM_{2.5}$ from anthropogenic emissions	µg/m^3
SURF_PM25water	Water in $PM_{2.5}$ at 50% relative humidity	µg/m^3
SURF_ug_NH4_F	NH_4^+ fine aerosol as ammonium sulphate and ammonium	µg/m^3
SURF_ug_NO3_F	NO_3^- fine aerosol as ammonium nitrate	µg/m^3
SURF_ug_NO3_C	NO_3^- coarse aerosol associated with sea salt and mineral dust	µg/m^3
SURF_ug_SO4	SO_4^{2-} sulphate aerosol	µg/m^3

https://doi.org/10.5194/egusphere-2026-3188
Preprint. Discussion started: 2 July 2026

SURF_ug_SIA	Secondary Inorganic Aerosols	µg/m^3
SURF_ug_ECCOARSE	Elemental carbon coarse	µg/m^3
SURF_ug_ECFINE	Elemental carbon fine	µg/m^3
SURF_ug_PM_OM25	Organic matter fine aerosol	µg/m^3
SURF_ug_PM_OMCOARSE	Organic matter coarse aerosol	µg/m^3
	Ozone metrics for health impact assessment	
SOMO35	Sum of the daily maximum of 8 hours running average over 35 ppb	ppb.day
SOMO35_max6m	SOMO35, Max of 6 month sum of daily maximum 8 hours mean over 35 ppb	ppb.day
SOMO0	Sum of the daily maximum of 8 hours running average (no threshold)	ppb.day
SOMO0_max6m	SOMO0, Max of 6 month sum of daily maximum 8 hours mean	ppb.day
DMAX_O3_max6m	Max of 6 month moving average of ozone daily maximum (0:00-24:00)	ppb
DMAX_O3_max3m	Max of 3 month moving average of ozone daily maximum (0:00-24:00)	ppb
	Ozone metrics for vegetation and crops impact assessment	
EUAOT40_Crops	AOT40 over crops (EU definition uses day hours from 8:00-20:00)	ppb.h
EUAOT40_Forests	AOT40 over forests (EU definition uses day hours from 8:00-20:00)	ppb.h
MMAOT40_IAM_CR	AOT40 over generic crop (Mapping Manual update, IAM_CR land cover class in EMEP model)	ppb.h
MMAOT40_IAM_DF	AOT40 over generic deciduos forest (Mapping Manual update, IAM_DF land cover class in EMEP model)	ppb.h
MMAOT40_IAM_MF	AOT40 over generic forest (Mapping Manual update, IAM_MF land cover class in EMEP model)	ppb.h
MMAOT40_TC	AOT40 over temperate/boreal crop (Mapping Manual update, TC land cover class in EMEP model)	ppb.h
POD0_IAM_CR	Phyto-toxic ozone dose, accumulated stomatal ozone flux over 0 nmole O_3 m^{-2} (PLA)s^{-1} over generic crop (IAM_CR)	mmole/m^2
POD0_IAM_DF	Phyto-toxic ozone dose, accumulated stomatal ozone flux over 0 nmole O_3 m^{-2} (PLA)s^{-1} over generic deciduous forest (IAM_DF)	mmole/m^2
POD0_IAM_MF	Phyto-toxic ozone dose, accumulated stomatal ozone flux over 0 nmole O_3 m^{-2} (PLA)s^{-1} over generic forest (IAM_MF)	mmole/m^2
POD1_IAM_CR	Phyto-toxic ozone dose, accumulated stomatal ozone flux over 1 nmole O_3 m^{-2} (PLA)s^{-1} over generic crop (IAM_CR)	mmole/m^2

https://doi.org/10.5194/egusphere-2026-3188
Preprint. Discussion started: 2 July 2026

POD1_IAM_DF	Phyto-toxic ozone dose, accumulated stomatal ozone flux over 1 nmole O_3 m^{-2} $(PLA)s^{-1}$ over generic deciduous forest (IAM_DF)	mmole/m^2
POD1_IAM_MF	Phyto-toxic ozone dose, accumulated stomatal ozone flux over 1 nmole O_3 m^{-2} $(PLA)s^{-1}$ over generic forest (IAM_MF)	mmole/m^2
POD3_IAM_CR	Phyto-toxic ozone dose, accumulated stomatal ozone flux over 3 nmole O_3 m^{-2} $(PLA)s^{-1}$ over generic crop (IAM_CR)	mmole/m^2
POD1_CF	Phyto-toxic ozone dose, accumulated stomatal ozone flux over 1 nmole O_3 m^{-2} $(PLA)s^{-1}$ over coniferous forest (CF)	mmole/m^2
POD1_DF	Phyto-toxic ozone dose, accumulated stomatal ozone flux over 1 nmole O_3 m^{-2} $(PLA)s^{-1}$ over deciduous forest (CF)	mmole/m^2
POD3_TC	Phyto-toxic ozone dose, accumulated stomatal ozone flux over 3 nmole O_3 m^{-2} $(PLA)s^{-1}$ over crops (TC)	mmole/m^2
M12_O3_Maize	Mean of ozone 12 hours daylight means (8:00-20:00) for Maize	ppb
M12_O3_Soybeans	Mean of ozone 12 hours daylight means (8:00-20:00) for soybeans	ppb
M7_O3_Wheat	Mean of ozone 7 hours daylight means (9:00-16:00) for wheat	ppb
M7_O3_Rice	Mean of ozone 7 hours daylight means (9:00-16:00) for rice	ppb
	Dry deposition	
DDEP_OXN_m2Conif	Dry deposition of Oxidized nitrogen to coniferous forest	mgN/m^2
DDEP_OXN_m2Crops	Dry deposition of Oxidized nitrogen to crops	mgN/m^2
DDEP_OXN_m2Decid	Dry deposition of Oxidized nitrogen to deciduous forest	mgN/m^2
DDEP_OXN_m2Grid	Dry deposition of Oxidized nitrogen for a grid cell	mgN/m^2
DDEP_OXN_m2Seminat	Dry deposition of Oxidized nitrogen to semi-natural	mgN/m^2
DDEP_OXN_m2Water_D	Dry deposition of Oxidized nitrogen to water surfaces	mgN/m^2
DDEP_RDN_m2Conif	Dry deposition of Reduced nitrogen to coniferous forest	mgN/m^2
DDEP_RDN_m2Crops	Dry deposition of Reduced nitrogen to crops	mgN/m^2
DDEP_RDN_m2Decid	Dry deposition of Reduced nitrogen to deciduous forest	mgN/m^2
DDEP_RDN_m2Grid	Dry deposition of Reduced nitrogen for a grid cell	mgN/m^2
DDEP_RDN_m2Seminat	Dry deposition of Reduced nitrogen to semi-natural	mgN/m^2
DDEP_RDN_m2Water_D	Dry deposition of Reduced nitrogen to water surfaces	mgN/m^2
DDEP_SOX_m2Conif	Dry deposition of Oxidized sulphur to coniferous forest	mgS/m^2
DDEP_SOX_m2Crops	Dry deposition of Oxidized sulphur to crops	mgS/m^2
DDEP_SOX_m2Decid	Dry deposition of Oxidized sulphur to deciduous forest	mgS/m^2
DDEP_SOX_m2Grid	Dry deposition of Oxidized sulphur for a grid cell	mgS/m^2

https://doi.org/10.5194/egusphere-2026-3188
Preprint. Discussion started: 2 July 2026

DDEP_SOX_m2Seminat	Dry deposition of Oxidized sulphur to semi-natural	mgS/m^2
DDEP_SOX_m2Water_D	Dry deposition of Oxidized sulphur to water surfaces	mgS/m^2
	Wet deposition	
WDEP_HNO3	Wet deposition of HNO_3	mgN/m^2
WDEP_OXN	Wet deposition of oxidized nitrogen	mgN/m^2
WDEP_RDN	Wet depostion of reduced nitrogen	mgN/m^2
WDEP_SO2	Wet deposition of SO_2	mgS/m^2
WDEP_SOX	Wet depostion of oxidized sulphur	mgS/m^2
	Other	
AOD_550nm	Aerosol Optical Depth at 550 nm	

790

Table A2: Overview of the 39 JRC-FASST source regions in the global domain (0.5° × 0.5°), and comparison with the previous TM5-FASST source regions (1° x 1°)*.

JRC-FASST Source Region	Horizontal resolution	Countries	ISO Codes	TM5-FASST Source Region (Van Dingenen et al., 2018
EAF	0.5 x 0.5	Eastern Africa	CAF TCD SDN ETH SOM KEN UGA COD RWA TZA MDG ERI DJI COM BDI BID MUS REU SYC SDS SOL	EAF
NOA	0.5 x 0.5	Northern Africa (excluding EGY)	MAR DZA ESH TUN LBY SAH	NOA
SAF	0.5 x 0.5	Southern Africa (excluding RSA)	AGO NAM ZMB BWA ZWE MOZ MWI MYT	SAF
WAF	0.5 x 0.5	Western Africa	COG CNQ GAB GIN CMR NGA NER MLI BEN GHA BFA CIV SEN GMB GNB SLE LBR STP CPV SHN TGO GNQ MRT	WAF
RSA	0.5 x 0.5	Republic of South Africa, Swaziland and Lesotho	ZAF SWZ LSO	RSA
EGY	0.5 x 0.5	Egypt	EGY	EGY
AUS	0.5 x 0.5	Australia	AUS	AUS
NZL	0.5 x 0.5	New Zealand	NZL	NZL
CHN	0.5 x 0.5	China, Hong Kong and Macao	CHN HKG MAC	CHN
COR	0.5 x 0.5	South Korea	KOR	COR
JPN	0.5 x 0.5	Japan	JPN	JPN

https://doi.org/10.5194/egusphere-2026-3188
Preprint. Discussion started: 2 July 2026

MON	0.5 x 0.5	Mongolia and North Korea	MNG PRK	MON
TWN	0.5 x 0.5	Taiwan	TWN	TWN
MEX	0.5 x 0.5	Mexico	MEX	MEX
RCAM	0.5 x 0.5	Centarl America and Caribbean	PAN NIC HND GTM SLV ANT KNA LCA VCT TTO TCA VIR BLZ AIA ATG ABW BHS BRB VGB CYM DMA CUB DOM GRD GLP HTI JAM MTQ MSR PRI CRI	RCAM
GLF	0.5 x 0.5	Gulf states	BHR IRQ KWT OMN QAT SAU ARE YEM IRN	GLF
MEME	0.5 x 0.5	Mediterranean Middle East	ISR JOR PSE LBN SYR PSX	MEME
CAN	0.5 x 0.5	Canada and Greenland	CAN GRL	CAN
USA	0.5 x 0.5	United States	USA SPM BMU	USA
KAZ	0.5 x 0.5	Kazakstan	KAZ	KAZ
RIS	0.5 x 0.5	Rest of former Soviet Union	KGZ TKM UZB TJK	RIS
ARG	0.5 x 0.5	Argentina, Falklands and Uruguay	ARG FLK URY	ARG
BRA	0.5 x 0.5	Brazil	BRA	BRA
CHL	0.5 x 0.5	Chile	CHL	CHL
RSAM	0.5 x 0.5	Rest of South America	BOL COL ECU GUF GUY PER SUR VEN PRY PRA	RSAM
NDE	0.5 x 0.5	India, Maldives and Sri Lanka	IND LKA MDV	NDE
RSAS	0.5 x 0.5	Rest of South Asia	AFG BGD BTN NPL PAK	RSAS
IDN	0.5 x 0.5	Indonesia and East Timor	IDN TLS	IDN
MYS	0.5 x 0.5	Malaysia, Singapore and Brunei	MYS SGP BRN	MYS
PHL	0.5 x 0.5	Philippines	PHL	PHL
RSEA	0.5 x 0.5	Rest of East Asia	KHM LAO MMR	RSEA
THA	0.5 x 0.5	Thailand	THA	THA
VNM	0.5 x 0.5	Vietnam	VNM	VNM
PAC	0.5 x 0.5	Pacific Islands and Papua New Guinea	FJI NCL SLB VUT FSM GUM KIR MHL NRU MNP PLW NFK TKL ASM COK PYF NIU PCN TON TUV WLF WSM PNG	PAC

https://doi.org/10.5194/egusphere-2026-3188
Preprint. Discussion started: 2 July 2026

RUS	**0.5 x 0.5**	**Russia**	**RUS**	**in RUS and RUE**
EUR	**0.5 x 0.5**	**Europe (EU27, Switzerland, Norway, Iceland and United Kingdom)**		**AUT BGR BLX CHE GER SWE ESP POL FIN FRA GBR NOR GRC RCZ HUN ITA ROM (HRV in RCEU)**
TURP	**0.5 x 0.5**	**Türkiye, Armenia, Gerogia and Azerbajan**	**TUR ARM GEO AZE**	**TUR (ARM GEO AZE in RUS)**
UKRP	**0.5 x 0.5**	**Ukraine, Belarus and Moldova**	**BLR MDA UKR**	**UKR**
WEB	**0.5 x 0.5**	**Western Balkans**	**SRB MKD BIH ALB MNE XKX**	**RCEU excluding HRV**

* In bold are highlighted the source regions which are different from the previous TM5-FASST source regions. In the new version the entire Russia (RUS) is considered as a single source, compared to previous version which was divided in the European and Asian part of Russia (RUS and REU). A new source region is including all Europe (EUR) at the global level, it includes all EU27 countries, Switzerland, Norway, Iceland and United Kingdom. A separate source region was included at global level for Turkey, and Caucasian countries, Armenia, Georgia and Azerbaijan (TURP). All western Balkan countries were included in a single source region at the global scale (WEB).

Table A3: Overview of the 41 JRC-FASST source regions in Europe (0.1° × 0.1°), and comparison with the previous TM5-FASST source regions (1° x 1°).

JRC-FASST Source Region	Horizontal resolution	Countries	ISO Codes	TM5-FASST Source Region (Van Dingenen et al., 2018
AUT	0.1 x 0.1	Austria	AUT	in AUT
BGR	0.1 x 0.1	Bulgaria	BGR	BGR
BEL	0.1 x 0.1	Belgium	BEL	in BLX
CHE	0.1 x 0.1	Switzerland and Liechtenstein	CHE	CHE
DEU	0.1 x 0.1	Germany	DEU	GER
DNK	0.1 x 0.1	Denmark	DNK	in SWE
ESP	0.1 x 0.1	Spain and Gibraltar	ESP	in ESP
EST	0.1 x 0.1	Estonia	EST	in POL
FIN	0.1 x 0.1	Finland	FIN	FIN
FRA	0.1 x 0.1	France and Andorra	FRA AND	FRA
GBR	0.1 x 0.1	Great Britain	GBR GGY IMN JEY	in GBR
IRL	0.1 x 0.1	Ireland	IRL	in GBR
LTU	0.1 x 0.1	Lithuania	LTU	in POL

https://doi.org/10.5194/egusphere-2026-3188
Preprint. Discussion started: 2 July 2026

LUX	0.1 x 0.1	Luxembourg	LUX	in BLX
LVA	0.1 x 0.1	Latvia	LVA	in POL
NLD	0.1 x 0.1	Netherlands	NLD	in BLX
NOR	0.1 x 0.1	Norway and Iceland	NOR ISL	NOR
POL	0.1 x 0.1	Poland	POL	in POL
PRT	0.1 x 0.1	Portugal	PRT	in ESP
SWE	0.1 x 0.1	Sweden	SWE	in SWE
CYP	0.1 x 0.1	Cyprus	CYP	in GRC
CZE	0.1 x 0.1	Czech Republic	CZE	in RCZ
GRC	0.1 x 0.1	Greece	GRC	in GRC
HRV	0.1 x 0.1	Croatia	HRV	in RCEU
HUN	0.1 x 0.1	Hungary	HUN	HUN
ITA	0.1 x 0.1	Italy, Malta, San Marino and Monaco	ITA VAT SMR MCO MLT	ITA
ROU	0.1 x 0.1	Romania	ROU	ROM
SVK	0.1 x 0.1	Slovakia	SVK	in RCZ
SVN	0.1 x 0.1	Slovenia	SVN	in AUT
TUR	0.1 x 0.1	Turkiye	TUR	TUR
ARM	0.1 x 0.1	Armenia	ARM	in RUS
GEO	0.1 x 0.1	Georgia	GEO	in RUS
AZE	0.1 x 0.1	Azerbaijan	AZE	in RUS
UKR	0.1 x 0.1	Ukraine	UKR	in UKR
MDA	0.1 x 0.1	Moldova	MDA	in UKR
BLR	0.1 x 0.1	Belarus	BLR	in UKR
ALB	0.1 x 0.1	Albania	ALB	in RCEU
BIH	0.1 x 0.1	Bosnia and Herzegovina	BIH	in RCEU
MKD	0.1 x 0.1	North Macedonia	MKD	in RCEU
MNE	0.1 x 0.1	Montenegro	MNE	in RCEU
SRB	0.1 x 0.1	Serbia and Kosovo	SRB XKX	in RCEU

https://doi.org/10.5194/egusphere-2026-3188
Preprint. Discussion started: 2 July 2026

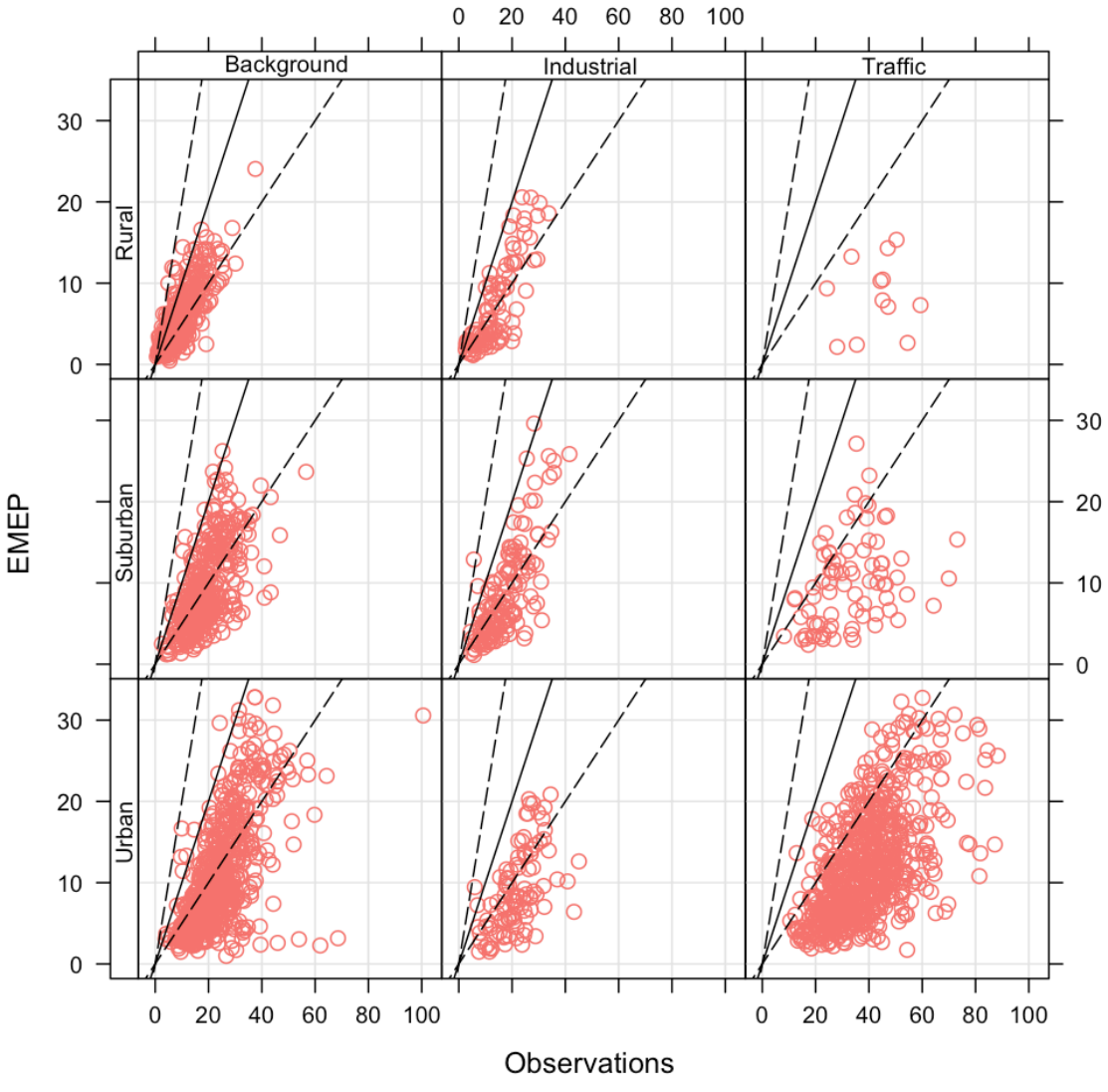

Figure A1: Comparison with observations in Europe (EEA) and EMEP simulation for 2015: annual mean NO_2 concentrations.

https://doi.org/10.5194/egusphere-2026-3188
Preprint. Discussion started: 2 July 2026

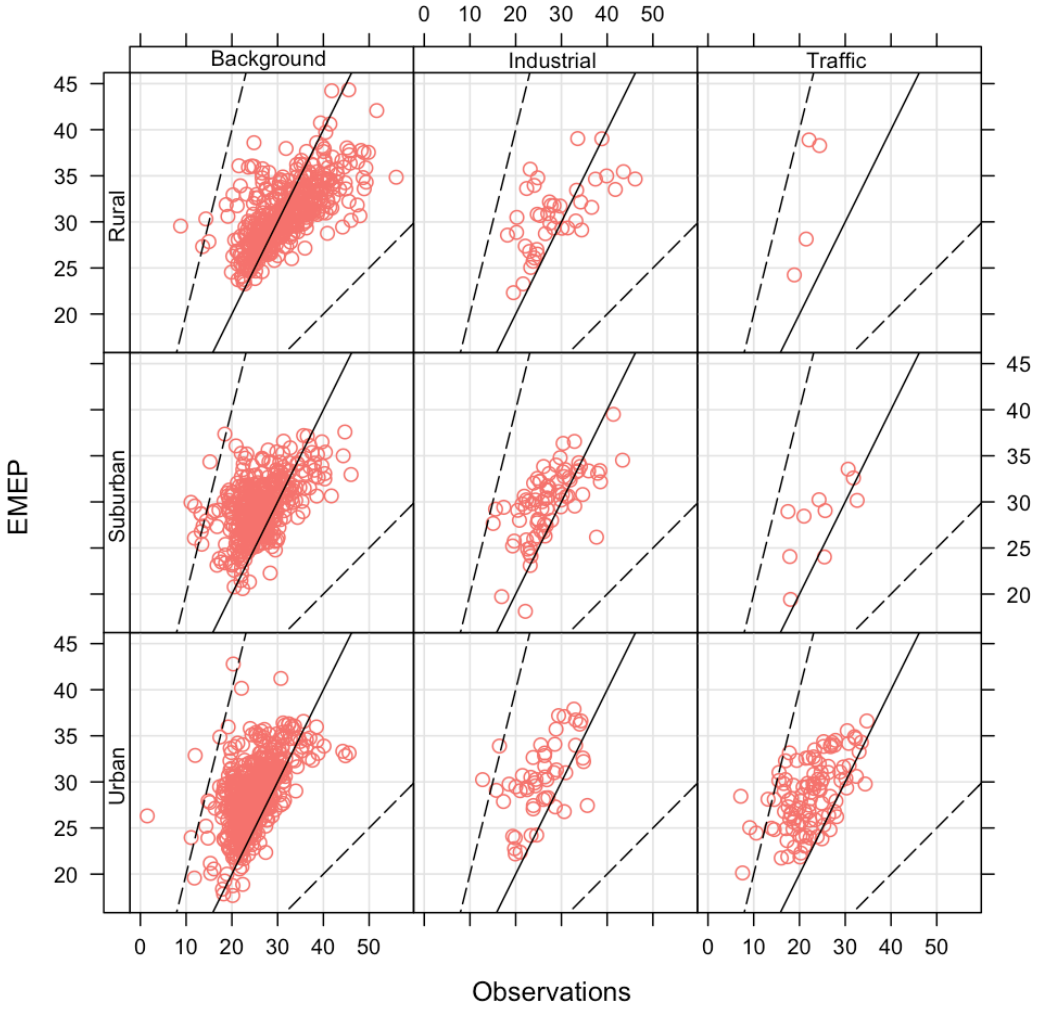

Figure A2: Comparison with observations in Europe (EEA) and EMEP simulation for 2015: annual mean O_3 concentrations.

https://doi.org/10.5194/egusphere-2026-3188
Preprint. Discussion started: 2 July 2026

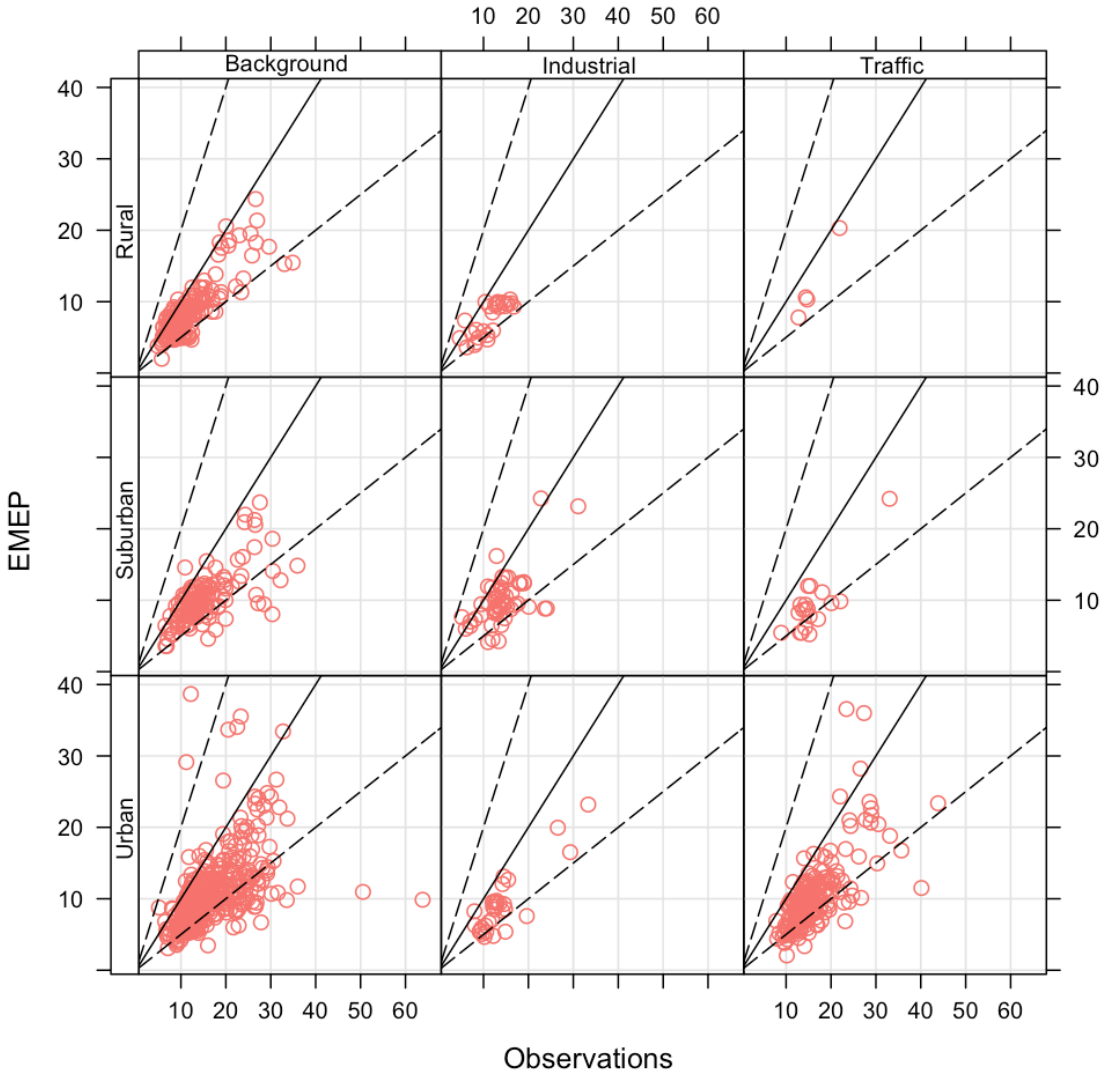

Figure A3: Comparison with observations in Europe (EEA) and EMEP simulation for 2015: annual mean $PM_{2.5}$ concentrations.

https://doi.org/10.5194/egusphere-2026-3188
Preprint. Discussion started: 2 July 2026

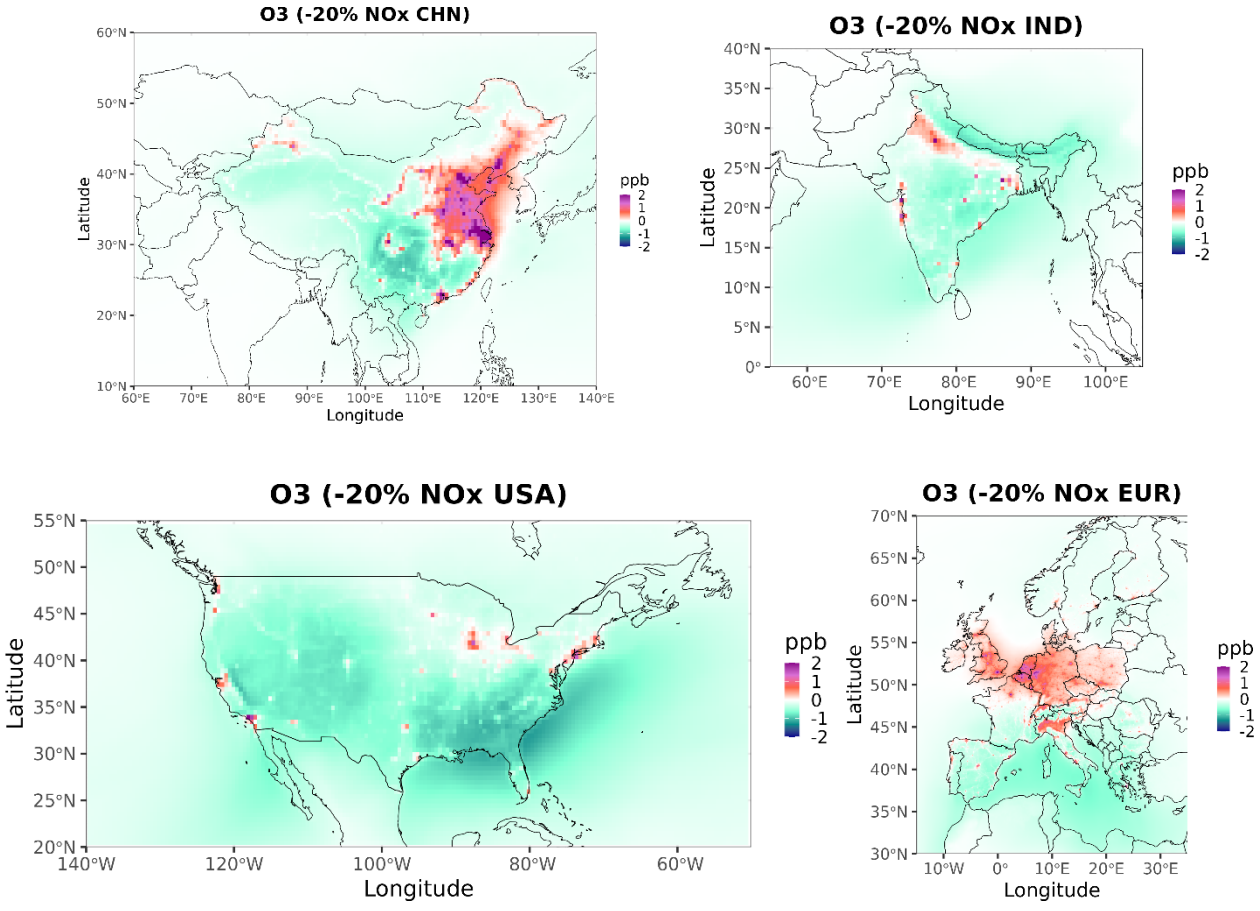

Figure A4: Changes in O_3 annual mean concentrations due to -20% NO_x emission reductions in different source regions: China (CHN), India (IND), United States of America (USA), and Europe (EUR, EU27, Norway, UK, Switzerland).

https://doi.org/10.5194/egusphere-2026-3188
Preprint. Discussion started: 2 July 2026

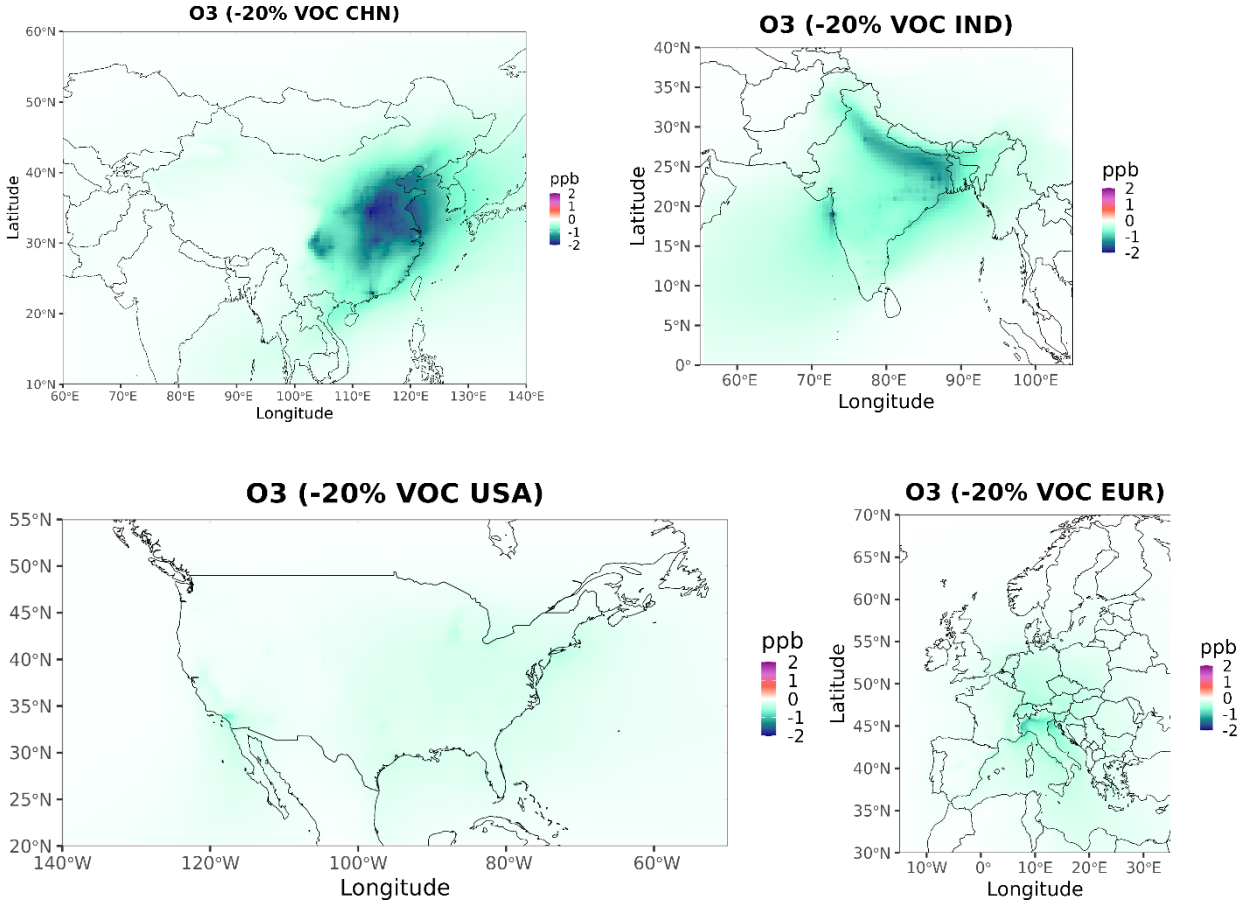

Figure A5: Changes in O_3 annual mean concentrations due to -20% VOC emission reductions in different source regions: China (CHN), India (IND), United States of America (USA), and Europe (EUR, EU27, Norway, UK, Switzerland).

https://doi.org/10.5194/egusphere-2026-3188
Preprint. Discussion started: 2 July 2026

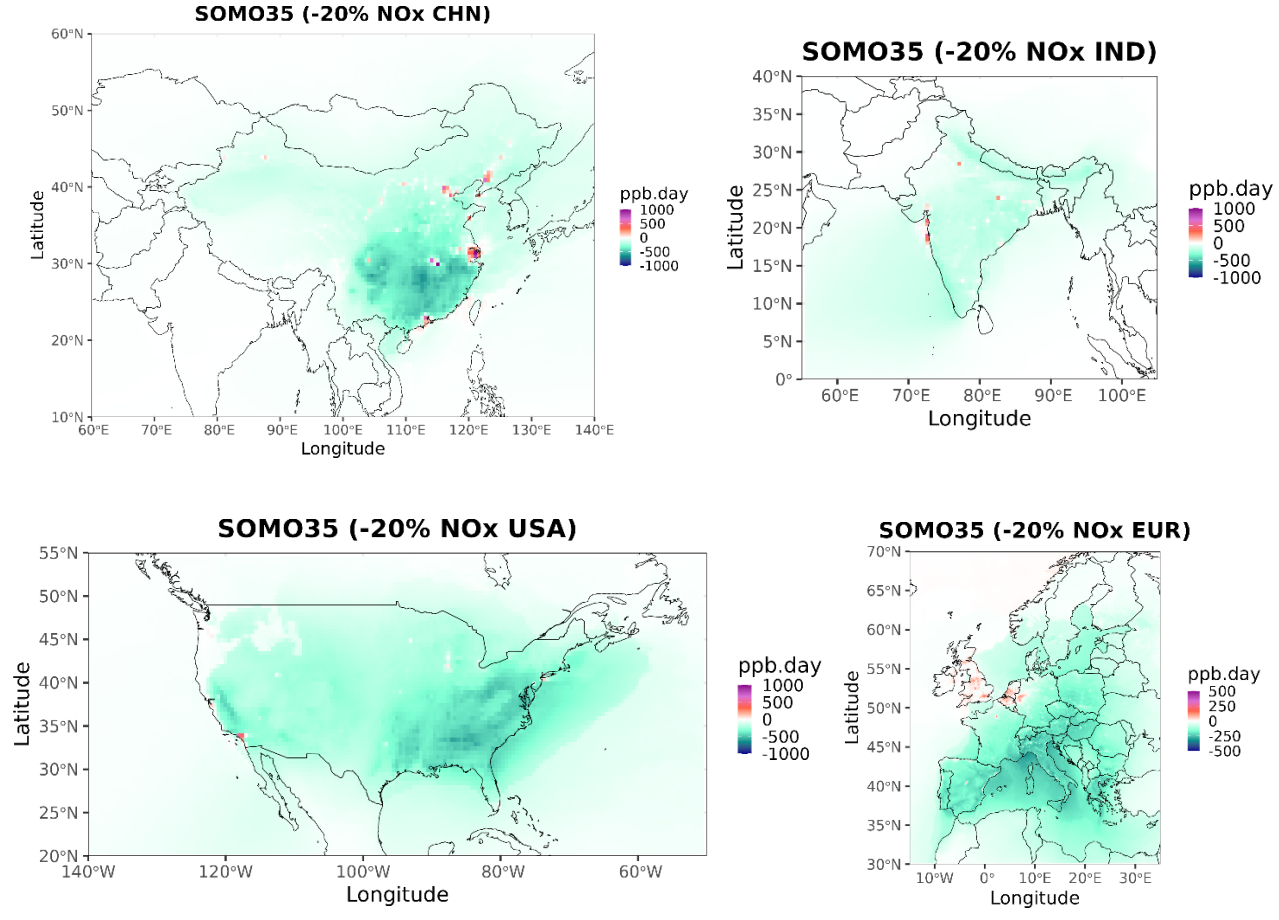

Figure A6: Changes in annual maximum 6 months SOMO35 concentrations due to -20% NO_x emission reductions in different source regions: China (CHN), India (IND), United States of America (USA), and Europe (EUR, EU27, Norway, UK, Switzerland).

https://doi.org/10.5194/egusphere-2026-3188
Preprint. Discussion started: 2 July 2026

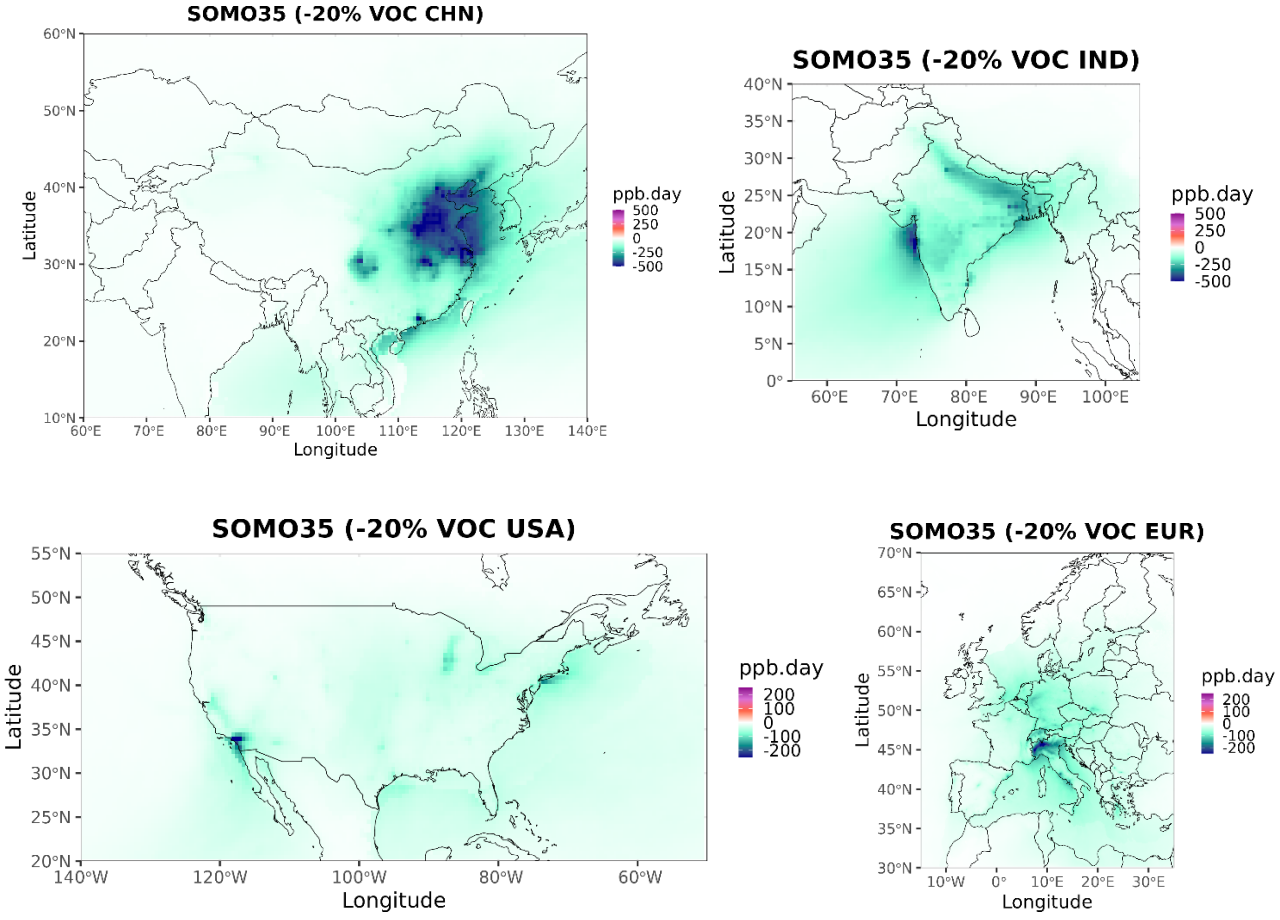

Figure A7: Changes in annual maximum 6 months SOMO35 concentrations due to -20% VOC emission reductions in different source regions: China (CHN), India (IND), United States of America (USA), and Europe (EUR, EU27, Norway, UK, Switzerland).

https://doi.org/10.5194/egusphere-2026-3188
Preprint. Discussion started: 2 July 2026

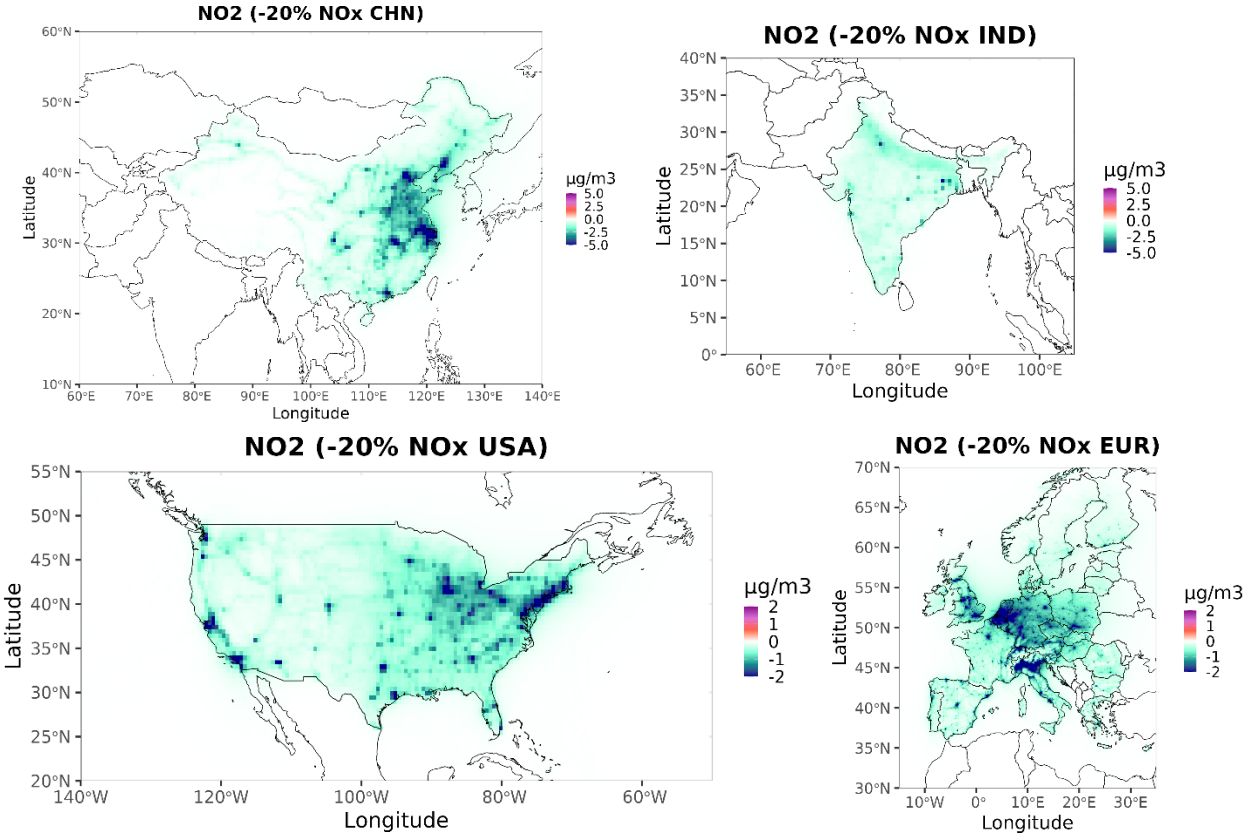

Figure A8: Changes NO_2 annual mean concentrations due to -20% NO_x emission reductions in different source regions: China (CHN), India (IND), United States of America (USA), and Europe (EUR, EU27, Norway, UK, Switzerland).

https://doi.org/10.5194/egusphere-2026-3188
Preprint. Discussion started: 2 July 2026

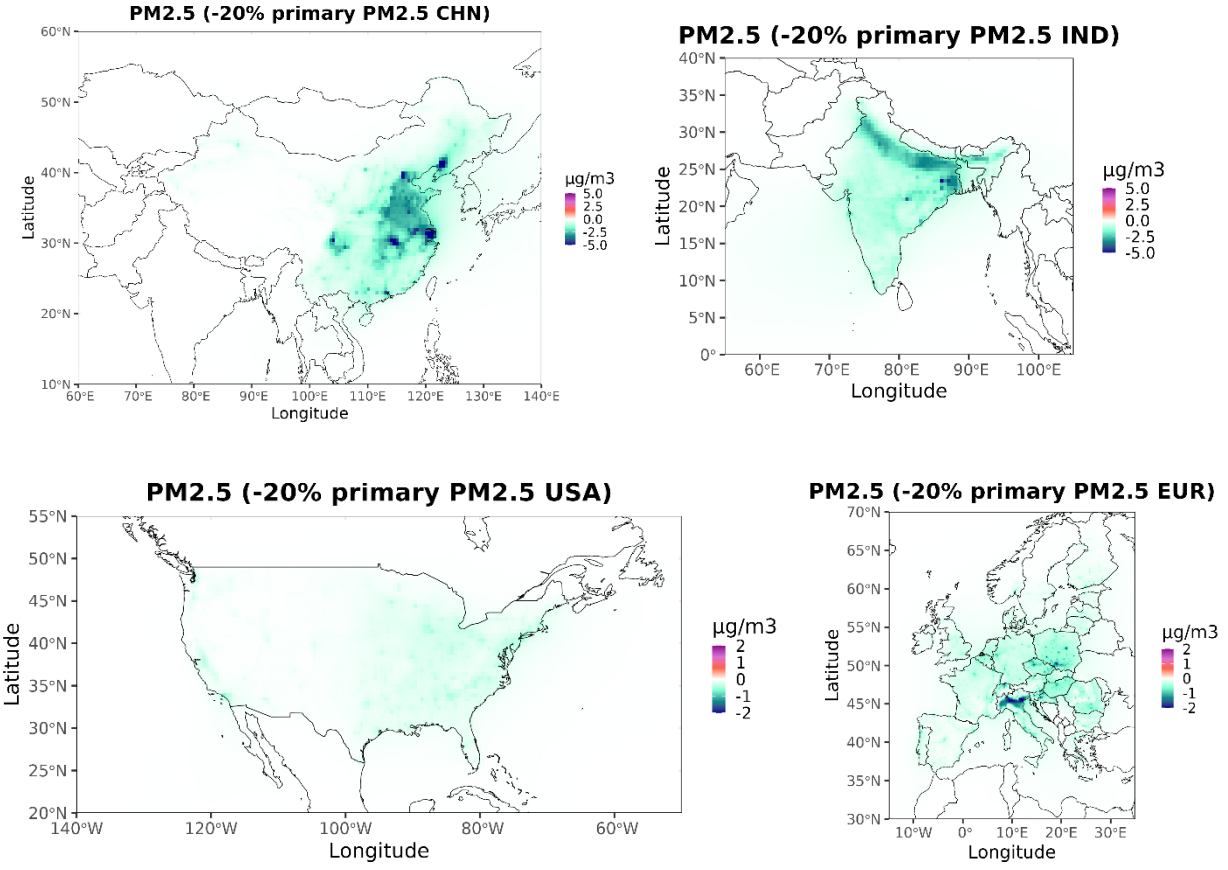

Figure A9: Changes $PM_{2.5}$ annual mean concentrations due to -20% primary $PM_{2.5}$ emission reductions in different source regions: China (CHN), India (IND), United States of America (USA), and Europe (EUR, EU27, Norway, UK, Switzerland).

https://doi.org/10.5194/egusphere-2026-3188
Preprint. Discussion started: 2 July 2026

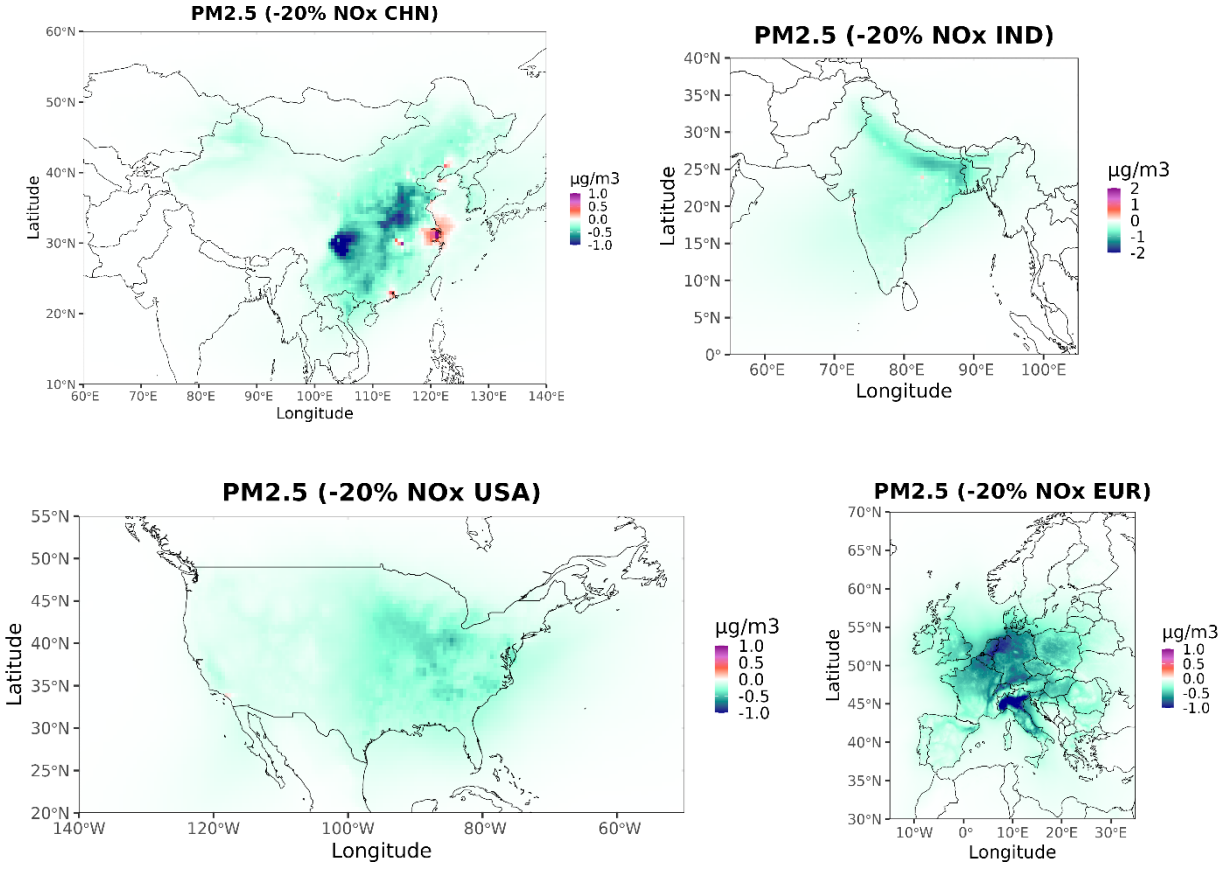

Figure A10: Changes $PM_{2.5}$ annual mean concentrations due to -20% NO_x emission reductions in different source regions: China (CHN), India (IND), United States of America (USA), and Europe (EUR, EU27, Norway, UK, Switzerland).

https://doi.org/10.5194/egusphere-2026-3188
Preprint. Discussion started: 2 July 2026

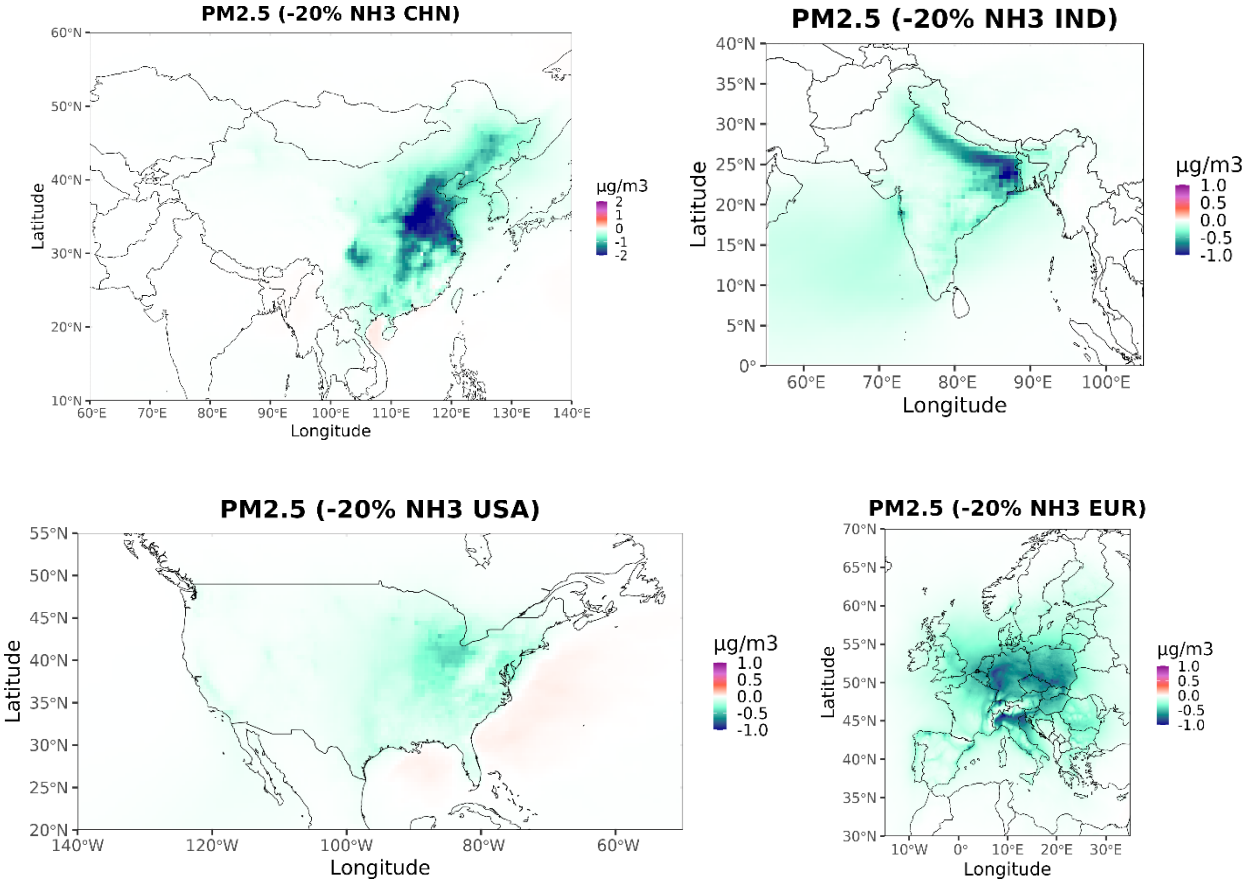

Figure A11: Changes $PM_{2.5}$ annual mean concentrations due to -20% NH_3 emission reductions in different source regions: China (CHN), India (IND), United States of America (USA), and Europe (EUR, EU27, Norway, UK, Switzerland).

https://doi.org/10.5194/egusphere-2026-3188
Preprint. Discussion started: 2 July 2026

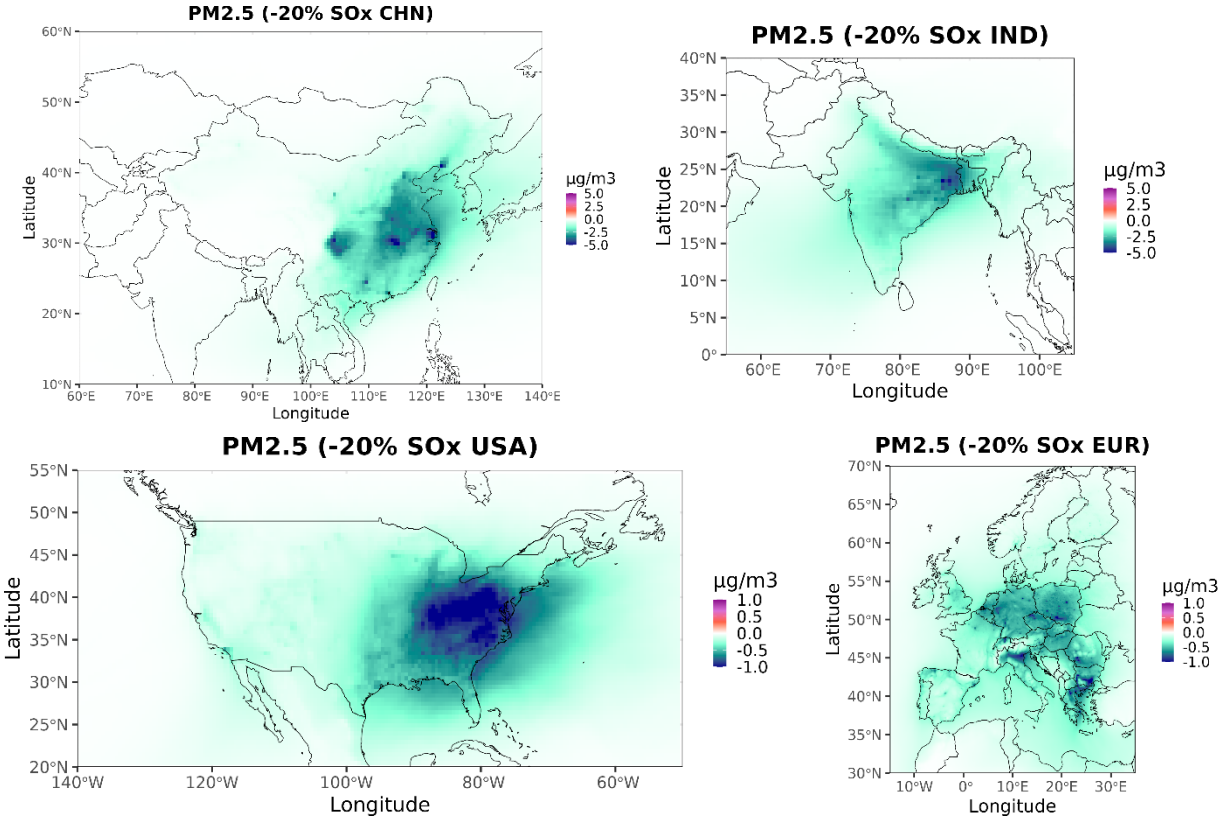

Figure A12: Changes $PM_{2.5}$ annual mean concentrations due to -20% SO_x emission reductions in different source regions: China (CHN), India (IND), United States of America (USA), and Europe (EUR, EU27, Norway, UK, Switzerland).

https://doi.org/10.5194/egusphere-2026-3188
Preprint. Discussion started: 2 July 2026

Data availability

The EDGAR emissions used for establishing the FASST source–receptor matrices are publicly available at: https://edgar.jrc.ec.europa.eu/. References to ancillary data (population, crop, and health statistics) have been included in the paper and in Appendix A. The FASST tool is publicly accessible via the Joint Research Centre FASST Webpage, available at: https://tm5-fasst.jrc.ec.europa.eu// (Joint Research Centre, 2026). The data presented in this paper are available at https://doi.org/10.5281/zenodo.20508569. FASST embedded source–receptor matrices are available from: JRC-FASST@ec.europa.eu.

Author contributions

Conceptualisation: CB, RVD, LP. Data curation: ADM, LP, AG. Formal analysis: ADM, LP, AG. Methodology: CB, RVD, LP. Software: CB, RVD, LP. Supervision: CB. Validation: RVD, ADM, LP, AG. Writing – original draft: LP, CB. Writing – review & editing: CB, RVD, LP, ADM, AG.

Competing interests

The authors declare they have no competing interests.

Disclaimer

Copernicus Publications adds a standard disclaimer: “Copernicus Publications remains neutral with regard to jurisdictional claims made in the text, published maps, institutional affiliations, or any other geographical representation in this paper. While Copernicus Publications makes every effort to include appropriate place names, the final responsibility lies with the authors. Views expressed in the text are those of the authors and do not necessarily reflect the views of the publisher.”

Please feel free to add disclaimer text at your choice, if applicable.

Acknowledgements

Besides the author’s statement of gratitude to and recognition of the people and institutions that helped the author’s research and writing, authors are also asked to include relevant research infrastructure they have benefitted from during their research, where research was conducted or data/resources were used. Examples are Field Stations and Marine Laboratories (FSMLs).

Financial support

There was no external financial support for the development of this work..

https://doi.org/10.5194/egusphere-2026-3188
Preprint. Discussion started: 2 July 2026

Review statement

The review statement will be added by Copernicus Publications listing the handling editor as well as all contributing referees according to their status anonymous or identified.

References

Alcamo, J., Shaw, R., and Hordijk, L. (Eds.): The RAINS Model of Acidification – Science and Strategies in Europe, 1st Edn., Springer Netherlands, 1990.

Alexeeff, S.E., Liao, N.S., Liu, X., Van Den Eeden, S.K., and Sidney, S.: Long-term $PM_{2.5}$ exposure and risks of ischemic heart disease and stroke events: review and meta- analysis. J. Am. Heart Assoc. 10, e016890, 2021.

Amann, M., Bertok, I., Borken-Kleefeld, J., Cofala, J., Heyes, C., Höglund-Isaksson, L., Klimont, Z., Nguyen, B., Posch, M., Rafaj, P., Sandler, R., Schöpp, W., Wagner, F., and Winiwarter, W.: Cost-effective control of air quality and greenhouse gases in Europe: Modeling and policy applications, Environ. Model. Softw., 26, 1489–1501, https://doi.org/10.1016/j.envsoft.2011.07.012, 2011.

Anagha, K. S. and Kuttippurath, J.: Surface ozone pollution-driven risks for the yield of major food crops under future climate change scenarios in India, Environmental Research, 275, 121390, https://doi.org/10.1016/j.envres.2025.121390, 2025.

Ananthapavan, J., Moodie, M., Milat, A.J., and Carter, R.: Systematic review to update 'value of a statistical life' estimates for Australia. IJERPH 18, 6168. https://doi.org/ 10.3390/ijerph18116168, 2021.

Belis, C. A., Van Dingenen, R., Klimont, Z., and Dentener, F.: Scenario analysis of PM2.5 and ozone impacts on health, crops and climate with TM5-FASST: A case study in the Western Balkans, Journal of Environmental Management, 319, 115738, https://doi.org/10.1016/j.jenvman.2022.115738, 2022.

Belis, C.A., Van Dingenen, R., 2023. Air quality and related health impact in the UNECE region: source attribution and scenario analysis. Atmospheric Chemistry and Physics 23, 8225–8240. https://doi.org/10.5194/acp-23-8225-2023

Belis, C.A., Matkovic, V., Ballocci, M., Jevtic, M., Millo, G., Mata, E., and Van Dingenen, R.: Assessment of health impacts and costs attributable to air pollution in urban areas using two different approaches. A case study in the Western Balkans. Environ. Int. 2023, 182, 108347, 2023

Belis, C.A., Pirovano, G., Villani, M.G., Calori, G., Pepe, N., and Putaud, J.P.: Comparison of source apportionment approaches and analysis of non-linearity in a real case model application. Geoscientific Model Development 14, 4731–4750. https://doi.org/10.5194/gmd-14-4731-2021, 2021.

Brauer M.,et al.: Global burden and strength of evidence for 88 risk factors in 204 countries and 811 subnational locations, 1990–2021: a systematic analysis for the Global Burden of Disease Study 2021, The Lancet, Volume 403, Issue 10440, 2024, Pages 2162-2203, ISSN 0140-6736, https://doi.org/10.1016/S0140-6736(24)00933-4, 2024.

Cao, M., Xing, J., Sahu, S. K., Duan, L., and Li, J.: Accurate prediction of air quality response to emissions for effective control policy design, Journal of Environmental Sciences, 123, 116–126, https://doi.org/10.1016/j.jes.2022.02.009, 2023.

https://doi.org/10.5194/egusphere-2026-3188
Preprint. Discussion started: 2 July 2026

Chen, J., and Hoek, G.,: Long-term exposure to PM and all-cause and cause-specific mortality: a systematic review and meta-analysis. Environ. Int. 143, 105974, 2020.

Ciarlantini, S., Frontuto, V., Pezzoli, A., Gavros, A., and Belis, C.A.:, Econometric model derived from meta-analysis to estimate VSL and VOLY associated to air pollution at a global level. Journal of Environmental Management 379, 124824. https://doi.org/10.1016/j.jenvman.2025.124824, 2025.

Clappier, A., Thunis, P., Beekmann, M., Putaud, J.P., and de Meij, A.: Impact of SOx, NOx and NH_3 emission reductions on $PM_{2.5}$ concentrations across Europe: Hints for future measure development, Environment International, Volume 156, 2021, ISSN 0160-4120, https://doi.org/10.1016/j.envint.2021.106699, 2021

Crippa, M., Solazzo, E., Huang, G., Guizzardi, D., Koffi, E., Muntean, M., Schieberle, C., Friedrich, R., and Janssens-Maenhout, G.: High resolution temporal profiles in the Emissions Database for Global Atmospheric Research (EDGAR), Nature Scientific Data, doi:10.1038/s41597-020-0462-2, 2019.

De Meij, A., Cuvelier, C., Thunis, P., Pisoni, E., and Bessagnet, B.: Sensitivity of air quality model responses to emission changes: comparison of results based on four EU inventories through FAIRMODE benchmarking methodology, Geosci. Model Dev., 17, 587–606, https://doi.org/10.5194/gmd-17-587-2024, 2024.

Dentener, F., Keating, T., Akimoto, H., Pirrone, N., Dutchak, S., and Zuber, A.: Convention on Long-range Transboundary Air Pollution, United Nations and UNECE Task Force on Emission Inventories and Projections, Hemispheric transport of air pollution 2010: prepared by the Task Force on Hemispheric Transport of Air Pollution acting within the framework of the Convention on Long-range Transboundary Air Pollution, United Nations, New York, Geneva, 2010.

EMEP Status Report 1/04: Transboundary acidification, eutrophication and ground level ozone in Europe, Joint MSC-W & CCC & CIAM & ICP-M&M & CCE Report, https://emep.int/publ/reports/2004/Status_report_int_del1.pdf, 2004.

EMEP Status Report 1/2017: Transboundary particulate matter, photo-oxidants, acidifying and eutrophying components, Joint MSC-W & CCC & CEIP Report, https://emep.int/publ/reports/2017/EMEP_Status_Report_1_2017.pdf, 2017.

EMEP Status Report 1/2020: Transboundary particulate matter, photo-oxidants, acidifying and eutrophying components, Joint MSC-W & CCC & CEIP Report, https://emep.int/publ/reports/2020/EMEP_Status_Report_1_2020.pdf, 2020.

Forastiere, F., Spadaro, J. V., Ancona, C., Jovanovic Andersen, Z., Cozzi, I., Gumy, S., Loncar, D., Mudu, P., Medina, S., Perez Velasco, R., Walton, H., Zhang, J., and Krzyzanowski, M.: Choices of morbidity outcomes and concentration-response functions for health risk assessment of long-term exposure to air pollution, Environmental epidemiology (Philadelphia, Pa.), 8, p314, 10.1097, 2024.

Ge, Y., Heal, M. R., Stevenson, D. S., Wind, P., and Vieno, M.: Evaluation of global EMEP MSC-W (rv4.34) WRF (v3.9.1.1) model surface concentrations and wet deposition of reactive N and S with measurements, Geosci. Model Dev., 14, 7021–7046, https://doi.org/10.5194/gmd-14-7021-2021, 2021.

Ge, Y.: Dataset for evaluation of global EMEP MSC-W (rv4.34)-WRF (v3.9.1.1) model surface concentrations and wet deposition of reactive N and S with measurements. Zenodo. https://doi.org/10.5281/zenodo.5037080, 2021.

https://doi.org/10.5194/egusphere-2026-3188
Preprint. Discussion started: 2 July 2026

Grell G. A., and Dévényi, D.: A generalized approach to parameterizing convection combining ensemble and data assimilation techniques. Geophys Res Lett. doi:10.1029/2002GL015311, 2002.

Gu, B., Zhang, L., Dingenen, R. V., Vieno, M., Grinsven, H. J. V., Zhang, X., Zhang, S., Chen, Y., Wang, S., Ren, C., Rao, S., Holland, M., Winiwarter, W., Chen, D., Xu, J., and Sutton, M. A.: Abating ammonia is more cost-effective than nitrogen oxides for mitigating $PM_{2.5}$ air pollution, Science, 374, 758–762, https://doi.org/10.1126/science.abf8623, 2021.

Hamra Ghassan, B., Guha, N., Cohen, A., Laden, F., Raaschou-Nielsen, O., Samet Jonathan, M., Vineis, P., Forastiere, F., Saldiva, P., Yorifuji, T., and Loomis, D.: Outdoor particulate matter exposure and lung cancer: a systematic review and meta-analysis. Environ. Health Perspect. 122, 906–911, 2014.

Harmsen, M.J.H.M., van Dorst, P., van Vuuren, D.P. et al. Co-benefits of black carbon mitigation for climate and air quality. Climatic Change 163, 1519–1538 https://doi.org/10.1007/s10584-020-02800-8, 2020.

Harrison, R.M., Beddows, D.C.S., Tong, C., and Damayanti, S.: Non-linearity of secondary pollutant formation estimated from emissions data and measured precursor-secondary pollutant relationships. npj Clim Atmos Sci 5, 71 (2022). https://doi.org/10.1038/s41612-022-00297-9, 2022.

Health Effects Institute (HEI). 2025. State of Global Air 2025: A Report on Air Pollution and Its Role in the Worlds' Leading Causes of Death. Boston, MA: Health Effects Institute, 2025

Heroux, M.-E., Anderson, H.R., Atkinson, R., Brunekreef, B., Cohen, A., Forastiere, F., Hurley, F., Katsouyanni, K., Krewski, D., Krzyzanowski, M., Künzli, N., Mills, I., Querol, X., Ostro, B., and Walton, H.: Quantifying the health impacts of ambient air pollutants: recommendations of a WHO/Europe project. Int. J. Public Health 60, 619–627, 2015.

Hong, S., J. Dudhia, and S. Chen, 2004: A Revised Approach to Ice Microphysical Processes for the Bulk Parameterization of Clouds and Precipitation. Mon. Wea. Rev., 132, 103–120, https://doi.org/10.1175/1520-0493(2004)132<0103:ARATIM>2.0.CO;2., 2004.

Hong, S. Y. and Lim, J. O. J., The WRF single–moment 6–class microphysics scheme (WSM6), J. Korean Meteor. Soc., 42, 129 – 151, 2006.

Huangfu, P., and Atkinson, R.: Long-term exposure to NO_2 and O_3 and all-cause and respiratory mortality: A systematic review and meta-analysis. Environ. Int. 144, 105998, 2020.

Iacono, M.J., J.S. Delamere, E.J. Mlawer, M.W. Shephard, S.A. Clough, and W.D. Collins: Radiative forcing by long-lived greenhouse gases: calculations with the AER radiative transfer models, J. Geophys. Res., 113, D13103, doi:10.1029/2008 JD009944, 2008.

IEA, 2017, https://www.oecd.org/en/publications/co2-emissions-from-fuel-combustion-2017_co2_fuel-2017-en.html

IPCC AR6, Szopa, S., V. Naik, B. Adhikary, P. Artaxo, T. Berntsen, W.D. Collins, S. Fuzzi, L. Gallardo, A. Kiendler-Scharr, Z. Klimont, H. Liao, N. Unger, and P. Zanis, Short-Lived Climate Forcers Supplementary Material. In Climate Change 2021: The Physical Science Basis. Contribution of Working Group I to the Sixth Assessment Report of the Intergovernmental Panel on Climate Change [Masson-Delmotte, V., P. Zhai, A. Pirani, S.L. Connors, C. Péan, S. Berger, N. Caud, Y. Chen, L. Goldfarb,

https://doi.org/10.5194/egusphere-2026-3188
Preprint. Discussion started: 2 July 2026

M.I. Gomis, M. Huang, K. Leitzell, E. Lonnoy, J.B.R. Matthews, T.K. Maycock, T. Waterfield, O. Yelekçi, R. Yu, and B. Zhou (eds.)] 2021.

Janić, Zaviša I., Nonsingular implementation of the Mellor-Yamada level 2.5 scheme in the NCEP Meso model, National Centers for Environmental Prediction (U.S.)); https://repository.library.noaa.gov/view/noaa/11409, 2001.

Logan, J. A.: An analysis of ozonesonde data for the troposphere: Recommendations for testing 3-D models and development of a gridded climatology for tropospheric ozone, J. Geophys. Res., 10, 16115–16149, 1998.

Kasdagli, M.-I., Orellano, P., Pérez Velasco, R., and Samoli, E.: Long-Term Exposure to Nitrogen Dioxide and Ozone and Mortality: Update of the WHO Air Quality Guidelines Systematic Review and Meta-Analysis, International Journal of Public Health, Volume 69 - 2024, 10.3389/ijph.2024.1607676, 2024.

Khreis, H., Kelly, C., Tate, J., Parslow, R., Lucas, K., and Nieuwenhuijsen, M.: Exposure to traffic-related air pollution and risk of development of childhood asthma: a systematic review and meta-analysis. Environ. Int. 100, 1–31, 2017.

Maes, J., Bruzón, A. G., Barredo, J. I., Vallecillo, S., Vogt, P., Rivero, I. M., and Santos-Martín, F.: Accounting for forest condition in Europe based on an international statistical standard, Nature Communications, 14, 3723, https://doi.org/10.1038/s41467-023-39434-0, 2023.

Matsui, T., Zhang, S.Q., Lang, S.E., Tao W., Ichoku, C., and Peters-Lidard, C.D.: Impact of radiation frequency, precipitation radiative forcing, and radiation column aggregation on convection-permitting West African monsoon simulations. Clim Dyn 55, 193–213 (2020). https://doi.org/10.1007/s00382-018-4187-2, 2020.

Ménégoz, M., Salas Y Melia, D., Legrand, M., Teyssédre, H., Michou, M., Peuch, V. H., Martet, M., Josse, B., and Dombrowski-Etchevers, I.: Equilibrium of sinks and sources of sulphate over Europe: Comparison between a six-year simulation and EMEP observations, Atmospheric Chemistry and Physics, 9, 4505-4519, 2009. 10.1034/j.1600-0889.2001.530507, 2009.

Mills, G., Buse, A., Gimeno, B., Bermejo, V., Holland, M., Emberson, L., and Pleijel, H.: A synthesis of AOT40-based response functions and critical levels of ozone for agricultural and horticultural crops, Atmos. Environ., 41, 2630–2643, https://doi.org/10.1016/j.atmosenv.2006.11.016, 2007.

Mlawer, E. J., S. J. Taubman, P. D. Brown, M. J. Iacono, and S. A. Clough: Radiative transfer for inhomogeneous atmospheres: RRTM, a validated correlated-k model for the longwave, J. Geophys. Res., 102(D14), 16663–16682, doi:10.1029/97JD00237, 1997.

Narain, U., and Sall, C.: Methodology for Valuing the Health Impacts of Air Pollution. World Bank, Washington, DC. https://doi.org/10.1596/24440, 2016.

OECD, Environmental Outlook on the Triple Planetary Crisis: Stakes, Evolution and Policy Linkages, OECD Publishing, Paris, https://doi.org/10.1787/257ffbb6-en, 2025.

Pachón, J. E., Opazo, M. A., Lichtig, P., Huneeus, N., Bouarar, I., Brasseur, G., Li, C. W. Y., Flemming, J., Menut, L., Menares, C., Gallardo, L., Gauss, M., Sofiev, M., Kouznetsov, R., Palamarchuk, J., Uppstu, A., Dawidowski, L., Rojas, N. Y., Andrade,

https://doi.org/10.5194/egusphere-2026-3188
Preprint. Discussion started: 2 July 2026

M. D. F., Gavidia-Calderón, M. E., Delgado Peralta, A. H., and Schuch, D.: Air quality modeling intercomparison and multiscale ensemble chain for Latin America, Geosci. Model Dev., 17, 7467-7512, 10.5194/gmd-17-7467-2024, 2024.

Park, J., Kim, H.-J., Lee, C.-H., Lee, C.H., and Lee, H.W.: Impact of long-term exposure to ambient air pollution on the incidence of chronic obstructive pulmonary disease: a systematic review and meta-analysis. Environ. Res. 194, 110703, 2021.

Pommier, M., Fagerli, H., Gauss, M., Simpson, D., Sharma, S., Sinha, V., Ghude, S. D., Landgren, O., Nyiri, A., and Wind, P.: Impact of regional climate change and future emission scenarios on surface O_3 and $PM_{2.5}$ over India, Atmos. Chem. Phys., 18, 103-127, 10.5194/acp-18-103-2018, 2018.

Rao, S., Klimont, Z., Smith, S. J., Dingenen, R. V., Dentener, F., Bouwman, L., Riahi, K., Amann, M., Bodirsky, B. L., Vuuren, D. P. van, Reis, L. A., Calvin, K., Drouet, L., Fricko, O., Fujimori, S., Gernaat, D., Havlik, P., Harmsen, M., Hasegawa, T., Heyes, C., Hilaire, J., Luderer, G., Masui, T., Stehfest, E., Strefler, J., Sluis, S. van der, and Tavoni, M.: Future air pollution in the Shared Socio-economic Pathways, Global Environmental Change, 42, 346–358, https://doi.org/10.1016/j.gloenvcha.2016.05.012, 2017.

von Schneidemesser, E., Driscoll, C., Rieder, H.E., Schiferl, L.D., 2020. How will air quality effects on human health, crops and ecosystems change in the future? Philosophical Transactions of the Royal Society A: Mathematical, Physical and Engineering Sciences 378, 20190330. https://doi.org/10.1098/rsta.2019.0330

Simpson, D., Fagerli, H., Jonson, J., Tsyro, S., Wind, P., and Tuovinen, J.-P.: The EMEP Unified Eulerian Model. Model Description, EMEP MSC-W Report 1/2003, The Norwegian Meteorological Institute, Oslo, Norway, 2003.

Simpson, D., Benedictow, A., Berge, H., Bergström, R., Emberson, L. D., Fagerli, H., Flechard, C. R., Hayman, G. D., Gauss, M., Jonson, J. E., Jenkin, M. E., Nyíri, A., Richter, C., Semeena, V. S., Tsyro, S., Tuovinen, J.-P., Valdebenito, Á., and Wind, P.: The EMEP MSC-W chemical transport model – technical description, Atmos. Chem. Phys., 12, 7825–7865, https://doi.org/10.5194/acp-12-7825-2012, 2012.

Skamarock, W. C., J. B. Klemp, J. Dudhia, D. O. Gill, D. M. Barker, W. Wang, and J. G. Powers: A description of the Advanced Research WRF Version 2. NCAR Tech Notes-468+STR, 2005.

Sonwani, S., Hussain, S., and Saxena, P.: Air pollution and climate change impact on forest ecosystems in Asian region – a review, Ecosystem Health and Sustainability, 8, 2090448, https://doi.org/10.1080/20964129.2022.2090448, 2022.

Thunis, P., Clappier, A., Beekmann, M., Putaud, J. P., Cuvelier, C., Madrazo, J., and de Meij, A.: Non-linear response of $PM_{2.5}$ to changes in NOx and NH_3 emissions in the Po basin (Italy): consequences for air quality plans, Atmos. Chem. Phys., 21, 9309–9327, https://doi.org/10.5194/acp-21-9309-2021, 2021.

Thunis, P., Degraeuwe, B., Pisoni, E., Trombetti, M., Peduzzi, E., Belis, C. A., Wilson, J., Clappier, A., and Vignati, E.: PM 2.5 source allocation in European cities: A SHERPA modelling study, Atmospheric Environment, 187, 93–106, https://doi.org/10.1016/j.atmosenv.2018.05.062, 2018.

Tian, Y., Wang, S., and Jin, X.: Global patterns and trends in ground-level ozone chemical formation regimes from 1996 to 2022, Atmos. Chem. Phys., 25, 9127–9149, https://doi.org/10.5194/acp-25-9127-2025, 2025.

https://doi.org/10.5194/egusphere-2026-3188
Preprint. Discussion started: 2 July 2026

UNECEhttps://unece.org/fileadmin/DAM/env/documents/2017/AIR/EMEP/Final__new_Chapter_3_v2__August_2017_.pdf , 2017.

Turnock, S.T., Wild, O., Dentener, F.J., Davila, Y., Emmons, L.K., Flemming, J., Folberth, G.A., Henze, D.K., Jonson, J.E., Keating, T.J., Kengo, S., Lin, M., Lund, M., Tilmes, S., O'Connor, F.M., 2018. The impact of future emission policies on tropospheric ozone using a parameterised approach. Atmospheric Chemistry and Physics 18, 8953–8978. https://doi.org/10.5194/acp-18-8953-2018

United Nations Environment Programme. Global Environment Outlook 7: A future we choose – Why investing in Earth now can lead to a trillion-dollar benefit for all. Nairobi. https://wedocs.unep.org/handle/20.500.11822/49014, 2025.

van Caspel, W. E., Simpson, D., Jonson, J. E., Benedictow, A. M. K., Ge, Y., di Sarra, A., Pace, G., Vieno, M., Walker, H. L., and Heal, M. R.: Implementation and evaluation of updated photolysis rates in the EMEP MSC-W chemistry-transport model using Cloud-J v7.3e, Geosci. Model Dev., 16, 7433-7459, 10.5194/gmd-16-7433-2023, 2023.

Vandyck, T., Keramidas, K., Kitous, A., Spadaro, J. V., Van Dingenen, R., Holland, M., and Saveyn, B.: Air quality co-benefits for human health and agriculture counterbalance costs to meet Paris Agreement pledges, Nat Commun, 9, 4939, https://doi.org/10.1038/s41467-018-06885-9, 2018.

Van Dingenen, R., Dentener, F., Crippa, M., Leitao, J., Marmer, E., Rao, S., Solazzo, E., and Valentini, L.: TM5-FASST: a global atmospheric source–receptor model for rapid impact analysis of emission changes on air quality and short-lived climate pollutants, Atmos. Chem. Phys., 18, 16173–16211, https://doi.org/10.5194/acp-18-16173-2018, 2018.

Vieno, M., Dore, A. J., Stevenson, D. S., Doherty, R., Heal, M. R., Reis, S., Hallsworth, S., Tarrason, L., Wind, P., Fowler, D., Simpson, D. and Sutton, M. A.: Modelling surface ozone during the 2003 heat-wave in the UK, Atmos. Chem. Phys., 10, 7963-7978, 2010.

Vieno, M., Heal, M. R., Hallsworth, S., Famulari, D., Doherty, R. M., Dore, A. J., Tang, Y. S., Braban, C. F., Leaver, D., Sutton, M. A. and Reis, S.: The role of long-range transport and domestic emissions in determining atmospheric secondary inorganic particle concentrations across the UK, Atmos. Chem. Phys., 14, 8435-8447, 2014.

Vieno, M., Heal, M. R., Williams, M. L., Carnell, E. J., Nemitz, E., Stedman, J. R. and Reis, S.: The sensitivities of emissions reductions for the mitigation of UK $PM_{2.5}$, Atmos. Chem. Phys., 16, 265-276, 2016.

World Health Organization, Exposure to health damaging air pollutants: technical brief. Geneva (Air Quality, Energy and Health Science and Policy Summaries). https://doi.org/10.2471/B09461, 2025.

Wild, O., Fiore, A.M., Shindell, D.T., Doherty, R.M., Collins, W.J., Dentener, F.J., Schultz, M.G., Gong, S., MacKenzie, I.A., Zeng, G., Hess, P., Duncan, B.N., Bergmann, D.J., Szopa, S., Jonson, J.E., Keating, T.J., Zuber, A., 2012. Modelling future changes in surface ozone: a parameterized approach. Atmospheric Chemistry and Physics 12, 2037–2054. https://doi.org/10.5194/acp-12-2037-2012

Xiao, X., D. S.Cohan, D. W.Byun, and F.Ngan: Highly nonlinear ozone formation in the Houston region and implications for emission controls, J. Geophys. Res., 115, D23309, doi:10.1029/2010JD014435, 2010.

https://doi.org/10.5194/egusphere-2026-3188
Preprint. Discussion started: 2 July 2026

Xu, Y., Kobayashi, K., and Feng, Z.: Wheat yield response to elevated O3 concentrations differs between the world's major producing regions, Science of The Total Environment, 907, 168103, https://doi.org/10.1016/j.scitotenv.2023.168103, 2024.

Yang, B.-Y., Fan, S., Thiering, E., Seissler, J., Nowak, D., Dong, G.-H., and Heinrich, J.: Ambient air pollution and diabetes: a systematic review and meta-analysis. Environ. Res. 180, 108817, 2020.

Ye, Q., Li, J., Chen, X., Chen, H., Yang, W., Du, H., Pan, X., Tang, X., Wang, W., Zhu, L., Li, J., Wang, Z., Wang, Z., 2021. High-resolution modeling of the distribution of surface air pollutants and their intercontinental transport by a global tropospheric atmospheric chemistry source–receptor model (GNAQPMS-SM). Geoscientific Model Development 14, 7573–7604. https://doi.org/10.5194/gmd-14-7573-2021

Wang, X. and Mauzerall, D. L.: Characterizing distributions of surface ozone and its impact on grain production in China, Japan and South Korea: 1990 and 2020, Atmos. Environ., 38, 4383–4402, https://doi.org/10.1016/j.atmosenv.2004.03.067, 2004.

Zhong, Q., Tao, S., Ma, J., Liu, J., Shen, H., Shen, G., Guan, D., Yun, X., Meng, W., Yu, X., Cheng, H., Zhu, D., Wan, Y., and Hu, J.: PM2.5 reductions in Chinese cities from 2013 to 2019 remain significant despite the inflating effects of meteorological conditions, One Earth, 4, 448–458, https://doi.org/10.1016/j.oneear.2021.02.003, 2021.